



UNIVERSITA' DELLA CALABRIA

Dipartimento di Biologia, Ecologia e Scienze della Terra

Dottorato di Ricerca in Scienze della vita

Con il contributo di FSE

CICLO XXXIII

EDIBLE OLEOGELS: A RHEOLOGICAL AND MICROSTRUCTURAL ANALYSIS FOR STRUCTURED EMULSIONS DESIGN

Settore Scientifico Disciplinare ING-IND/24

Coordinatore: Ch.mo Prof. Maria Carmela Cerra

Firma  Firma oscurata in base alle linee guida del Garante della privacy

Supervisor: Prof. Domenico Gabriele

Firma  Firma oscurata in base alle linee guida del Garante della privacy

Dott.ssa Francesca Romana Lupi

Firma  Firma oscurata in base alle linee guida del Garante della privacy

Dottorando: Dott. Samuele Salvino

Firma  Firma oscurata in base alle linee guida del Garante della privacy

Table of Contents

Introduction	4
Research	5
Scientific Activity.....	5
1. Edible oleogels: an overview.....	6
1.1 Gels, organogels, oleogels.....	6
1.2 Organogel applications	7
1.3 Replacing solid fats in food products.....	7
1.4 Oleogelators properties.....	9
1.5 working principle of LMWOs	10
1.6 Organic production	11
1.7 Food gelators.....	12
1.7.1 Organic gelators.....	12
1.7.2 Nonorganic gelators.....	16
References	17
2. Materials and methods.....	22
2.1 Raw Materials and sample preparation.....	22
2.1.1 Raw Materials.....	22
2.1.2 Oleogels preparation.....	22
2.1.3 Emulsions preparation	23
2.2 Methods	23
2.2.1 Rheological Investigations.....	23
2.2.2 Spectroscopic investigations.....	25
2.2.3 Thermal Investigation.....	27
2.3 Insight on techniques used for the oleogel characterisation.....	28
2.3.1 Rheology.....	28
2.3.2 Differential Scanning Calorimetry	30
2.3.3 Spectroscopy.....	31
References	34
3. Results and Discussion	36
3.1 Rheological and spectroscopic analysis of Extra-Virgin Olive oil	36
3.2 Rheological, thermal and spectroscopic analysis of oleogels.....	37
3.2.1 Myverol.....	38

3.2.2 Policosanol.....	43
3.2.3 Carnauba wax	48
3.2.4 Beeswax	53
3.2.5 Manuka Beeswax.....	57
3.3 Comparison between oleogelators	61
3.3.1 Crystal onset temperature	61
3.3.2 Relative properties of gels during crystallisation	63
3.3.3 Structure Development Rate: Kinetics of gel structuring.....	66
3.4 Edible oleogels as fat phase for emulsion preparation.....	67
3.4.1 R-based oleogels.....	68
3.4.2 Rheological tests on a potentially marketable emulsion.....	69
References	71
Conclusions and perspectives	73

Introduction

Oleogelation is a reliable method for structuring healthy cis-unsaturated fats (which mainly composes vegetable liquid oils) to replace saturated and trans-unsaturated fats (abundant in vegetal and animal hardstocks): Their chronic consumption is believed to be dangerous for the cardiovascular apparatus of consumers. Organogelation occurs when, at a certain temperature, a relatively small amount of some specific amphiphilic compounds called oleogelators self-assembles into a 3D network via non-covalent, weak and reversible interactions such as van der Waals and H-bonding in the case of Low Molecular Weight Organogelators (LMWO). LMWOs are able to retain a large amount of oil, giving the system an overall solid-like behaviour even if they are composed of liquids for the most part and, therefore, they exhibit similar organoleptic features to widely used solid fats. Rheological (both small amplitude oscillatory and steady shear tests), thermal (Differential Scanning Calorimetry) and spectroscopic (Nuclear Magnetic Resonance, InfraRed, and Visible spectrophotometry) studies were carried out with a thermal cooling ramp on binary systems composed by olive oil and edible oleogelators (obtained from plant-based raw material processing, such as monoacylglycerols, policosanol, beeswax, Carnauba wax and Manuka wax). With the binary mixtures it was possible to highlight the formation kinetics of interactions and provide a better understanding of the link between macroscopic and microscopic variables. The overall aim was the formulation of a predictable pattern, which could be used in the fat industry to improve the technology of the process, especially in using the oleogels as the fat phase of water-in-oil emulsions. The application of oleogels in the process of edible emulsion making has been done under the supervision of the hosting company, since such material constitutes its core business and the production technology of such materials is continuously evolving and updating.

Research

The rheological and infrared spectroscopic part of the research, which constitute the majority of the work, were carried out at University of Calabria, in the Rheology and Food Engineering Laboratory of D.I.M.E.S. (Informatics, Model, Electronic and System Engineering Department). Other measurements were performed during a 6-month period in Switzerland at ETH Zürich, in the Food Process Engineering Laboratory of Institute of Food, Nutrition and Health (IFNH), Department for Health Sciences and Technology (D-HEST).

Scientific Activity

Three conferences were attended during the research period:

-ISFRS 2019 - Zurich, Switzerland - June 17-20, 2019 - Poster presentation, title " Simultaneous Microstructural and Rheological study of olive oil-based organogels as fat phase for shortenings and emulsions"

-AERC 2021 - Online Conference - April 13-15, 2021 - Poster presentation, title "Rheological, thermal and spectroscopic investigation of olive oil-based oleogels as fat phase for food emulsions"

-CReo Giovani 2021 - Online conference - September 13-14, 2021 - Oral Presentation, title "Rheological, thermal and spectroscopic investigation of olive oil-based oleogels".

1. Edible oleogels: an overview

1.1 Gels, organogels, oleogels

Gels have gained more and more attention over the past years because of their applications and their amazing chemical and physical properties. They are soft viscoelastic materials that hold a significant amount of liquid without allowing it to leak. This definition, although straightforward, is far from being rigorous and it has to be considered as an empirical and intuitive way for approaching this field. In fact, gels were said to be “easier to recognize than to define” a century ago from Lloyd [1]. A slightly better definition refers to gels as non-fluid colloidal network or polymer network expanded throughout its whole volume by a fluid [2]. This kind of material is believed to be composed by a self-assembling solid structuring agent (also called gelator) forming a three-dimensional fibrous network capable to entrap solvent molecules and preventing them from flowing in steady state. A gel is generally classified as hydrogel or organogel depending on the nature of the liquid component in the system: it is a hydrogel if the liquid is an aqueous (hydrophilic) phase, and if the liquid is an oil (hydrophobic) phase the system is referred to as an organogel. Gels can be further classified depending on the nature of the gelling molecules, which can be polymers or low molecular weight organogelators (LMOGs). Polymeric organogelators form a network which entraps the solvent molecules by either forming a cross-linked network in the case of chemical gels or an entangled one for physical gels, which can be further stabilised by weak intermolecular forces such as H-Bonding, π - π stacking, van der Waals forces [3]. On the other hand, LMOGs assemble themselves into supra-molecular structures via non covalent weak interactions [4] leading to the formation of sufficiently extended aggregates interacting with each other and with the solvent molecules to induce solvent gelation [3]. The physical gel, and especially the one whose formation is promoted by LMOGs, is very susceptible to external agents like temperature, pressure and pH [5], while a chemical gel, being held by irreversible covalent forces through long chain polymers, is stronger and more resistant to such agents. It is common among researchers, although not a general rule, to call “oleogels” the organogels which solvent is an edible oil generally liquid-like at room temperature. This notation will be used throughout this work.

1.2 Organogel applications

The most interesting feature of organogels is that, generally, a huge amount of liquid is contained within a small amount of assembled gelator. This, along with the fact that, for physical gels, no chemical reactions are involved and therefore the solvent keeps its chemical properties, probably leads to the most interesting feature of such systems: it is basically possible to transform a liquid-like solvent into a solid-like material without changing its chemical properties. Since the gel is basically a “non-flowing liquid” such materials are available for various applications: for example, gelling lubricants to prevent exudation from metallic surfaces, structuring of cosmetics for achieving the desired spreadability, making waste cooking oil solid-like for a safer disposal, gelling solvents used in restoration to prevent their infiltration into paintings, controlled release of drugs within a gel matrix, etc. [6]. Other more advanced perspectives concern tissue engineering, synthesis of inorganic nanostructures, biosensors, nanofibres [7]. Food and drug industries are particularly interested in organogels: the structuring of edible oils offers a solution to several problems, such as reducing oil mobility and migration, the ability to control the release of nutraceutical molecules, stabilising emulsions and replacing saturated fats and trans fats [6]. This work focuses on the latter, in particular, on the structuration of triglycerides as a possible solution to human health problems related to chronic fat consumption, that will be shortly explained.

1.3 Replacing solid fats in food products

Fats and oils, widely and traditionally used in the human diet, are mainly composed by triacylglycerols (TAGs), made of three fatty acids attached to the branches of a glycerol molecule, besides some impurities and some small amounts of mono- and diacylglycerols. The fatty acids on the TAGs molecule can be monounsaturated, polyunsaturated (called MUFA and PUFA, Mono and Poly Unsaturated Fatty Acids respectively) and saturated fatty acids. It was common sense to think that all fats are bad for human health, which led to the development of low-fat diets, but an increasing number of studies for this topic showed that only the chronic consumption of saturated and trans-unsaturated fatty acids of the TAGs are responsible of cardiovascular diseases [8], [9] since trans-fatty acids have shown to be responsible for an increase of the low-density lipoprotein (LDL), also known as the “bad cholesterol” and decrease the amount of high-density lipoprotein (HDL), the “good cholesterol”, while saturated fatty acids have been shown to increase the LDL levels without affecting the HDL levels [10]–[13]. Unfortunately, they also play a crucial role in providing desirable solid-like structure and texture of the food, therefore, trying to eliminate them without affecting the final

organoleptic properties required by the customer is very challenging. Furthermore, food manufacturers are reluctant in changing successful industrial food products. The negative effects could be avoided by consuming polyunsaturated fats instead of saturated and trans-unsaturated fats [14]. The saturated fatty acid is held together by single covalent carbon-carbon bonds, which prevents it to twist in the tri-dimensional space allowing it to stay in a straight line. All unsaturated fatty acids have at least one carbon-carbon double bond: in the *trans* configuration the two carbon groups are on the opposite side of the carbon group, while in the *cis*-configuration they are on the same side. The *cis* configuration produces a bend in the molecule, whereas the *trans* configuration is similar to the saturated fat. Saturated and trans-unsaturated fatty acids have similar melting point, while cis-unsaturated fatty acids have a lower melting point than their trans-isomers [15]. The mechanical properties of fats are the result of the synergistic effect of solid fat content, polymorphism and fat crystal network microstructure, including the shape, size, area fraction and the distribution pattern of the fat crystals [16]. An alternative and interesting way for obtaining such structure using healthy low-melting point cis-saturated fatty acids, which are abundant in edible oils obtained from vegetal sources, is oleogelation. Theoretically, it is also possible to think about oleogels as substitutes of plant based meat analogues' fat phase [17]. Before digging deeper into oleogelation working principles, it is worth giving some highlights about this interesting and exponentially growing field.

1.3.1 Plant-based meat analogues

Meat is a very important part of the human daily diet, providing vital components for our body such as proteins, vitamins, minerals and fats [18]. Although global meat market is estimated to grow [19], meat consumption patterns are unpredictable due to a number of factors affecting the consumer's choice including price, safety, appearance and personal choices [20]. Furthermore, massive meat consumption puts in danger both the environment and the human health: indeed, it is a major responsible for greenhouse emissions [21] and cardiovascular diseases increased risk, the latter due to the high content of cholesterol and saturated fatty acids [22]. Plant based products are obtaining growing attention from customers looking for healthy, safe and sustainable food [20]. The use of plant based meat is therefore a possible answer for food industries which are asked to produce more healthy and eco-friendly products, as well as an answer to ethical concerns [23]. Plant based meat analogues are plant-based products that mimic the appearance, flavour and the fibrous texture of animal meat [24]. Several vegetal protein sources (e.g. cereals, vegetables, legumes, microalgae and fungi) are used to substitute animal proteins for producing a wide spectrum of meat-free products such as burger patties, sausages and nuggets [25]. To emulate the fibrous texture of meat muscle,

plant-based proteins must be processed from their original form (globular shape) to the textured protein (linear shape) by applying different techniques (e.g., extrusion, wet or electro-spinning, high-temperature conical simple shearing, freeze structuring, blends proteins, hydrocolloids and 3D printing) [17]. Lipids rich in saturated fatty acids (e.g., coconut oil and cocoa butter) or rich in unsaturated fatty acids (e.g., sunflower oil, canola oil, sesame oil and avocado oil) are used to intensify the flavour as well as to improve texture and mouthfeel of the plant-based meat analogues. The source and composition of fatty acids is extremely important to mimic meat flavour related to lipid oxidation and volatiles generated by Maillard reaction during thermal processing [26]. Oleogels could play a role in this. It has been shown that it is possible to enrich proper meat products with oleogel to increase the ratio of healthy PUFA with respect to other fatty acids, affecting neither the overall customer appreciation nor the final price [27].

1.4 Oleogelators properties

As they have been physically described so far, organogelators must be able to give a solid like behaviour to an otherwise liquid system and preventing it from escaping from the network. For food applications there are other requirements to be met [28] :

- (a) they have to comply with strict rules given by food ruling authorities;
- (b) they should be as cheap as possible, since specific materials often come from a synthesis or isolation process that results in high added value, and therefore high cost;
- (c) they must be able to structure TAGs at the lowest possible concentrations, i.e., be efficient, to overcome the cost problem and minimise any side effects caused by excessive ingestion of structuring agent;
- (d) they must have the same physical properties as the fat material they are supposed to replace, since most foods are typically stored at temperatures ranging from 5°C to 25°C and eaten at physiological temperatures (around 37°C). Hence, the organogelator should remain solid at least up to 37°C and then melt according to the different application.
- (e) they should be able to compete with the versatility of fats in terms of choice of physical properties: for example, from a technical point of view, it is possible to change the melting point and melting profile simply by mixing different fats and oils, by catalytic hydrogenation or by changing the conditions of the crystallisation process, which are fields widely known and studied, but when it comes to alternative structuring agents this is more difficult because of their earlier discovery [4].

(f) if the final product has to be sold with the “organic” label, the oleogelators must be labelled as organic as well, even if there is just a small amount of them. A short framework on organic production will follow later in this chapter after describing the working principle of organogelation.

1.5 working principle of LMWOs

Some LMWOs are capable of gelling certain edible oils even at low concentrations, ranging from 0.5 to 3% w/w [29]. The process of gelation with LMWOs is thermally reversible and temperature sensitive. Generally, high concentrations of oleogelators are required to gel oils with large amounts of impurities as the impurities interact with the gelators. These gelators have high gelation ability and the formed gel will have a long lifetime [30]. Although numerous gelators have been discovered along with different gelation patterns, it is not possible to determine *a priori* whether yet, given certain characteristics, a molecule can behave as a gelator, just as it is not possible to predict which solvent may be preferentially gelled. The discovery of new gelators remains almost randomised (the term serendipity is often used) and is usually followed by the search for potentially gelation-compatible solvents [3]. It is believed that the ability of an organogelator to gel a solvent is the result of balancing the solubility and insolubility of that gelator in that solvent: the molecule must be relatively insoluble to be able to crystallise or self-assemble, in order to form structures on an intermolecular scale; at the same time it must be relatively soluble to be able to interact with solvent molecules [4]. If the organogelator is insoluble, it precipitates; if it is completely soluble, a homogeneous solution will be formed. A technique for preparing LMOG-based organogels is to heat the gelator within the solvent above its melting temperature, and allow the over-saturated, isotropic solution to cool down to room temperature. Due to the temperature decrease, the gel molecules condense and, depending on the affinity solvent-solute it could lead to possible scenarios sketched in fig.1.1

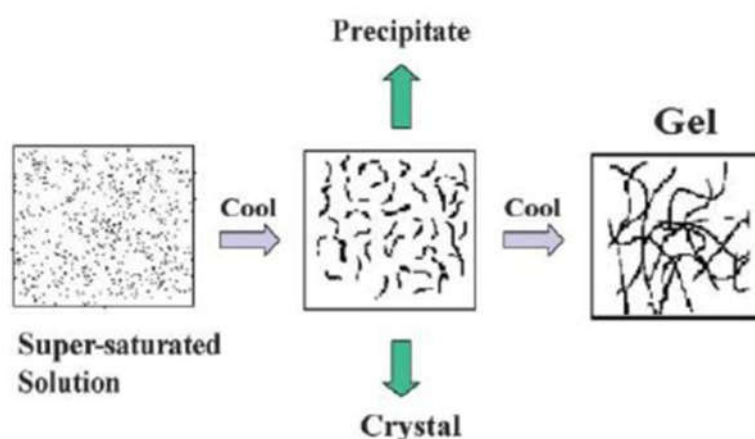


Fig. 1 .1 Possible scenarios during the cooling process of a solvent-solute system [31].

In particular, during the cooling process of such systems, the following materials can be produced:

- highly ordered aggregate (crystal);
- aggregate in a disordered manner to form an amorphous precipitate;
- gels, representing an intermediate situation.

1.6 Organic production

The definition and features of organic production are reported from the EU website [32]. An “organic” production must respect the rules on organic farming. These rules are designed to promote environment protection, maintain the biodiversity and build consumer trust in organic products. These regulations govern all areas of organic production and are based on several key principles, such as:

- prohibition of the use of GMOs;
- forbidding the use of ionising radiations;
- limiting the use of artificial fertilisers, herbicides and pesticides;
- prohibiting the use of hormones and restricting the use of antibiotics to only when necessary for animal health.

This means that organic producers need to adopt different approaches to maintaining soil fertility and animal and plant health including:

- crop rotation;
- cultivation of nitrogen fixing plants and other green manure crops to restore the fertility of the soil;
- prohibition of use of mineral nitrogen fertilisers;
- to reduce the impact of weeds and pests, organic farmers choose resistant varieties and breeds and techniques encouraging natural pest control;
- encourage the natural immunological defence of animals;
- in order to maintain animal health, organic producers need to prevent overstocking.

An organic product is granted to have a higher quality and traceability, which of course is something desirable for the consumer although the final price is often higher than the common product. Organic labelling process must face very strict rules, which observance is ensured by specific bodies authorised and supervised by major institutions like European Union. Such bodies make sure that both raw materials and production processes observe the rules of organic production. The European Union avails a group specifically created for the purpose of determining new substances or process techniques which satisfy the organic labelling rules: such group, called EGTOP (Expert Group for

Technical advice on Organic Production), grants that EU rules on organic production are effective and reasonable and, since the technological innovation of organic product is continuously evolving, makes sure that the EU is always updated on technical and scientific aspects regarding the organic production. On the EU website a list of edible and food production-related organic substances, based on EGTOP's advice, is available [33]. From such list some of them were selected and used in this research work.

1.7 Food gelators

There are different types of low molecular weight oleogelators which can be used for food production such as waxes, fatty acids and fatty alcohols, phytosterols, ceramides, lecithin, surfactant, TAG derivatives and others.

1.7.1 Organic gelators

For a product, whether partially or fully composed by an oleogel, to be given the organic label, all of its components must be labelled as organic as well. The following substances are present on the abovementioned EGTOP organic substances list [33].

1.7.1.1 Waxes

A wax is defined as a chemically heterogeneous material mainly containing long chain esters from fatty acids and fatty alcohols [34], along with smaller quantities of other products such as n-alkanes, fatty acids and fatty alcohols. They display hydrophobic tendencies, have high melting temperatures (50-80°C) and are solid at room temperature [35]. Waxes are widely used in cosmetics industry and in food industry as coating agents, but even if not approved as food additives by the EU, they are widely studied as gelling agents because of their promising behaviour.

1.7.1.1.1 Beeswax

Beeswax is obtained through secretion from bees, when building the hive (the hexagonal cells structure where they live). After removing the honey by draining, filtering, and centrifuging the hive is melted in boiling water or with steam. A hot water bath, along with active carbon and fossil shell flour to remove impurities, further refines the obtained wax. Wax obtained by pressure filtering is called "yellow beeswax" and removing the natural pigment leads to the "white beeswax" [36].

Beeswax is a complex mixture of saturated/unsaturated, linear/complex mono- and di- esters, hydrocarbons, free fatty acids and alcohols and other substances. More than 300 individual components have been found comparing waxes from different bees' species; although their concentration may depend globally on the species and the geographic location, the differences in components and their concentrations are quite small [37]. In the following figure (Fig. 1.2) the composition of a particular beeswax called *A. Mellifera* is reported.

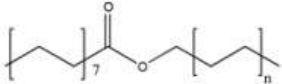
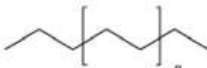
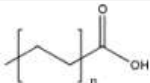
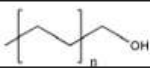
Components	<i>A. mellifera</i> L. (%)	General structural formulas
Esters total	57.4	
monoesters	40.8	
hydroxymonoesters	9.2	
diesters	7.4	
Hydrocarbons total	15.7	
alkanes	12.8	
alkenes	2.9	
Free fatty acids total	18.0	
Free fatty alcohols total	0.6	
Total	91.7	

Fig. 1.2 Composition of beeswax "*A. Mellifera*". Missing percentage refers to other components and impurities [37].

Beeswax is a promising oleogelator since has been found to gel vegetable oils with a minimum concentration of 2% w/w [38] but it has been shown that variations in composition of the same wax species influences the minimum concentration [39].

1.7.1.1.2 Manuka Beeswax

Manuka Beeswax is a particular beeswax, produced exclusively in New Zealand. Manuka is the Maori name for the plant *Leptosperunum scoparium*, also called "tea tree". His flowers, full of pollen and nectar, feed the bees which produce Manuka honey, very precious and with anti-bacterial properties, unlike ordinary honey [40]. Although a huge number of studies on Manuka honey are available, no published research work on Manuka beeswax can be found in literature.

1.7.1.1.3 Carnauba Wax

Carnauba wax (also called palm wax or Brazilian wax) is obtained from dried leaves of Brazilian palm tree *Copernicia prunifera* [41]. Wax is found on the outer leaves of the tree, which are either dried naturally by sun exposition or on a steam-warmed grill, to soften the wax; then, the leaves are cut and separated to get a mixture composed by wax at 60%, the remaining being ground leaves. The

main purification process is done by melting such mixture in a water and oxalic acid solution, obtaining a raw wax paste, which is heated up to its boiling point and pressure-forced through a filter at high temperature. Centrifugation expels the water, making the wax anhydrous. The final wax is a complex mixture consisting of aliphatic esters (wax esters), α -hydroxyl esters and cinnamic aliphatic diesters (referred to cinnamyl group, an aromatic group depicted in figure 1.3). It also contains free acids, free alcohols, hydrocarbons and resins. It is described as consisting mainly of straight-chain acids with even-numbered carbon chains from C24 to C28 and straight-chain alcohols with even-numbered carbon chains from C30 to C34. The average composition of the highest quality carnauba wax is reported in fig. 1.3 [42].

Compound	Amount (wt% of wax)
Aliphatic esters	38-40
Diesters of 4-hydroxycinnamic acid	20-23
Diesters of 4-methoxycinnamic acid	5-7
Esters of ω -hydroxycarboxylic acids	12-14
Free alcohols	10-12
Free acids	5-7
Hydrocarbons (paraffins)	0.3-1
Triterpene diols	0.4

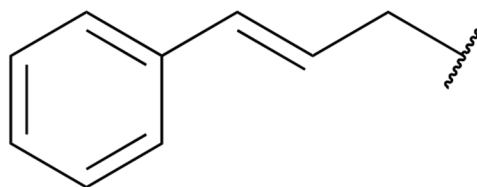


Fig. 1.3: Carnauba wax average composition [42] (left) and cinnamyl group (right).

Dassanayake et al. found that a minimum concentration as low as 4% w/w is required to gel vegetable oils [43].

1.7.1.2 Soy Lecithin

The definition of lecithin is given by European commission [33]. Lecithins are referred to as mixtures or fractions of phosphatides obtained from physical processing of animal or plant substances. Percentages of different components in lecithins depend on raw materials. The main source for lecithin production is the soybean oil: seeds are compressed, and water is added for the phosphatides hydrolysis, forming a muddy compound. Mud is separated from oil by centrifugation at 50-70°C. Oil contains <0.5% phosphatides while mud, containing 40-50% water is dried until reaching <1% water, obtaining the final lecithin which is cooled down under 50°C degrees to maintain properties. It can be stocked at room temperature for several months [44]. Lecithins obtained from soy beans have 60% phospholipid and 40% other components such as triacylglycerols, sterols and carbohydrates in various amounts. The components giving the lecithins their most interesting properties as emulsifiers and, in a certain set of condition, as oleogelators, are phospholipids and in particular phosphatidylcholine, at a point where just this molecule is commonly called “lecithin”. Phosphatidylcholine is a zwitterionic surfactant, given the simultaneous presence of both a negative and a positive electric charge. The structure of such molecules is reported in fig. 1.4 [45].

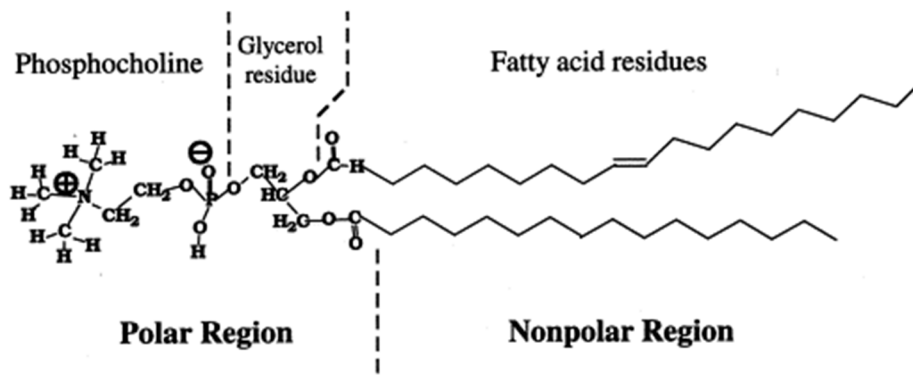


Fig. 1.4: Scheme of phosphatidylcholine. In the lower side the polar and nonpolar regions are highlighted, whereas in the upper side the chemical parts are distinguished. Electric charges are circled on the phosphocholine [45].

When dissolving lecithin alone in non-polar systems like vegetable oil, they form inverted spherical micelles, having the non-polar part oriented towards the bulk of the solvent interacting with fatty acids of the triacylglycerols molecules, and the polar part towards the inner side of the aggregate interacting with its similar parts of other surfactants. In literature, no stable oleogels formed by oil and lecithin only are described. Adding small amounts of a polar solvent, like water, causes the formation of tubular micelles: they interact forming a 3D network causing an abrupt increase in viscosity and later the gel formation [45][46]. A phase diagram has been built to help understanding the role of water in oleogel formation [47]:

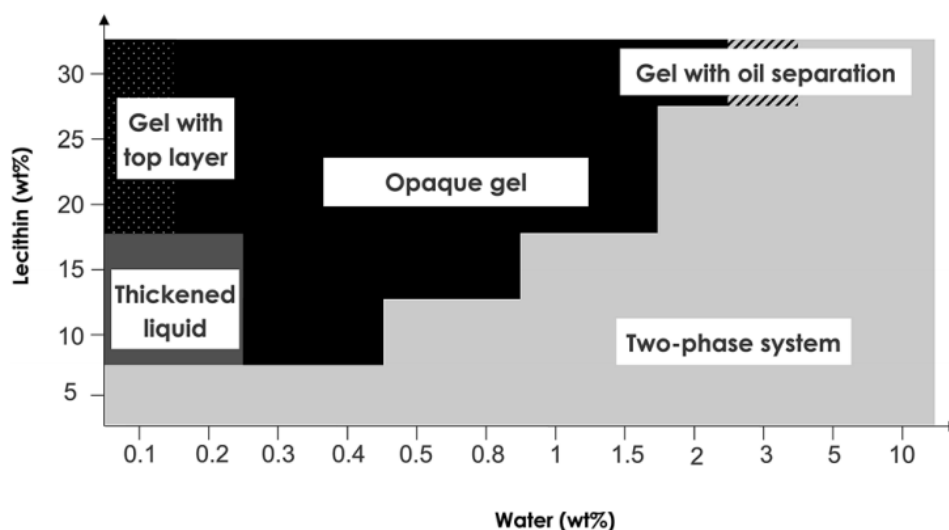


Fig. 1.5: Partial binary phase diagram of lecithin/water/canola oil system at room temperature. Sample left at rest for 24h. The “gel” criterion is the ability of the sample not to flow under its own weight.

Diagram shows that both lecithin and water play a fundamental role in gel construction and its kinetic stability. If the lecithin is kept under 7.5% concentration no gel formation is observed whatsoever.

1.7.2 Nonorganic gelators

Some substances are not entitled to the organic label, but they show good gelling abilities, and they can be used, whereas approved by local laws, as food additives and oleogelators.

1.7.2.1 Monoacylglycerols

Monoacylglycerols of fatty acids (MAGs) are of great interest because of their wide application fields. They show healthy benefits [48] and are able to self-assemble both within organic and aqueous environment [49] because of their amphiphilic nature: the glycerol head is the hydrophilic part, while the chain of the fatty acid is the hydrophobic part. MAGs are widely used as emulsifiers for example in food industries as structuring agents, such as the structuring of cod liver oil [50] or as a substitute for saturated fats in the production of biscuits in the form of an oil-in-water emulsion [51]. Lupi et al. [52] demonstrated that organogels based on Myverol®, a commercial monoacylglycerols mixture equally composed by glyceryl monopalmitate and glyceryl monostearate (on a weight basis), oil and cocoa butter can be used to produce water-in-oil emulsions with rheological properties similar to commercial margarines. The minimum concentration of Myverol to obtain a organogel is in the range between 1% and 1.5% w/w [53].

1.7.2.2 Policosanol

Fatty acids and fatty alcohols have been reported to gel edible oils [54]. As usually happens for organogelators, an increase in the length of the aliphatic chain of such molecules reduces the amount of organogelator needed to gel the system. Policosanol is a nutraceutical mixture of fatty alcohols having chain lengths greater than 24 carbons, the predominant being octacosanol with 28 carbons. In food applications, Lupi et al. [55] used policosanol to gel olive oil while highlighting its nutraceutical properties. The same authors concluded that it is possible to efficiently gel an oil phase with a policosanol concentration as low as 0.5%.

References

- [1] D. Lloyd, "The problem of gel structure." The Chemical Catalog Co, pp. 767–782, 1926.
- [2] J. Alemán *et al.*, "Definitions of terms relating to the structure and processing of sols, gels, networks, and inorganic-organic hybrid materials (IUPAC recommendations 2007)," *Pure Appl. Chem.*, vol. 79, no. 10, pp. 1801–1829, 2007.
- [3] A. Vintiloiu and J. C. Leroux, "Organogels and their use in drug delivery - A review," *J. Control. Release*, vol. 125, no. 3, pp. 179–192, 2008.
- [4] E. D. Co and A. G. Marangoni, "Organogels: An alternative edible oil-structuring method," *JAACS, J. Am. Oil Chem. Soc.*, vol. 89, no. 5, pp. 749–780, May 2012.
- [5] A. Thamizhanban, K. Lalitha, and S. Nagarajan, "Self-Assembled Soft Materials for Energy and Environmental Applications," pp. 443–470, 2019.
- [6] N. E. Hughes, A. G. Marangoni, A. J. Wright, M. A. Rogers, and J. W. E. Rush, "Potential food applications of edible oil organogels," *Trends Food Sci. Technol.*, vol. 20, no. 10, pp. 470–480, 2009.
- [7] E. D. Co and A. G. Marangoni, *Oleogels*. AOCS Press, 2018.
- [8] A. G. Liu, N. A. Ford, F. B. Hu, K. M. Zelman, D. Mozaffarian, and P. M. Kris-Etherton, "A healthy approach to dietary fats: Understanding the science and taking action to reduce consumer confusion," *Nutr. J.*, vol. 16, no. 1, Aug. 2017.
- [9] Y. Zhu, Y. Bo, and Y. Liu, "Dietary total fat, fatty acids intake, and risk of cardiovascular disease: A dose-response meta-analysis of cohort studies," *Lipids Health Dis.*, vol. 18, no. 1, Apr. 2019.
- [10] M. A. Rogers, "Novel structuring strategies for unsaturated fats - Meeting the zero-trans, zero-saturated fat challenge: A review," *Food Res. Int.*, vol. 42, no. 7, pp. 747–753, 2009.
- [11] A. Keys, "Diet and the epidemiology of coronary heart disease," *J Am Med Assoc*, vol. 164, pp. 1912–1919, 1957.
- [12] M. K. A. A. M. S. W. W. D Mozaffarian, "Trans fatty acids and cardiovascular disease," *N Engl J Med*, vol. 354, pp. 1601–1613, 2006.
- [13] J. M. M. F. M Brandt, "The 2006–2007 Food Label and Package Survey (FLAPS): nutrition

labelling, trans fat labelling,” *J Food Compos Anal*, vol. 225, pp. S74–S77, 2009.

- [14] H. M. Roche, “Fatty acids and the metabolic syndrome,” 2021.
- [15] B. S. Ghotra, S. D. Dyal, and S. S. Narine, “Lipid shortenings a review.pdf,” vol. 35, pp. 1015–1048, 2002.
- [16] D. Tang and A. G. Marangoni, “Quantitative study on the microstructure of colloidal fat crystal networks and fractal dimensions,” *Adv. Colloid Interface Sci.*, vol. 128–130, no. 2006, pp. 257–265, 2006.
- [17] F. Boukid, “Plant-based meat analogues: from niche to mainstream,” *Eur. Food Res. Technol.*, vol. 247, no. 2, pp. 297–308, 2021.
- [18] P. M. de C. C. Pereira and A. F. dos R. B. Vicente, “Meat nutritional composition and nutritive role in the human diet,” *Meat Sci*, vol. 93, no. 3, pp. 586–592, Mar. 2013.
- [19] ResearchandMarkets, “Processed Poultry & Meat Market Analysis 2020-2025 - Global Market Forecast to Grow at a CAGR of 7.35% During 2020 and 2025,” pp. 7–11, 2020.
- [20] N. M. Xazela, A. Hugo, U. Marume, and V. Muchenje, “Perceptions of rural consumers on the aspects of meat quality and health implications associated with meat consumption,” *Sustainability*, vol. 9, no. 5, p. 830, May 2017.
- [21] M. Shafiullah, U. Khalid, and M. Shahbaz, “Does meat consumption exacerbate greenhouse gas emissions? Evidence from US data,” *Environ. Sci. Pollut. Res.*, vol. 28, no. 9, pp. 11415–11429, Mar. 2021.
- [22] Y. Wang and M. A. Beydoun, “Meat consumption is associated with obesity and central obesity among US adults,” *Int J Obes*, vol. 33, no. 6, pp. 621–628, Jun. 2009.
- [23] C. Hartmann and M. Siegrist, “Consumer perception and behaviour regarding sustainable protein consumption: a systematic review,” *Trends Food Sci Technol*, vol. 61, pp. 11–25, Mar. 2017.
- [24] V. Joshi and S. Kumar, “Meat analogues: plant based alternatives to meat products—a review,” *Int J Food Ferment Technol*, vol. 5, no. 2, p. 107, 2015.
- [25] U. Fresán, M. A. Mejia, W. J. Craig, K. Jaceldo-Siegl, and J. Sabaté, “Meat analogs from different protein sources: a comparison of their sustainability and nutritional content,” *Sustain*, vol. 11, no. 12, 2019.

- [26] C. Diez-Simon, R. Mumm, and R. D. Hall, “Mass spectrometry-based metabolomics of volatiles as a new tool for understanding aroma and flavour chemistry in processed food products,” *Metabolomics*, vol. 15, no. 3, p. 41, Mar. 2019.
- [27] A. J. Martins *et al.*, “Omega-3 and Polyunsaturated Fatty Acids-Enriched Hamburgers Using Sterol-Based Oleogels,” *Eur. J. Lipid Sci. Technol.*, vol. 121, no. 11, Nov. 2019.
- [28] E. D. Co and A. G. Marangoni, “Organogels: An alternative edible oil-structuring method,” *JAOCs, J. Am. Oil Chem. Soc.*, vol. 89, no. 5, pp. 749–780, May 2012.
- [29] F. R. Lupi, V. Greco, N. Baldino, B. de Cindio, P. Fischer, and D. Gabriele, “The effects of intermolecular interactions on the physical properties of organogels in edible oils,” *J. Colloid Interface Sci.*, vol. 483, pp. 154–164, 2016.
- [30] M. Suzuki and K. Hanabusa, “Polymer organogelators that make supramolecular organogels through physical cross-linking and self-assembly,” *Chem. Soc. Rev.*, vol. 39, no. 2, pp. 455–463, Jan. 2010.
- [31] N. M. Sangeetha and U. Maitra, “Supramolecular gels: Functions and uses,” *Chem. Soc. Rev.*, vol. 34, no. 10, pp. 821–836, 2005.
- [32] EC, “Organic production and products | European Commission,” pp. 1–7, 2020.
- [33] CIR EU 673, “COMMISSION IMPLEMENTING REGULATION (EU) 2016/673 of 29 April 2016,” *Off. J. Eur. Union*, vol. 2001, no. May, pp. 20–30, 2016.
- [34] C. D. Doan, I. Tavernier, P. K. Okuro, and K. Dewettinck, “Internal and external factors affecting the crystallization, gelation and applicability of wax-based oleogels in food industry,” *Innov. Food Sci. Emerg. Technol.*, vol. 45, no. September 2017, pp. 42–52, 2018.
- [35] S. Jana and S. Martini, “Physical characterization of crystalline networks formed by binary blends of waxes in soybean oil,” *Food Res. Int.*, vol. 89, pp. 245–253, Nov. 2016.
- [36] EFSA, “Beeswax (E 901) as a glazing agent and as carrier for flavours Scientific Opinion of the Panel on Food additives, Flavourings, Processing aids and Materials in Contact with Food (AFC),” *EFSA J.*, vol. 615, pp. 1–28, 2007.
- [37] R. Aichholz and E. Lorbeer, “Investigation of combwax of honeybees with high-temperature gas chromatography and high-temperature gas chromatography–chemical ionization mass spectrometry: I. High-temperature gas chromatography,” *J. Chromatogr. A*, vol. 855, no. 2, pp. 601–615, Sep. 1999.

- [38] A. J. Martins, M. A. Cerqueira, L. H. Fasolin, R. L. Cunha, and A. A. Vicente, “Beeswax organogels: Influence of gelator concentration and oil type in the gelation process,” *Food Res. Int.*, vol. 84, pp. 170–179, 2016.
- [39] H. S. Hwang, S. Kim, M. Singh, J. K. Winkler-Moser, and S. X. Liu, “Organogel formation of soybean oil with waxes,” *JAOCs, J. Am. Oil Chem. Soc.*, vol. 89, no. 4, pp. 639–647, 2012.
- [40] R. J. Weston, K. R. Mitchell, and K. L. Allen, “Antibacterial phenolic components of New Zealand manuka honey,” *Food Chem.*, vol. 64, no. 3, pp. 295–301, Feb. 1999.
- [41] S. D. Koonce, “A n Historical R e v i e w of the Chemistry of Carnauba W a x,” 1941.
- [42] E. W. LE Vandenburg, “The structural constituents of carnauba wax,” *J Am Oil Chem Soc*, vol. 47, pp. 514–518, 1970.
- [43] L. S. K. Dassanayake, D. R. Kodali, S. Ueno, and K. Sato, “Physical properties of rice bran wax in bulk and organogels,” *JAOCs, J. Am. Oil Chem. Soc.*, vol. 86, no. 12, pp. 1163–1173, Jan. 2009.
- [44] W. Van Nieuwenhuyzen, “Lecithin production and properties,” *J. Am. Oil Chem. Soc.*, vol. 53, no. 6, pp. 425–427, 1976.
- [45] Y. A. Shchipunov, “Lecithin organogelA micellar system with unique properties,” *Colloids Surfaces A Physicochem. Eng. Asp.*, vol. 183–185, pp. 541–554, 2001.
- [46] F. R. Lupi, D. Gabriele, N. Baldino, L. Seta, B. de Cindio, and C. De Rose, “Stabilization of meat suspensions by organogelation: A rheological approach,” *Eur. J. Lipid Sci. Technol.*, vol. 114, no. 12, pp. 1381–1389, Dec. 2012.
- [47] M. Bodennec, Q. Guo, and D. Rousseau, “Molecular and microstructural characterization of lecithin-based oleogels made with vegetable oil,” *RSC Adv.*, vol. 6, no. 53, pp. 47373–47381, 2016.
- [48] F. R. Lupi, D. Gabriele, D. Facciolo, N. Baldino, L. Seta, and B. de Cindio, “Effect of organogelator and fat source on rheological properties of olive oil-based organogels,” *Food Res. Int.*, vol. 46, no. 1, pp. 177–184, 2012.
- [49] F. Valoppi, S. Calligaris, L. Barba, and M. C. Nicoli, “Structural and viscoelastic characterization of ternary mixtures of sunflower oil, saturated monoglycerides and aqueous phases containing different bases,” *Food Res. Int.*, vol. 74, pp. 224–230, 2015.

- [50] S. Calligaris, S. Da Pieve, G. Arrighetti, and L. Barba, "Effect of the structure of monoglyceride-oil-water gels on aroma partition," *Food Res. Int.*, vol. 43, no. 3, pp. 671–677, Apr. 2010.
- [51] A. Goldstein and K. Seetharaman, "Effect of a novel monoglyceride stabilized oil in water emulsion shortening on cookie properties," *Food Res. Int.*, vol. 44, no. 5, pp. 1476–1481, 2011.
- [52] F. R. Lupi, D. Gabriele, B. De Cindio, M. C. Sánchez, and C. Gallegos, "A rheological analysis of structured water-in-olive oil emulsions," *J. Food Eng.*, vol. 107, no. 3–4, pp. 296–303, 2011.
- [53] F. R. Lupi, D. Gabriele, and B. de Cindio, "Effect of Shear Rate on Crystallisation Phenomena in Olive Oil-Based Organogels," *Food Bioprocess Technol.*, vol. 5, no. 7, pp. 2880–2888, 2012.
- [54] R. R. J Daniel, "Organogelation of plant oils and hydrocarbons by long-chain saturated FA, fatty alcohols, wax esters and dicarboxylic acids," *J Am Oil Chem Soc*, vol. 80, pp. 417–421, 2003.
- [55] F. R. Lupi, D. Gabriele, V. Greco, N. Baldino, L. Seta, and B. de Cindio, "A rheological characterisation of an olive oil/fatty alcohols organogel," *Food Res. Int.*, vol. 51, no. 2, pp. 510–517, 2013.

2. Materials and methods

2.1 Raw Materials and sample preparation

2.1.1 Raw Materials

The solvent used as a common basis for all the studied samples was extra virgin olive oil ('O') (Assoproli, Italy). Tested substances as oleogelators are, as described in chapter one: Myverol 1804K ('M') (Kerry Group, Ireland), a powder mixture composed in equal parts by glyceryl-monopalmitate and glyceryl-monostearate; the oleogelator used from the company, which commercial name shall remain secret, is similar to Myverol but mainly composed by glyceryl-stearate and will be noted with the letter 'R'; policosanol ('P'), composed by fatty alcohols (60% octacosanol, A.C.E.F., Italy), carnauba wax ('C') a wax obtained from the leaves of the Copernicia cerifera tree, and composed by aliphatic esters/diesters and free alcohols, (Norevo GmbH, Germany); beeswax ('B') obtained from the melting and purifying of the honeycomb and composed by mono- and di-esters, hydrocarbons and free acids, (A.C.E.F., Italy); Manuka beeswax ('U'), a particular beeswax obtained from the Manuka Tree (Mossop's, New Zealand); powder soy lecithin (L) composed by phospholipids and soybean oil. All samples were prepared by adding the solute to the oil heated above the melting temperature of each substance. Set temperatures were 70°C for M, B, U, L and 85°C for P and C, using water as thermal bath on a temperature-controlled heating plate. The following table sums them up.

Substance	Substance ID	Tprep [°C]
Extra Virgin Olive Oil	O	-
Sunflower Oil	S	-
Myverol 1804K	M	70
Company Oleogelator	R	70
Lecithin	L	70
Beeswax	B	70
Manuka wax	U	70
Carnauba wax	C	85
Policosanol	P	85

Table 2.1: ID and preparation temperature (Tprep) for each sample.

2.1.2 Oleogels preparation

All oleogels (except R) were prepared at two different mass fractions: 3.4% w/w and 10% w/w. The first mass fraction is indicated with the notation "1", while the latter with "2". From now on, when referring to a bi-component system, the notation "OXn" will be used, with O being the olive oil, X being the substance and n being the concentration notation number. For example, OC1 is the oleogel

composed by 3.4% Carnauba wax in 96.6% Oil and OM2 is the oleogel composed by 10% Myverol in 90% Oil. Sunflower oil (“S”, deSantis, Italy) was also used as alternative oil, along with O, for preparing OR1 and SR1 samples.

2.1.3 Emulsions preparation

Emulsions were prepared starting from a structured fat phase composed by R, O and cocoa butter. Full composition of the system shall remain under confidentiality, although the mass fraction of R within such system is similar to the mass fraction of R in sample OR1 and the total amount of oil is 60% w/w. Cocoa butter is added to boost rheological properties of the system [10]. The system is emulsified with 21% aqueous phase using a rotor-stator disperser (Ultra Turrax T50, IKA, Germany) at 2200 rpm for 3 minutes. Fruit juice was used as aqueous phase. System was prepared and stored in the fridge at 4°C for 10 days before measurements. For the aqueous phase of emulsions different water-soluble fruit-flavouring powders and fruit juices were provided by Reoli S.r.L. (Italy).

2.2 Methods

Prepared samples were studied with different investigation techniques. Methods will be described in this section, whereas an insight on the techniques will be given later.

2.2.1 Rheological Investigations

All samples were tested on a stress-controlled rheometer (Haake Mars III, ThermoFischer Scientific, USA) using a parallel plate steel geometry (diameter=50 mm, gap=1±0.1 mm). Temperature was controlled throughout the whole duration of the tests on the lower plate of the rheometer using a particular Peltier system, the so-called Rheonaut (Resultec, Germany; deviation on temperature=±0.1°C) which allowed to simultaneously collect rheological data and FTIR spectra, as later reported. Oscillatory and shear tests were performed using three different cooling ramps: -0.5°C/min, -1°C/min and -5°C/min starting from the preparation temperature of each sample (70°C for M, B, U, L and R; 85°C for P and C) up to 10°C. Small Amplitude Oscillatory Tests (SAOTs) were performed in the linear viscoelastic region of each sample at 1Hz, and Step Rate Temperature Ramp Tests (SRTRT) were performed at the shear rate of 1 s⁻¹. Regarding the SAOTs, linearity was checked by performing on each sample amplitude sweep tests at different temperatures in order to register all changes in both G' and G'' throughout the temperature range. Such temperatures were

reached by cooling down each sample from its preparation temperature using the appropriate cooling rate and oscillating at smallest settable stress amplitude ($\tau = 0.001\text{Pa}$), and for time purposes it was not possible to check every single temperature; depending on the sample, at least 4 to 6 different temperatures were required in order to find the different ranges of stress to be changed in order to follow linear viscosity. These tests allowed the kinetics of the gel formation with respect to the change in temperature variation to be followed. Both SAOTs and SRTRTs were used to evaluate the onset of crystallisation temperature T_{co} corresponding to the temperature at which a sudden increase of the complex modulus G^* , and, contemporarily, a strong decrease in phase angle δ was encountered [1] (for SAOT, T_{CO_OSC}) as well as sudden increase in viscosity η (for SRTRT, T_{CO_ROT}); as an example, a visual representation of T_{co} for a SRTRT will be provided later in fig. 2.2. Furthermore, G^* , δ and η were evaluated at 25°C and 10°C and/or at a certain temperature “ T_X ” far away from each T_{co} following the system cooling, for example $T_5 = T_{co} - 5^\circ\text{C}$. Similarly, a “knee” temperature T_{KN} was defined as the temperature at which the prolongation of the “liquid line” (i.e., the locus of points of $\ln(G^*)$ or $\ln(\eta)$ vs T in the liquid phase in which no gel is formed; such properties only increase owing to the temperature decrease and, therefore, kinetic energy of the molecules following Arrhenius’ law) meets the prolongation of the “structuring line” (which is the line starting from the next point with respect to T_{CO} and ending before the final gel plateau starts forming at lower temperatures). To study the gel kinetics, a structure development rate (SDr) was defined as follows [2].

$$SDr(t) = \frac{dG'(t)}{dt} \quad (2.1)$$

To compare differences of gelation for different substances, a number was defined as the integral of that value to obtain an average gelation rate [3]:

$$SDr_{avg}(T_x) = \frac{1}{t(T_c) - t(T_x)} \int_{t(T_c)}^{t(T_x)} \left(\frac{dG'(t)}{dt} \right) dt \quad (2.2)$$

Where T_c is a characteristic critical temperature, i.e. T_{KN} or T_{CO} and T_x is the abovementioned distance from such critical temperature. In this case, T_x is chosen as a variable instead of t because the preparation temperature and hence the starting temperature is not the same for all samples (see table 2.1), while the distance from critical temperature can be used for comparison.

For emulsions, time cure tests were performed and linear viscoelasticity was investigated using the same method used for oleogels. Samples were heated up from 10°C to 70°C using the heating rate $+1^\circ\text{C}/\text{min}$. Frequency sweep tests were also carried out by taking the emulsion out of the fridge,

placing it on the rheometer plate at 10°C and then heated up until 25°C without applying any heating ramp.

2.2.2 Spectroscopic investigations

Different spectroscopic techniques were used. They are described in the following sections.

2.2.3.1 FTIR

Infrared absorption spectra were collected while measuring rheological properties using the Rheonaut tool towards which the infrared beam coming from the spectrometer Nicolet iS-10 (ThermoFischer Scientific, USA) was conveyed. Spectra were acquired in the mid-infrared region from a wavenumber (ν) of 4000 cm^{-1} to 400 cm^{-1} using a 0.482 cm^{-1} step through an average of 32 scans per spectrum as the temperature was decreased, allowing a set of spectra depending on temperature for each sample to be collected. Considered parameter is the wavenumber at which the absorption peak of the CH₂ symmetric stretching (SS) is observed (typically $\sim 2852 \text{ cm}^{-1}$ for vegetable oil-based systems [4]) as depicted in Fig 2.1.

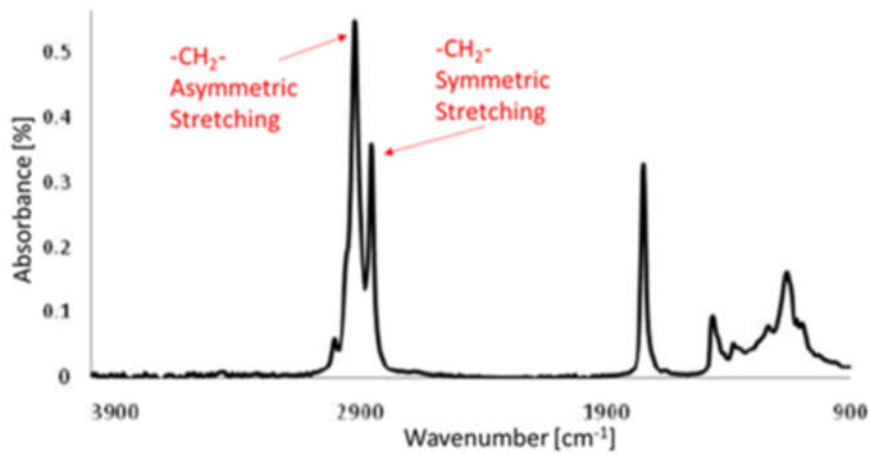


Fig 2.1: A typical infrared spectrum for vegetable oil systems. Symmetric and asymmetric -CH₂- stretching peaks are highlighted.

This value was then processed to get, for each sample, a relative shift of the peak absorption position (meaning it is calculated as the distance from the maximum starting temperature) with respect to the neat oil, with the aim of excluding the purely kinetic contribution to the gelation. Such parameter is called Relative Wavenumber Shift (RWS) and it has been obtained as follows in Eq. 2.3.

$$RWS(T) = \{[\nu(T) - \nu(T_{MAX})]_{SAMPLE} - [\nu(T) - \nu(T_{MAX})]_{PURE OIL}\} \quad (2.3)$$

Since the duration of each spectrum collection is about ~ 52 s, one spectrum per 1°C for the cooling rates -0.5°C/min and -1°C/min and one spectrum every 5°C for -5°C/min were acquired, therefore leading to a higher RWS resolution for the slower cooling rates. The values were used to evaluate the

onset of crystallisation temperature T_{CO_FTIR} corresponding to the temperature at which a sudden decrease of RWS was observed. Area between wavenumbers $3500-3200\text{cm}^{-1}$ was calculated since it corresponds to the OH-stretching modes, and therefore is an indicator of the presence of hydrogen bonding [5]. An explanation of the parameter meaning will be done.

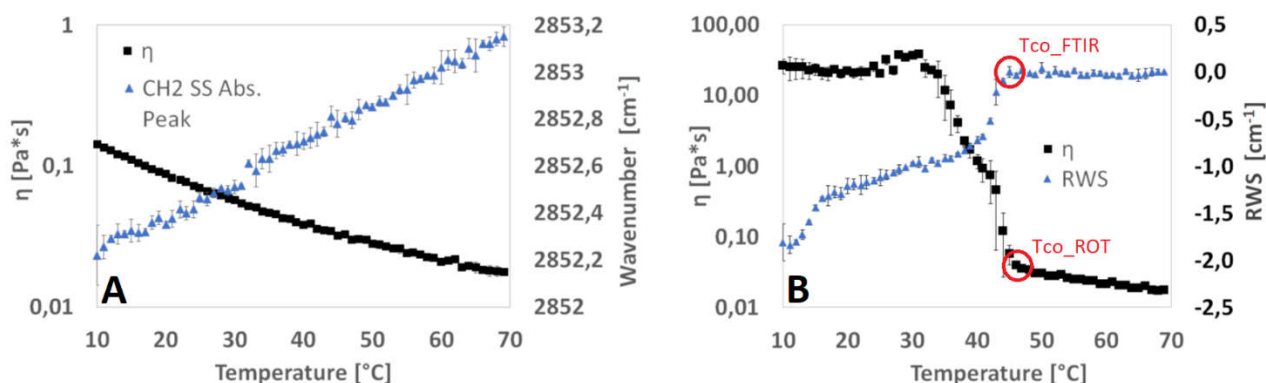


Fig. 2.2. (A) SRTRT viscosity and CH₂ symmetric stretching absorption peak wavenumber of O sample; (B) SRTRT viscosity and RWS of OM1 sample. T_{co_ROT} and T_{co_FTIR} for SRTRT are highlighted: in this case, they are the same.

In fig. 2.2A the viscosity and the CH₂ symmetric stretching absorption peak wavenumber of pure oil (O) simultaneously obtained during a SRTRT test are reported. The viscosity does not exhibit appreciable change throughout the temperature range, the small increase (not appreciable on a logarithmic scale) is only due to kinetic effects due to temperature decrease, and it can also be seen that the wavenumber has a linear behaviour which can be ascribable to kinetic effects as well. Viscosity only increases by one order of magnitude and the absorption peak only shifts by 1cm^{-1} . In fig. 2.2B the viscosity and RWS of OM1 (96.6% O + 3.4%M) sample simultaneously obtained during a SRTRT test are reported. It can be seen that at high temperatures viscosity only increases due to kinetic effects and RWS, which as defined in eq. 2.3 is the shift of the OM1 peak minus the shift of the O peak with respect to the pure oil, is zero because they are the same. When gelation occurs, simultaneous sudden increase of viscosity and decrease of RWS are observed at the same temperature, (T_{co_ROT} and T_{co_FTIR} are highlighted) and continue throughout the gelation, and finally the viscosity has increased by three orders of magnitude while RWS almost reaches -2cm^{-1} value. With eq. 2.3, the contribution of pure oil to OM1 peak shifting has been subtracted. RWS answers the question “how much the wavenumber of a sample decreases with respect to how much the wavenumber of the pure oil decreases?” and this is useful because this information tells us how much less does the CH₂ group stretch. As will be explained in paragraph 2.3.3.1, lower wavenumbers mean stronger interactions so RWS can be seen as a measurement of the gel’s “pure” interactions, since the kinetic contribution is subtracted.

2.2.3.2 NMR

Low-frequency nuclear magnetic resonance (Minispec mq20, Bruker, Germany) was carried out to evaluate the solid fat content (SFC) in the temperature range from preparation temperature down to 10°C. Organogels were prepared separately and injected NMR tubes (which were previously heated to avoid gelation on the tube walls) and eventually put into an external water bath (RC 20, LAUDA-Brinkmann LP, USA) at high temperature to erase previous thermal history caused by the injection. The temperature of the water bath was then lowered progressively using a step of 5°C measuring the SFC each time. This procedure provided an average cooling rate approximately equal to -1 °C/min. The onset of crystallisation temperature (TCO_NMR) was defined as the temperature at which a sudden increase of the SFC versus temperature was observed [3].

2.2.3.3 UV/VIS

The change in absorption intensity of the samples was recorded through UV-vis spectroscopy (Cary UV-Vis spectrometer, Agilent Technologies, USA). Samples were prepared separately and injected into pre-heated UV-quartz cuvettes. A preliminary absorption spectrum (200 – 800 nm) was collected on the pure oil to find the maximum absorption wavelength exhibited by the pure oil, which was found to be 415 nm (belonging to the visible spectrum). Then a light beam at that constant wavelength was shot to the samples while changing the temperature at the controlled cooling rates 0.5°C/min, -1 °C/min and -5 °C/min from 90°C to 10°C for all samples at the same time. The higher temperature with respect to the preparation temperature was set to be sure that all samples, surrounded by hot air, lost their thermal history. The temperature at which a sudden increase of the absorption intensity is observed was used to define the visible crystal onset temperature TCO_VIS.

2.2.3 Thermal Investigation

Differential Scanning Calorimetry (DSC) was performed on the samples (DSC 3, Mettler Toledo, USA). Samples (10 mg) were sealed in aluminium pans, kept at 70°C (M, B, U, L samples) or 85°C (P, C samples) for 10 min to erase a potential previous thermal history, and then cooled down to 10°C using cooling rates -0.5°C/min, -1°C/min and -5°C/min, while recording the heat flow as a function of temperature. As described by Lupi et al [3], the onset of crystallisation temperature evaluated by DSC (TCO_DSC) was estimated as the temperature corresponding to the beginning of the first exothermic peak.

2.3 Insight on techniques used for the oleogel characterisation

A brief explanation of used techniques to explain where the abovementioned quantities come from and understand their usefulness in oleogel characterisation.

2.3.1 Rheology

Rheology is probably the most useful tool available to understand the physical properties of gels [6]. It is almost impossible to find studies on gels without involving Rheology. In fact, when dealing with the mechanical properties of soft materials, the term *Rheology of a material* is used. That is because this branch of Physics deals with the mechanic properties of soft materials, i.e. materials which are neither treatable as elastic solids nor as viscous liquids and, as mentioned in chapter 1, mechanical properties are intrinsically involved in the process of understanding what a gel is. Most food products (and, in our case, oleogels) fall in this range of behaviour.

2.3.1.1 Steady shear flow and shear viscosity

In a steady shear flow, a shear stress is continuously (i.e. in steady state conditions) applied to a fluid. Given a certain volume of fluid, shear stress (τ) is the stress component applied tangentially to it through a surface of that volume (normal stresses also exist, which are applied on the normal directions of such control volume). It is equal to the force vector (a vector has both magnitude and direction) divided by the area of application and it is expressed in units of force per unit area (Pa). Shear rate, denoted by the symbol $\dot{\gamma}$, is the velocity gradient established in that fluid as a result of a shear stress applied in steady state. It is defined as the first-time derivative of the strain. It is expressed in units of reciprocal seconds s^{-1} . Viscosity is the internal friction of a fluid or its tendency to resist flow. Shear viscosity is defined as the ratio between shear stress and shear rate in steady state conditions, as reported in eq. 2.4:

$$\eta(\dot{\gamma}) = \frac{\tau}{\dot{\gamma}} \quad (2.4)$$

Generically it is denoted by the symbol η and it is a function of $\dot{\gamma}$. Its measurement unit in the S.I. is Pa*s. The viscosity of so-called Newtonian fluids, like water, pure oil and honey, does not depend on shear rate. Depending on the flow system and choice of shear rate and shear stress, there are several constitutive equations to evaluate the viscosity.

2.3.1.2 Oscillatory shear flow and viscoelasticity

As we said before, many materials, like most foods, do not behave as viscous liquids or elastic solids but their behaviour falls in between, and for that reason they are said to be viscoelastic. Although steady shear flow provides very useful information, is not enough to appreciate the behaviour of viscoelastic materials. Small amplitude oscillatory shear tests (SAOTs), can be used to determine viscoelastic properties of foods. In a SAOT experiment, a sinusoidal oscillating input, which could either be a stress or strain, is applied to the material with a fixed frequency and the phase difference between the input and the materials response in terms of oscillating strain (if stress is applied) or stress (if strain is applied), as well as the amplitude ratio are measured. If, for example, a fixed strain γ_0 is applied on the material oscillating over time at a frequency ω following the equation 2.4:

$$\gamma(t) = \gamma_0 \cos(\omega t) \quad (2.5)$$

The generated stress in the viscoelastic material can be split into two components: an elastic component in phase with the strain and a 90° out of phase viscous component. For deformation within the linear viscoelastic range, equation 2.6 expresses the generated stress $\sigma(t)$ in terms of an elastic or storage modulus G' and a viscous or loss modulus G'' .

$$\sigma(t) = G'\gamma_0 \sin(\omega t) + G''\gamma_0 \cos(\omega t) \quad (2.6)$$

For a viscoelastic material the resultant stress is also sinusoidal but shows a phase lag of δ radians when compared with the strain. The phase angle δ covers the range of 0° (solid materials) to 90° (purely viscous materials) as the viscous component increases. In this sense, also equation 2.7 also expresses the sinusoidal variation of the resultant stress:

$$\sigma(t) = \sigma_0 \sin(\omega t + \delta) \quad (2.7)$$

And by combining eqs. 2.6 and 2.7:

$$G' = \left[\frac{\sigma_0}{\gamma_0} \right] \cos \delta \quad (2.8)$$

$$G'' = \left[\frac{\sigma_0}{\gamma_0} \right] \sin \delta \quad (2.9)$$

The storage modulus G' expresses the quantity of energy stored in the material (or recoverable) per cycle of deformation, which is the main feature of purely elastic solids. G'' is a measure of the energy which is lost as viscous dissipation per cycle of deformation, process occurring in viscous liquids. Therefore, for a perfectly elastic solid, all the energy is stored, that is, G'' is zero and the stress and the strain will be in phase; in contrast, for a liquid with no elastic properties all the energy is dissipated as heat, that is, G' is zero and the stress and the strain will be out of phase by 90° (fig. 2.3).

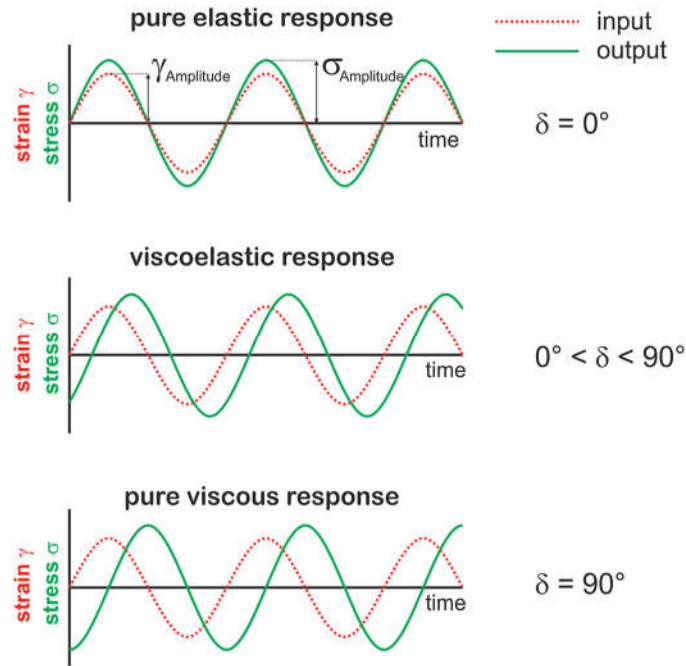


Fig 2.3: Stress versus strain response of a perfectly elastic solid, a viscoelastic material and a newtonian liquid in Dynamic Tests [7]

The complex modulus, used in this study, is defined as the geometric average of the storage and the loss modulus, as in eq. (2.10):

$$|G^*| = \sqrt{(G')^2 + (G'')^2} \quad (2.10)$$

2.3.2 Differential Scanning Calorimetry

Differential scanning calorimetry (DSC) gives information about organogel thermal transitions, particularly useful when evaluating the amount of energy involved during gelation. In DSC the sample is heated up or cooled down and the difference in thermal energy required to increase the temperature of the sample with respect to a reference is measured and plotted as a function of temperature. When the gel experiences a physical transformation, such as a phase transition from liquid to structured system, more heat has to be withdrawn in comparison to the reference in order to maintain both at the same temperature, since crystallisation is an exothermic process. The difference in heat flow associated with this exothermic phase transition allows the measurement of the amount of heat absorbed or released by integration of the DSC graph. DSC should be performed in both heating and cooling modes to evaluate both endothermic and exothermic transitions and assess the thermo-reversibility of the phase transition [8]. DSC data are also used as an indicator for the amount of solids in the gelled system and to identify if polymorphic transitions in crystalline networks occur [9].

2.3.3 Spectroscopy

If rheology and calorimetry help us in understanding the macroscopic mechanical and thermal behaviour of the material, they provide no information about where such properties arise from. In order to try to understand this, we have to look at microstructure of the substance. Spectroscopy refers to a wide set of different techniques using radiation to obtain data on the structure and properties of matter. It deals with measuring and interpreting spectra, as response from material that arise from the interaction of electromagnetic radiation, which is energy transmitted as electromagnetic (EM) waves, with matter. Its working principle is based on the absorption, emission, or scattering of electromagnetic radiation by atoms or molecules. The response of the sample is typically recorded as a function of radiation wavelength, and a plot of such responses represents a spectrum. Any source of EM waves (from low-energy radio waves to high-energy gamma-rays) can result in producing a spectrum, the higher being the energy and therefore the frequency and the lower being the wavelength, i.e., the distance between two consecutive peaks of the Em wave and therefore the dimension of the observable object. Energy, frequency and wavelength of the photons are bound as described by the equations 2.11

$$E = h\nu = \frac{hc}{\lambda} \quad (2.11)$$

Where E is the energy, ν is the frequency, λ is the wavelength, h is the Planck constant and c is the speed of light in vacuum. An overview of the spectroscopy techniques is reported in fig. 2.4:

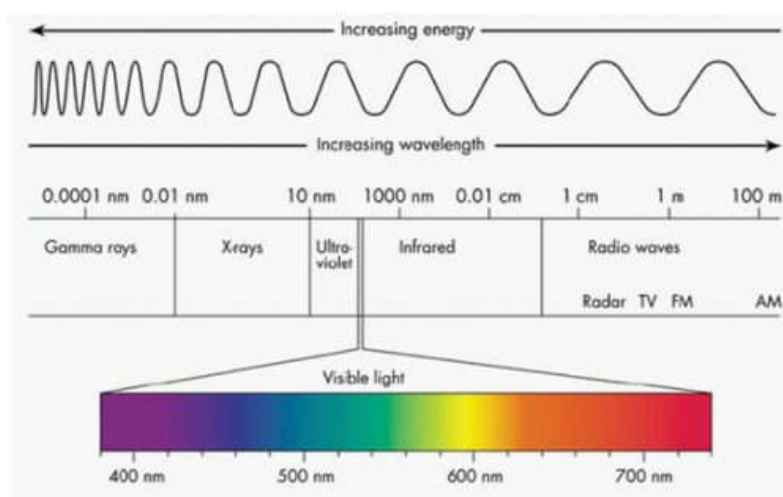


Fig. 2.4: Overview of EM spectrum from high energies to high wavenumbers (left to right). Visible region is highlighted [10].

Optical spectroscopy refers to all techniques that use nonionising radiation. This covers the region from the far ultraviolet (UV) to the far infrared (IR). In the medium, absorption of light causes a transition from an energetic ground state to a particular excited state. Depending on the energy of light and on the chemical nature of the interacting compound, the excited states may differ very much.

2.3.3.1 Infrared Spectroscopy

The mid (fundamental) infrared (IR or MIR) region extends from 4000 to 400 cm^{-1} . It is surrounded by the far infrared (FIR) region from 400 to 10 cm^{-1} and the near infrared (NIR) region from 12 500 to 4000 cm^{-1} . Infrared spectroscopy is the most used spectroscopic technique. The features of an IR spectrum (number of infrared absorption bands, their intensities, and their shapes) are directly related to the molecular structure of a compound. The IR spectrum is a unique physical property of an individual compound; it is its molecular fingerprint [11]. The IR region comprises fundamental vibrations of bound atoms. Whenever such bound atoms vibrate, they absorb infrared energy, that is, they exhibit IR absorption bands. The term “group frequencies” describes the IR bands repeating themselves in molecules having the same functional groups of atoms and are visible in the same area on a spectrum (these vibrations are distinguishable while others are overlapped). These group frequencies can be divided into three types [12].

- 1) those showing a rather constant position regardless of their environment;
- 2) those changing according to their molecular environment in a somewhat predictable manner;
- 3) those having unpredictable positions or intensities.

The second type is very useful for gel investigations. Among them, the stretching vibrations involving the bond linking the atoms or groups of atoms are often strongly affected by non-covalent intermolecular interactions [13]. For example, for vegetable oil-based systems, asymmetric and symmetric stretching of the group $-\text{CH}_2-$ are quite visible and distinguishable (Fig. 2.1). In order to understand the vibration of the group, Hooke’s law can be used [14]. When vibrating, a group can be classically seen as a spring with elastic constant k holding together two masses m_1 and m_2 . The reduced mass μ of the system is defined as follows:

$$\mu = \frac{m_1 m_2}{m_1 + m_2} \quad (2.12)$$

And the resonance frequency of such system is given by

$$\nu = \frac{1}{2\pi} \sqrt{\frac{k}{\mu}} \quad (2.13)$$

When going back to the smaller scale, m_1 and m_2 becomes the atomic masses of the diatomic group (as an example, but considering μ it does not matter), and k becomes the stiffness of the covalent bond. A shift to lower frequencies could mean, according to eq. 2.13, either a lower k or a higher μ . But since the covalent bond cannot change, it is straightforward to think that the overall reduced mass μ is increased through the weak non-covalent interactions with the chemical environment. This has

already been reported, regarding to the decreasing of $-\text{CH}_2-$ stretching absorption peak frequency, as a decrease in chain fluidity [15] and it can be speculated that this may be a consequence of Van der Waals interactions holding the gel together.

2.3.3.2 NMR spectroscopy

Nuclear magnetic resonance takes place on the right-side of fig 2.3, at high wavenumbers in the radiofrequencies. The utility of NMR spectroscopy when dealing with gels lays in the fact that NMR data give information about the chemical nature the molecular or collective mobility of an observed component. The aspects to be considered are the analysis of the variation of chemical shifts, spin relaxation times, or intensity of the NMR signals along with concentration, solvent composition, or temperature. Those data can be used to gather information on the nature of the intermolecular interactions, the critical organogelator concentration values, the change in the motion of the molecules or thermodynamic parameters associated with the gel formation [16]. Nuclear Magnetic Resonance is based on the interaction between an external magnetic field and a nucleus that possesses spin $I \neq 0$ and spin angular momentum [17]. The angular momentum within a static external magnetic field allows magnetization of the nuclei. In Fourier transform NMR spectrometers a second magnetic field perpendicular to the previous one, which oscillates at the proper resonance radio frequency, is sent to the sample for short times (pulse). Predetermined combinations of pulses allow to obtain 1D and 2D spectra which gives information on chemical environment, abundance, connectivity through bonds and space proximity to considered nuclei.

Solid Fat Content (SFC) is generally accepted analysis of fats and oils in the food industry, and therefore is useful if the final gel product must substitute a traditional fat. The traditional extraction methods for SFC determination are slow, irreproducible and require additional chemicals. Direct measurements of SFC by NMR (nuclear magnetic resonance) provides quick and accurate determination of SFC value [18]. Solid Fat Content determination by NMR is based on direct ratio measuring between the solid and liquid parts of the sample. After excitation of the sample by powerful 90°RF pulse FID (Free Induction Decay) is detected. FID is the signal accompanies relaxation process of hydrogen proton magnetic spins back to equilibrium state after disturbing. FID contains contributions from both solid and liquid parts. The protons of liquid content are more rapid in comparison with protons of solid. It provides faster signal decay from solids than from liquids. Thus, these contributions can be distinguished [19].

References

- [1] F. R. Lupi, D. Gabriele, N. Baldino, P. Mijovic, O. I. Parisi, and F. Puoci, “Olive oil/policosanol organogels for nutraceutical and drug delivery purposes,” *Food Funct.*, vol. 4, no. 10, pp. 1512–1520, 2013.
- [2] J. A. L. da Silva, M. P. Gonçalves, and M. A. Rao, “Kinetics and thermal behaviour of the structure formation process in HMP/sucrose gelation,” *Int. J. Biol. Macromol.*, vol. 17, no. 1, pp. 25–32, Jan. 1995.
- [3] F. R. Lupi, V. Greco, N. Baldino, B. de Cindio, P. Fischer, and D. Gabriele, “The effects of intermolecular interactions on the physical properties of organogels in edible oils,” *J. Colloid Interface Sci.*, vol. 483, pp. 154–164, 2016.
- [4] N. Vlachos, Y. Skopelitis, M. Psaroudaki, V. Konstantinidou, A. Chatzilazarou, and E. Tegou, “Applications of Fourier transform-infrared spectroscopy to edible oils,” *Anal. Chim. Acta*, vol. 573–574, pp. 459–465, Jul. 2006.
- [5] C. H. Chen and E. M. Terentjev, “Aging and metastability of monoglycerides in hydrophobic solutions,” *Langmuir*, vol. 25, no. 12, pp. 6717–6724, Jun. 2009.
- [6] S. Sahoo *et al.*, “Organogels: Properties and applications in drug delivery,” *Des. Monomers Polym.*, vol. 14, no. 2, pp. 95–108, 2011.
- [7] M. T. K. Kubo, M. L. Rojas, A. C. Miano, and P. E. D. Augusto, “Chapter 1 Rheological Properties of Tomato Products,” *Food Chem. Funct. Anal.*, vol. 2019-January, no. 9, pp. 1–25, 2019.
- [8] D. Smith, “Molecular gels—nanostructured soft materials.” Wiley-VCH , pp. 111–153, 2008.
- [9] M. Perneti, K. F. van Malssen, E. Flöter, and A. Bot, “Structuring of edible oils by alternatives to crystalline fat,” *Curr. Opin. Colloid Interface Sci.*, vol. 12, no. 4–5, pp. 221–231, 2007.
- [10] S. Baier, “What is Full Spectrum Lighting? | Lumenistics,” 19-Mar-2012. [Online]. Available: <https://lumenistics.com/what-is-full-spectrum-lighting/>.
- [11] H. Booth, “R. M. Silverstein, G. C. Bassler and T. C. Morrill. Spectrometric identification of organic compounds. Wiley, Chichester, 1991, pp. x + 419, £50.25 (cloth), ISBN 0 471 63404

- 2,” *Magn. Reson. Chem.*, vol. 30, no. 4, pp. 364–364, Apr. 1992.
- [12] A. Lee Smith, “Are Group Frequencies Obsolete?:,” <http://dx.doi.org/10.1366/0003702874447392>, vol. 41, no. 7, pp. 1101–1105, Aug. 2016.
- [13] H. Bouas-Laurent and J. P. Desvergne, “Optical Spectroscopic Methods as Tools to Investigate Gel Structures,” *Mol. Gels Mater. with Self-Assembled Fibrillar Networks*, pp. 363–429, 2006.
- [14] B. H. Stuart, “Infrared Spectroscopy: Fundamentals and Applications,” *Infrared Spectrosc. Fundam. Appl.*, pp. 1–224, Jul. 2005.
- [15] M. Suzuki, Y. Nakajima, M. Yumoto, M. Kimura, H. Shirai, and K. Hanabusa, “Effects of Hydrogen Bonding and van der Waals Interactions on Organogelation Using Designed Low-Molecular-Weight Gelators and Gel Formation at Room Temperature,” *Langmuir*, vol. 19, no. 21, pp. 8622–8624, 2003.
- [16] Y. E. Shapiro, “Structure and dynamics of hydrogels and organogels: An NMR spectroscopy approach,” *Prog. Polym. Sci.*, vol. 36, no. 9, pp. 1184–1253, Sep. 2011.
- [17] K. Sridharan, “NMR Spectroscopy,” *Spectr. Methods Transit. Met. Complexes*, pp. 135–176, Jan. 2016.
- [18] K. Van Putte and J. Van Den Enden, “Fully automated determination of solid fat content by pulsed NMR,” *J. Am. Oil Chem. Soc.*, vol. 51, no. 7, pp. 316–320, 1974.
- [19] “SFC - NMR Testing Laboratory.” [Online]. Available: <https://www.process-nmr.com/sfc/>.

3. Results and Discussion

In this chapter obtained results will be reported. First, the behaviour of pure oil is shown. Then, for each oleogelator separately, results obtained with different techniques are shown. Later, comparisons between different oleogelators are highlighted. In the final section, results regarding the study of potentially edible emulsions based on R oleogels and an edible water-based system like fruit juice will be shown as well.

3.1 Rheological and spectroscopic analysis of Extra-Virgin Olive oil

The rheological time cure tests performed on the sample 'O' being cooled down from 85°C to 5°C using a cooling ramp of -1°C/min (Fig. 3.1) highlighted a liquid-like behaviour, with the phase angle δ being very close to the 90° throughout the whole temperature range examined. The increase in G^* is only due to the kinetic effect induced by temperature decrease. Lower temperatures must be reached for the oil to crystallise.

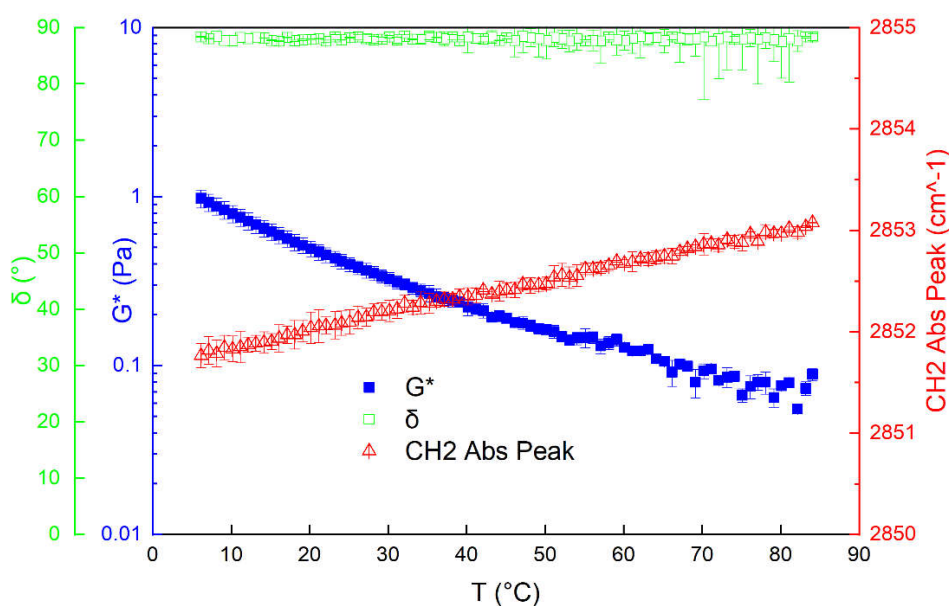


Fig 3.1: Time cure test for sample O, cooling rate -1°C/min

During the rheological measurement, simultaneously FT-IR spectra were acquired thanks to the Rheonaut tool. Only for sample O, the wavenumber absorption peak corresponding to the symmetric stretching of the -CH₂- group is reported instead of the parameter RWS (Relative Wavenumber Shift) because, as defined by eq. 2.3, the latter would be zero throughout the whole examined range of temperatures. The absolute value of the position (in terms of wavenumber) peak is compatible with

the characteristic peaks of vegetable oils, which is around 2854 cm^{-1} [1]. As the temperature is lowered, the peak shifts towards lower wavenumbers (or lower frequencies) which means a decrease in chain fluidity [2]. This happens in a linear fashion, which can be ascribed to the abovementioned kinetic effect. In similar way, SRTRT test using the shear rate 1 s^{-1} was performed on the sample O while cooling it down from 70°C to 10°C with a ramp of $-1^\circ\text{C}/\text{min}$. The results are reported in fig. 3.2, where viscosity (η) is plotted against Temperature. Again, the increase in viscosity is due to kinetic effects and no spontaneous crystallisation can be seen. The behaviour of the absorption peak is equivalent to the one seen on the time cure test.

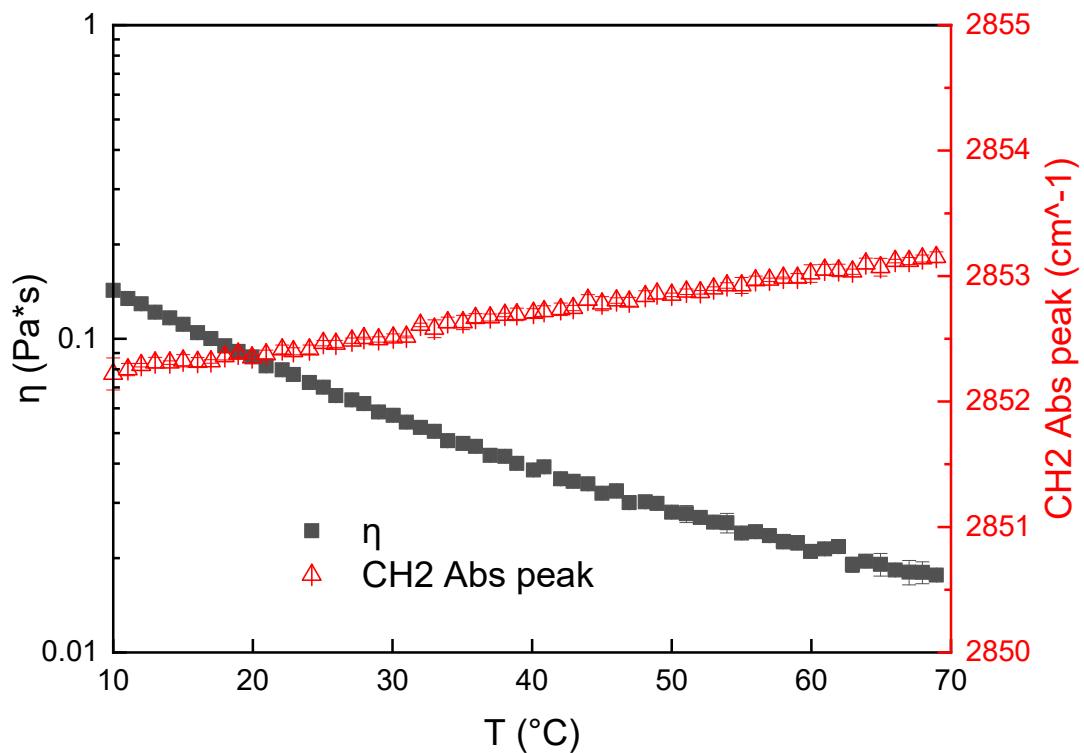


Fig 3.2: SRTRT test for sample O, cooling rate $-1^\circ\text{C}/\text{min}$

3.2 Rheological, thermal and spectroscopic analysis of oleogels

In this section, results regarding oil-oleogelator systems are shown. First, rheological data and infrared spectra are presented for the two different cooling rates $-1^\circ\text{C}/\text{min}$ and $-5^\circ\text{C}/\text{min}$; as for sample O, this has been done simultaneously since both IR spectra and rheological measurements were performed on the same sample at the same time thanks to the Rheonaut tool. Despite such results follow a similar pattern, they will be reported in different plots (one plot for each combination

substance/type of test/cooling rate) to appreciate what happens to the rheological and spectroscopic properties.

3.2.1 Myverol

Results regarding rheological, spectroscopic and thermal behaviour of sample OM1 will be reported.

3.2.1.1 Rheological and FTIR Analysis

Simultaneous rheological and spectroscopic results on OM1 sample are shown in Fig 3.3. At high temperatures, the binary system is melted in an isotropic phase, and the increase in G^* modulus upon cooling is only due to kinetic effects, recalling the behaviour described for sample O. Similarly, RWS is zero because the relative shifting of the examined peak is the same as the one exhibited by the oil.

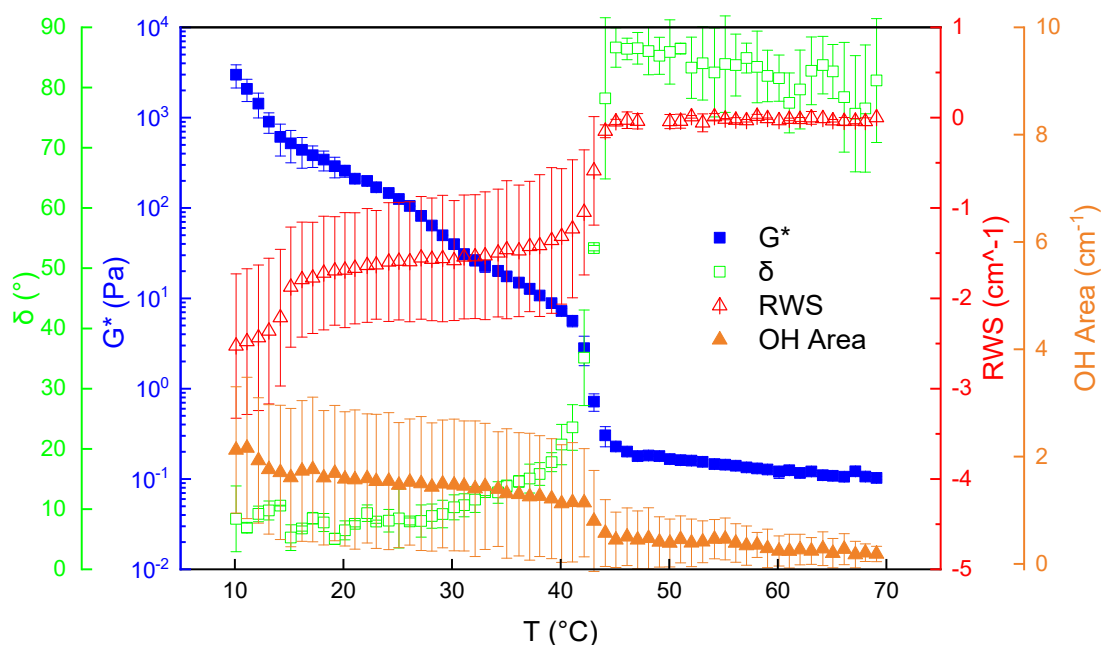


Fig 3.3: Time cure test and FTIR parameters for sample OM1, cooling rate $-1^{\circ}\text{C}/\text{min}$

This behaviour is observed in every examined spectrum plotted against T for all the samples studied. Similarly, OH area (which is measured in cm^{-1} because it comes from the integration of absorbance, which is dimensionless, over the wavenumber on the spectrum), can be considered as constant because it slightly grows within the error bars, which are wide owing to the experimental difficulties in repeating tests encountered for some samples, especially for infrared acquisitions. When the temperature reaches a critical value of crystal onset ($T=T_{\text{CO_OSC}}$) a sudden change both in complex modulus, which increases, and in phase angle, which decreases, is observed. This means that the system is starting to crystallise by forming small clusters. As temperature is further lowered,

interactions between aggregates take place, as can be seen from the subsequent sudden decrease in RWS, which is proportional to the decreasing of the absorption frequency of the $-CH_2-$ group symmetric stretching, meaning the chains are becoming less fluid because of the interacting with their chemical environment. This could be a way to measure van der Waals interactions [3]. It is interesting to acknowledge that the change in all monitored variables happens at the same temperature. This is also true for the OH area increase: despite its wide error bars, a slight step can be seen. The increase of OH Area means the formation of hydrogen bonds is taking place [3].

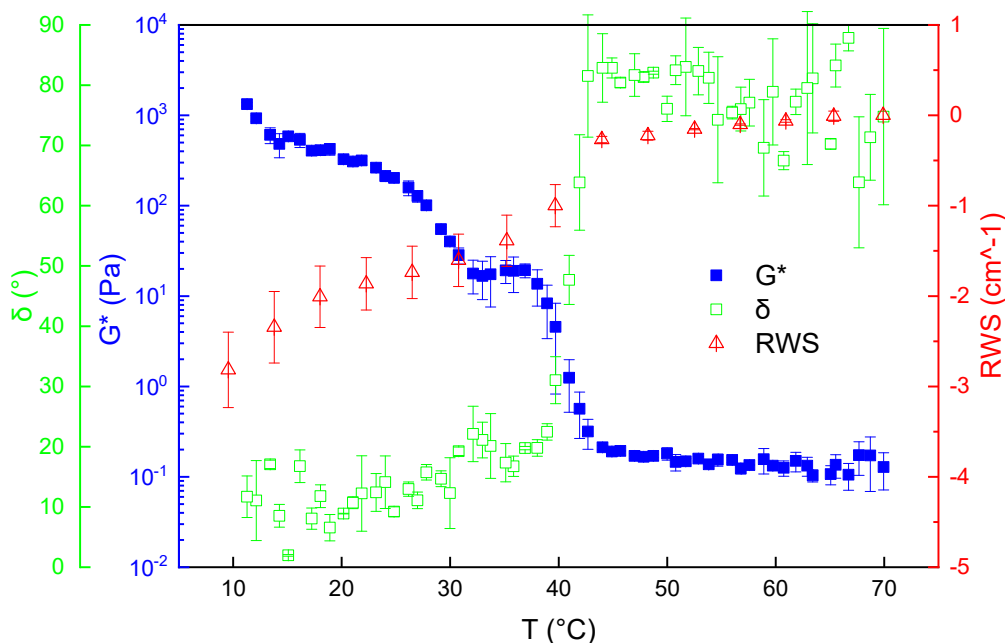


Fig 3.4: Time cure test and RWS for sample OM1, cooling rate $-5^{\circ}\text{C}/\text{min}$

As the temperature further decreases, the system becomes more structured as the clusters interact with each other to form a 3D network. When the phase angle reaches 45° , the system becomes a solid-like material, which means the gel is formed, and at lower temperatures the gel stiffness increases. A slight slope change of both G^* and RWS at around 15°C probably means that the system is facing a second transition [4]. The same test has been performed using a cooling rate of $-5^{\circ}\text{C}/\text{min}$, which is reported in fig. 3.4. The results are similar to the previous one. OH area is not reported since an increase was not appreciated. A sudden increase in G^* modulus is observed at around the same temperature of the slower cooling rate. A comparison between all results in terms of onset temperature and properties will be discussed later. RWS has a minor resolution because the time required for acquiring a single FTIR spectrum is around 1min, and in that time for that cooling ramp the temperature has decreased by 5°C . A small plateau can be seen between $40-30^{\circ}\text{C}$ in both G^* and δ . This could be a kinetic effect induced by the very fast cooling. Data regarding the phase angle δ are more scattered with respect to

the slower cooling rate because a constant low stress was used (0.01Pa) in order not to interfere too much with the crystallisation phenomena since the viscoelastic linearity range shifted very quickly. The small increase in G^* slope at low temperatures can be seen as well. SRTRT were also performed on the sample at both the cooling rates. Results are reported in fig. 3.5.

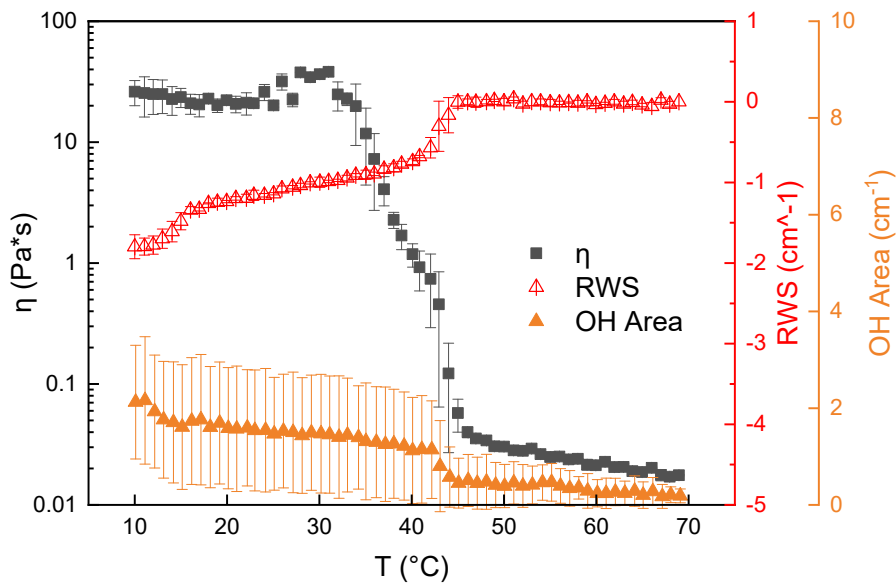


Fig 3.5: SRTRT and and FTIR parameters for sample OM1, cooling rate -1°C/min

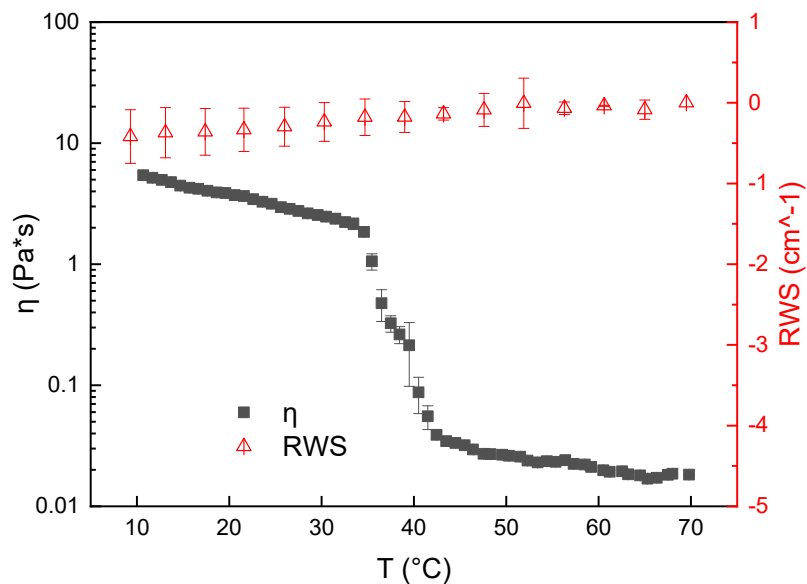


Fig 3.6: SRTRT and FTIR parameters for sample OM1, cooling rate -5°C/min

At high temperatures, the system behaves like sample O (fig 3.2) with viscosity increasing only because of kinetic effect. When $T=T_{CO_ROT}$ a sudden increase in viscosity and OH rea as well as a

sudden decrease in RWS is observed. Slope changes can be seen both in viscosity and in RWS. This is probably due to polymorphic transitions: as suggested by Lupi et al [4] crystallisation initially occurs in the α -crystalline polymorph, then it proceeds through α -crystals nucleation and their partial or complete polymorphic transition into β' crystals; final the formation and growth of crystalline aggregates leads to the final gel network structure. Increase in OH is small as well but was slightly appreciable. In all other measurement, it was not at all and therefore will not be reported again. Results of the same test executed at higher cooling rate is reported in figure 3.6. It is straightforward to note that a decrease in RWS is not appreciable, and yet the gelation is visible thanks to the exponential increase in viscosity. On the other hand, at the same cooling rate, a decrease in RWS in the oscillatory test was visible. This means that the type of test can influence the IR spectra. Viscosity also reaches a lower value with respect to the lower cooling rate.

3.2.1.2 DSC Analysis

Differential Scanning Calorimetry tests were performed on M, OM1 and OM2 samples at two different rates, $1^{\circ}\text{C}/\text{min}$ and $5^{\circ}\text{C}/\text{min}$. First by cooling, which is represented in the exothermic zone in the upper part of the plot (positive values), and then by heating, in the lower endothermic zone (negative values). Results for rate $1^{\circ}\text{C}/\text{min}$ showed in figure 3.7.

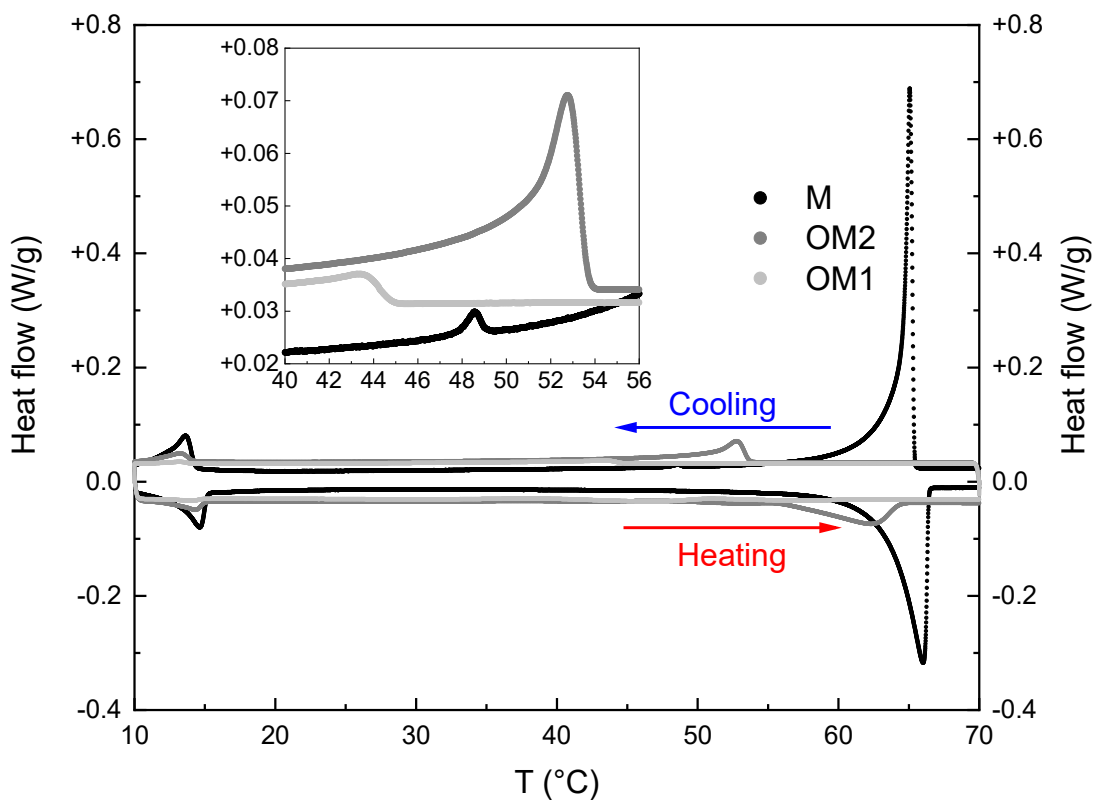


Fig 3.7: DSC thermogram, of myverol-based samples, rate $1^{\circ}\text{C}/\text{min}$ In the smaller plot, a portion of the cooling profile is magnified to highlight crystallisation of samples OM1 and OM2.

Cooling down sample M, two major exothermic peaks are highlighted, one at high T ($\sim 65^{\circ}\text{C}$) and the other at lower T ($\sim 14^{\circ}\text{C}$). The first one is responsible for the first crystallisation phenomena, and it can be seen at lower temperatures: the lower is the amount of gelator, the lower is the T_{co} [4]. The exothermic crystallisation peak is shifted to $\sim 53^{\circ}\text{C}$ for the sample OM2 (visible on the main plot) and $\sim 44^{\circ}\text{C}$ for the sample OM1 (visible on the smaller plot), which agrees with the qualitative behaviour seen in rheological tests performed on sample OM1. A small peak can be seen for sample M at 48°C on the cooling curve in the magnified portion of the thermogram. This is probably a small phase transition and is not visible on samples OM1 and OM2. At $\sim 14^{\circ}\text{C}$ the small peak recalls the change in slope seen on the rheological tests, due to a crystal polymorph. Similarly, the melting profile suggests the disruption of the polymorphic crystalline form at low temperatures and of the gel structure at higher temperatures. The same test was conducted at higher rate. Results are shown in fig. 3.8. Results quite similar to the slower cool cooling rates, except for the fact that heat flow values are higher. That is because in order for the structure to change, the same energy quantity is required, but since it is done in small amounts of time the power involved is higher.

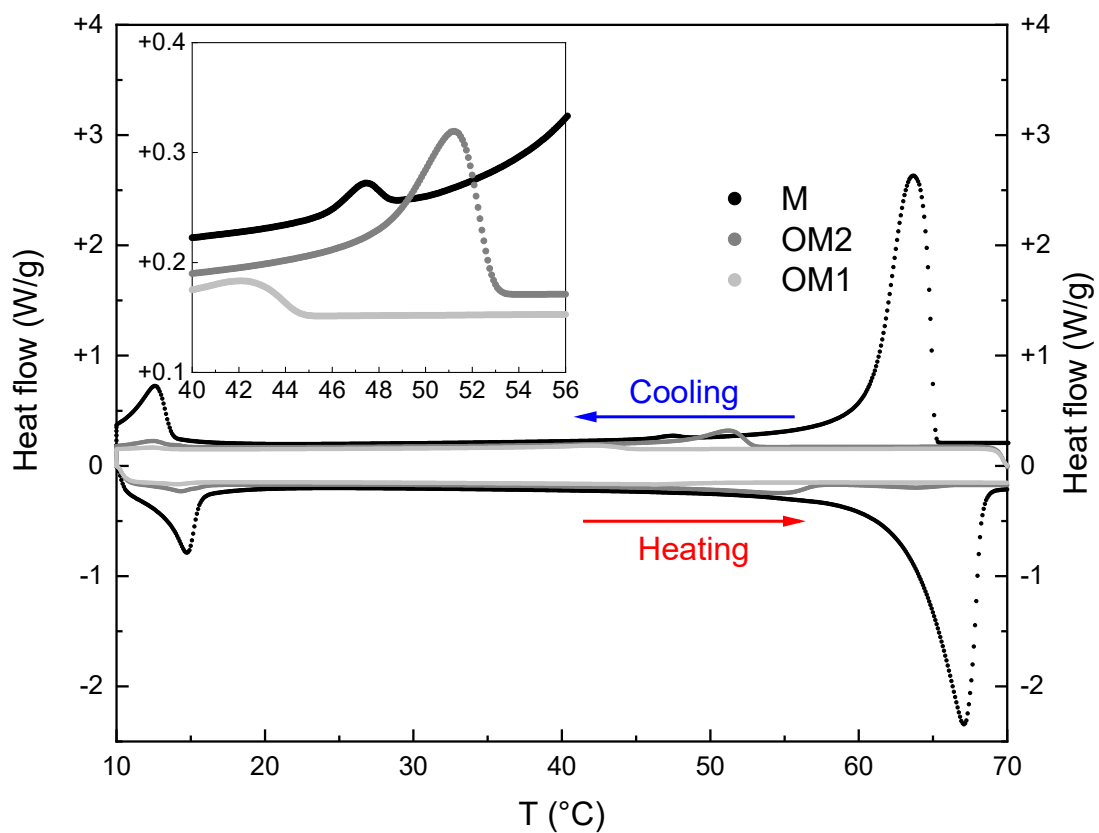


Fig 3.8: DSC thermogram, of myverol-based samples, rate $5^{\circ}\text{C}/\text{min}$. In the smaller plot, a portion of the cooling profile of the three samples is magnified to highlight crystallisation of samples OM1 and OM2.

3.2.1.3 SFC

SFC was collected for samples OM1 and OM2. Unfortunately, it was very difficult to control temperature upon time, a ramp of $\sim 0.5^\circ\text{C}/\text{min}$ was obtained. Results are shown in fig. 3.9.

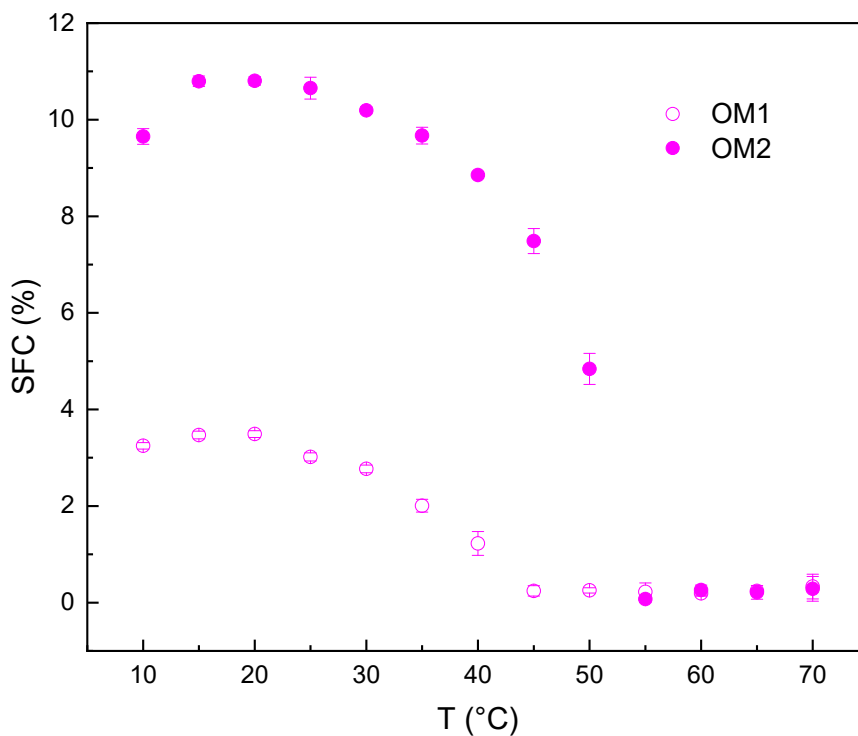


Fig 3.9: SFC of samples OM1 and OM2

It is interesting to note that, as temperature is lowered, SFC for both samples is very close to their mass fractions. The onset of crystallisation, which is the point corresponding to a sudden slope change, is clearly visible and coherent with the previous results.

3.2.2 Policosanol

3.2.2.1 Rheological and FTIR Analysis

Fig. 3.10 and 3.11 show oscillatory test and SRTRT, respectively. The first thing to note, with respect to equivalent OM1 sample, is that RWS does not change. This also happens for the faster cooling rate, as it will be seen. Despite that, change in G^* and η is sudden when the temperature reaches the crystal onset threshold. Lupi et al [5] found that policosanol-based oleogels were held together both by Hydrogen bonding and van der Waals interactions, but those spectra were acquired during static measurements at room temperature. Hence, it could be that imposed flow for such system hinders the

reflection of the light beam. Further and problem-oriented measurements should be done in order to explain this issue.

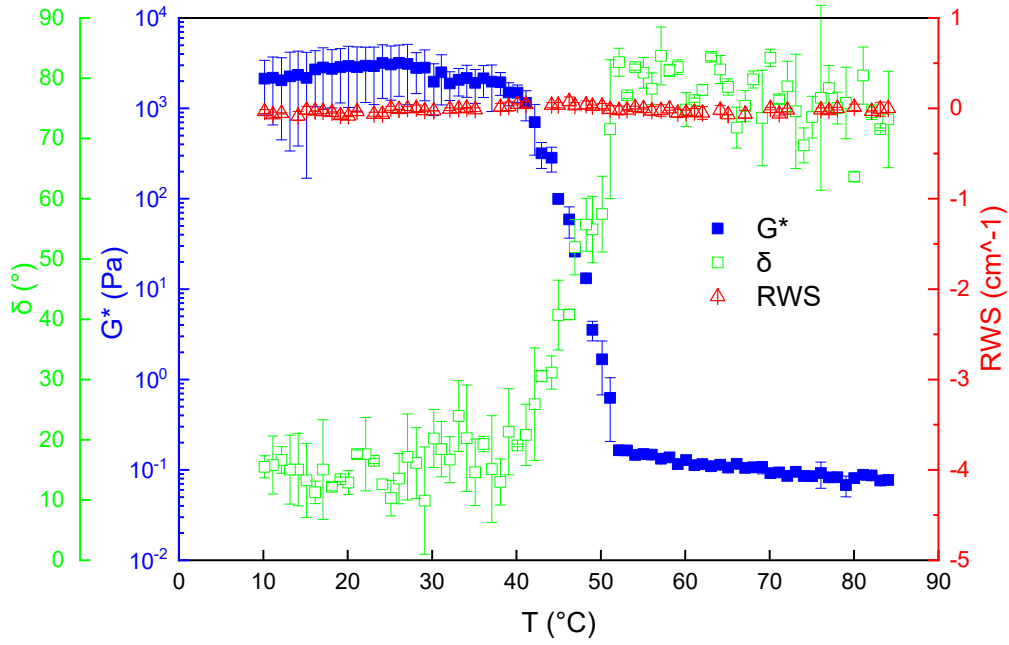


Fig 3.10: Time cure test and RWS for sample OP1, cooling rate $-1^\circ\text{C}/\text{min}$

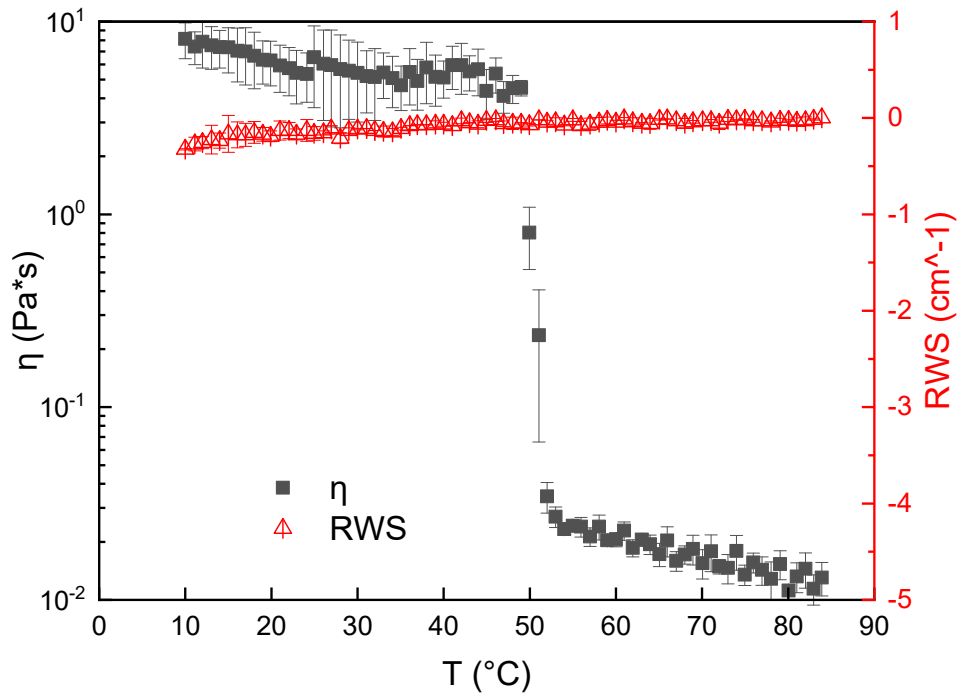


Fig 3.11: SRTRT and and RWS for sample OP1, cooling rate $-1^\circ\text{C}/\text{min}$

Fig. 3.12 and 3.13 show the same test on the same sample performed at a higher cooling rate. Results are similar: no significant decrease of RWS throughout the whole examined range and a sudden increase of G^* and δ .

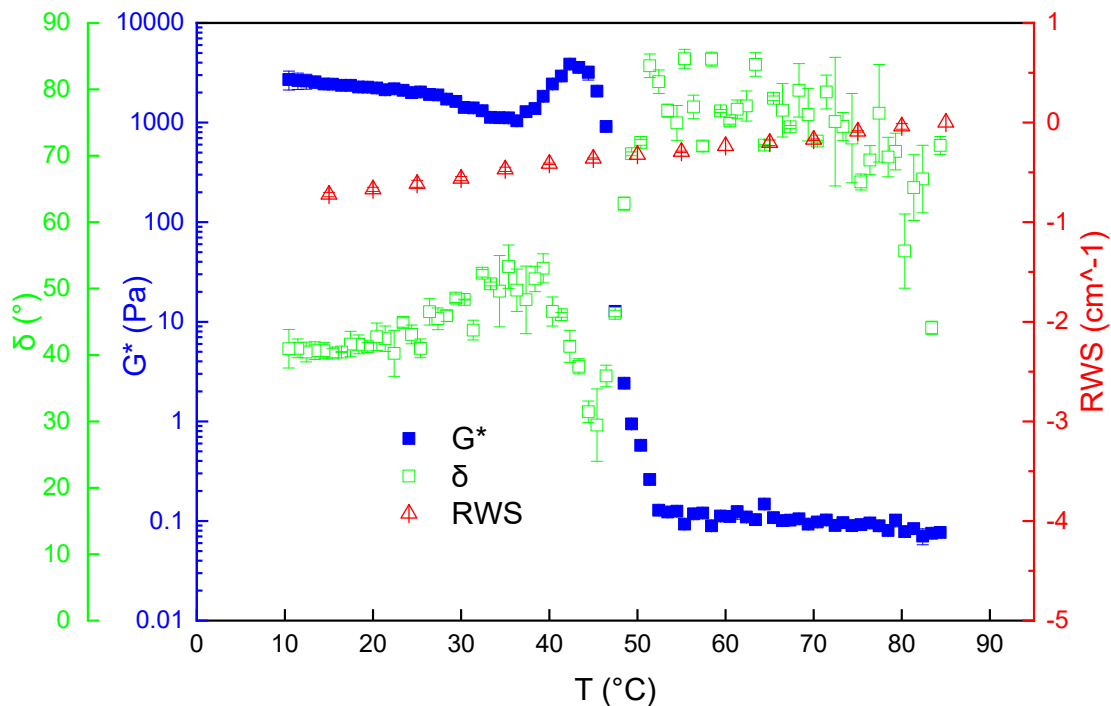


Fig 3.12: Time cure test and RWS for sample OP1, cooling rate $-5^{\circ}\text{C}/\text{min}$

The scattered trend of δ is due, again, to the choice of a lower stress that fits better the viscoelasticity region without changing it within small amounts of time in a situation where temperature is already changing abruptly. This also led to a peak in G^* , which, for such a system that increases its strength when temperature is lowered, is questionable and could be investigated further. In fact, final values of G^* appear higher for $-1^{\circ}\text{C}/\text{min}$ ramp; at the same time, SRTRT during faster cooling, as shown in fig. 3.12 seems to be similar to slower cooling, although the latter leads to slightly higher final viscosity values. Therefore, it can be stated that such data show that a faster cooling rate hinders the formation of the 3D network, although the crystal onset temperature does not seem to be affected by it.

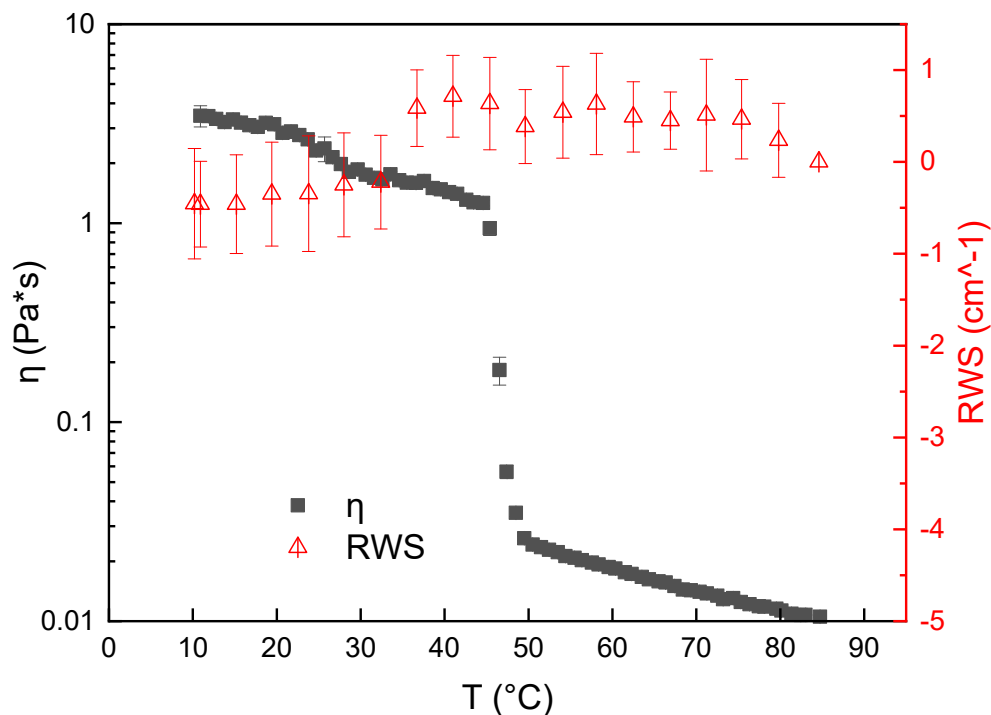


Fig 3.13: SRTRT and FTIR parameters for sample OP1, cooling rate $-5^{\circ}\text{C}/\text{min}$

3.2.2.2 DSC Analysis

DSC tests executed on policosanol-based samples are reported in fig. 3.14. Unlike the DSC tests performed on myverol-based samples, normalisation with respect to sample weight was not carried for the sake of a better reading of the plot. Results on cooling rate of $-1^{\circ}\text{C}/\text{min}$ are showed only. The relatively thin and strong crystallisation peak of P sample can be expected from a compound which is composed by a low variety of molecules: policosanol is a fatty alcohol mainly composed by n-octacosanol ($\sim 60\%$) and its crystallisation peak $\sim 80^{\circ}\text{C}$ is responsible for the crystallisation of OP2 at $\sim 60^{\circ}\text{C}$ and OP1 at $\sim 50^{\circ}\text{C}$. This is coherent with the rheological data that showed for both oscillatory and steady tests the T_{co} being similar to that value. It is also remarkable that, while the melting profile of P is almost symmetrical with respect to the cooling one, the melting peaks of samples OP1 and OP2 are broader than the crystallisation peaks.

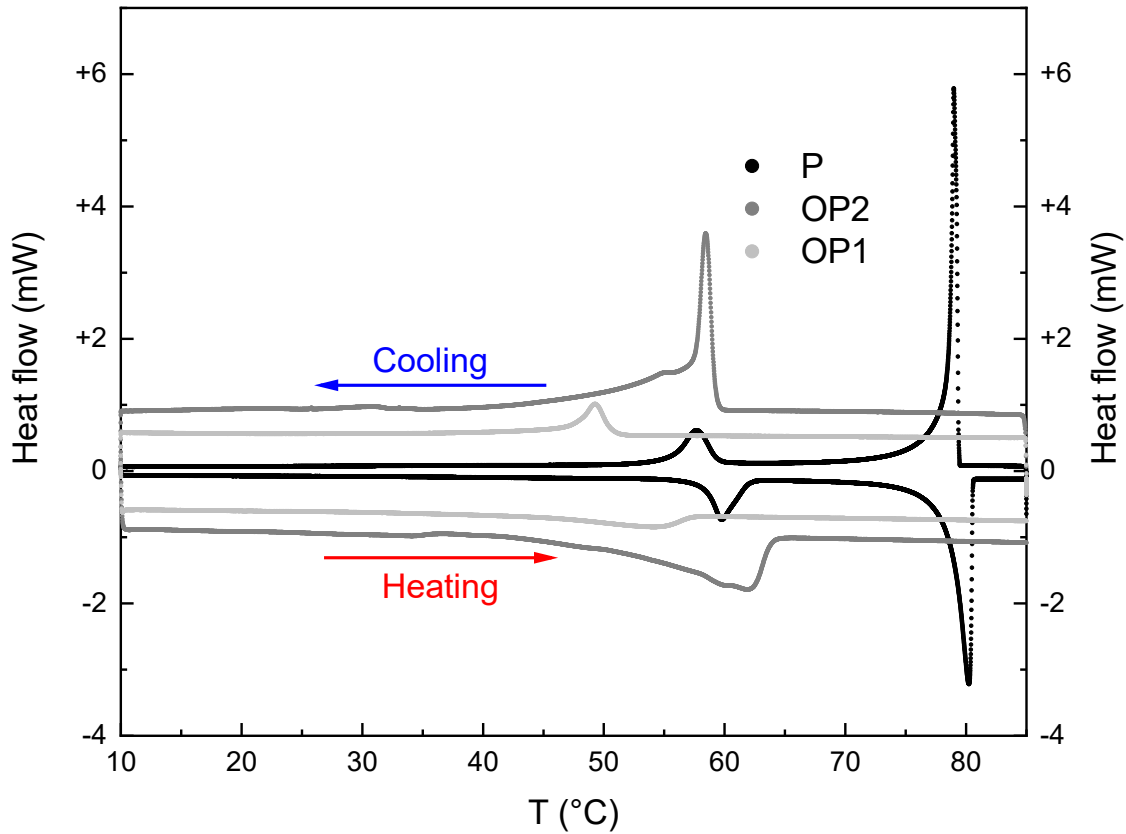


Fig 3.14: DSC thermogram, of Policosanol-based samples, rate 1°C/min

3.2.1.3 SFC

Solid fat content data for systems OP1 and OP2 are showed in fig. 3.15.

The interesting fact to note is that at the lower temperature values, SFC for OP1 is closer to 3.4%, which is the mass fraction of Policosanol in sample OP1, than SFC for OP2 is to 10%, which is the mass fraction of policosanol in sample OP2. that P2. Since SFC gives an insight on the crystallinity of the system, it could be speculated that, with due proportion, policosanol is a more efficient gelator at lower concentrations. An abrupt increase corresponding to the crystal onset is clearly visible, even though, while the one for OP2 is consistent with DSC measurement, the one for OP1 seems to start almost at the same time of OP2 and therefore way before the T_{co} seen during rheological and thermal tests. The smaller peak which is both visible on cooling ($\sim 57^{\circ}\text{C}$) and heating ($\sim 60^{\circ}\text{C}$) curves of P probably refers to the enthalpy change occurring during a polymorphic transition and it cannot be seen on samples OP1 and OP2.

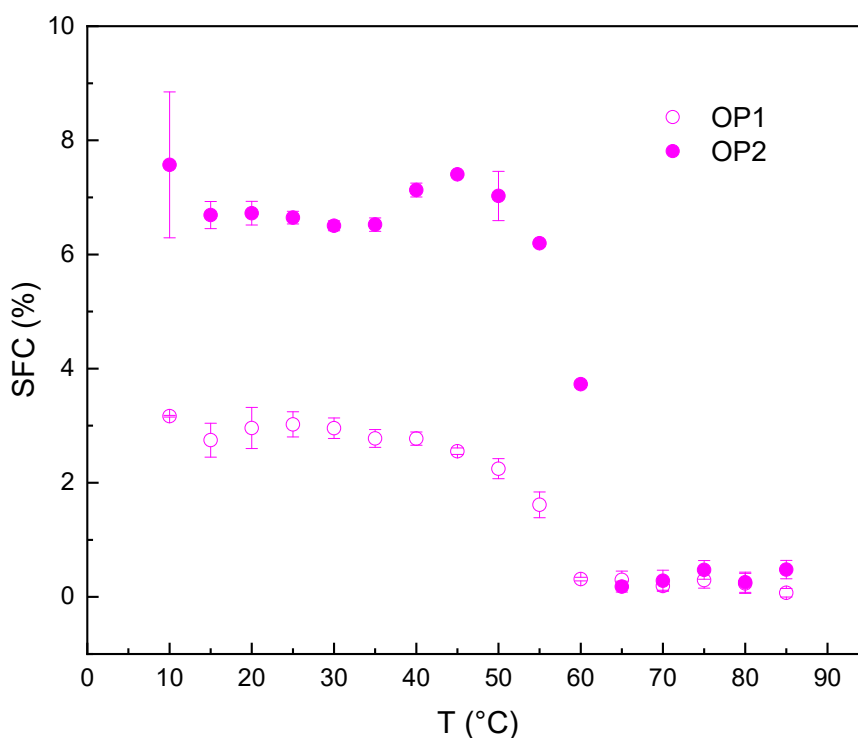


Fig 3.15: SFC of samples OP1 and OP2

3.2.3 Carnauba wax

3.2.3.1 Rheological and FTIR Analysis

Rheological data for sample OC1 at a cooling ramp of $-1^{\circ}\text{C}/\text{min}$ are reported in figures 3.16 and 3.17. It is worth noting that there is a difference in the gelling ability of the two samples: while according to the SAOT results (fig 3.16) the crystallisation happens in a smooth way, in SRTTRT (fig 3.17) it happens abruptly. Furthermore, for oscillatory tests crystallisation phenomenon begins at temperatures higher than steady state tests. This is confirmed by RWS decreasing in both tests, even if it reaches the same final value. A step in phase angle δ at high temperatures in fig. 3.16 is due to a stress change to maintain the linear viscoelasticity. The same issue did not affect G^* . From the same measurement, it can be seen that there is a very strong transition indicating the gel formation after a smooth crystallisation, as shown by the high G^* and low δ values. On the other hand, for the SRTTRT, despite the sudden increase of viscosity, its final value seems to be modest with respect to the one of other oleogels (OP1 and OM1) studied at the same conditions. Once again, steady shear seems to hinder the formation of the gel structure.

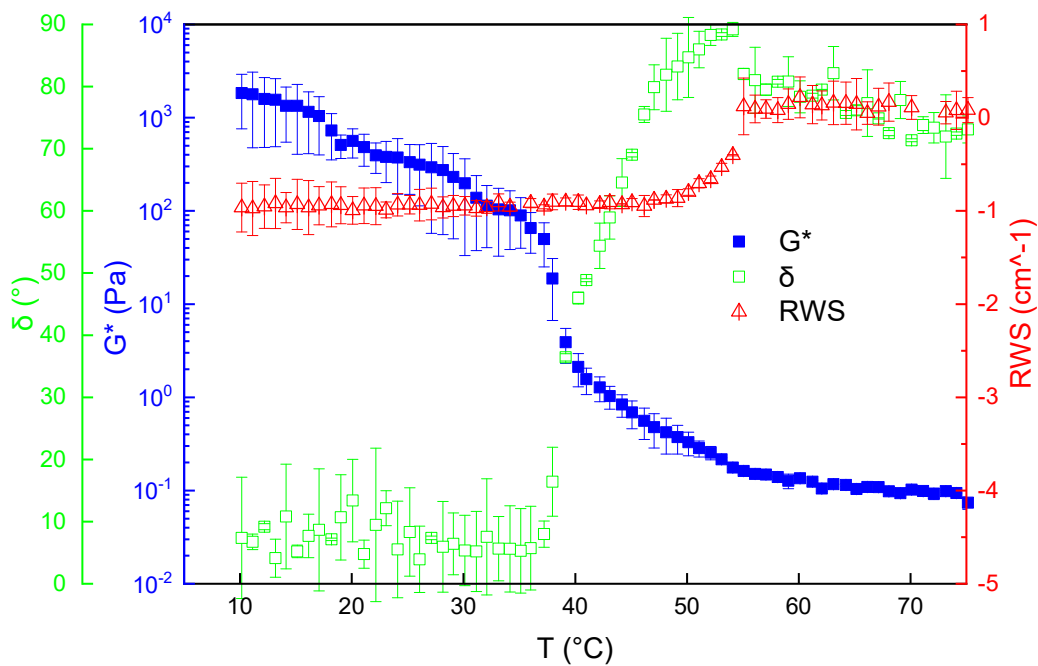


Fig 3.16: Time cure test and RWS for sample OC1, cooling rate $-1^{\circ}\text{C}/\text{min}$

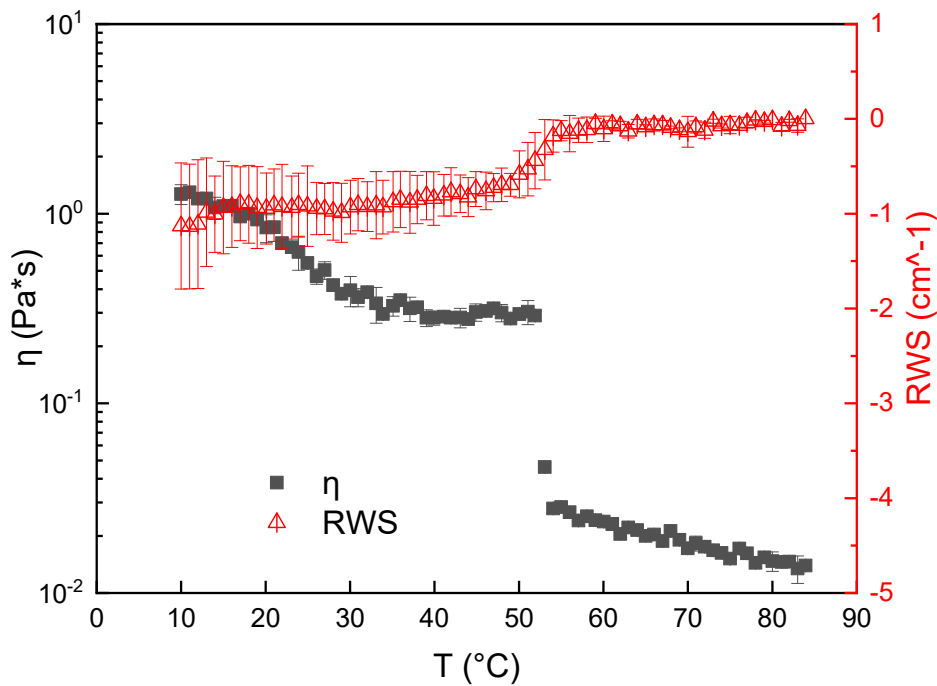


Fig 3.17: SRTRT and RWS for sample OC1, cooling rate $-1^{\circ}\text{C}/\text{min}$

Figures 3.18 and 3.19 show the behaviour of the same sample with the higher cooling rate $-5^{\circ}\text{C}/\text{min}$. The behaviour of the system when tested with the faster cooling rate during oscillatory measurements is quite different with respect to the slower $-1^{\circ}\text{C}/\text{min}$ cooling rate (fig 3.18). In SAOTs, crystallisation

seems slightly hindered by the higher cooling ramp although the final G^* is similar. Also, despite the wide error bars, a lower RWS is observed but this does not seem to significantly affect the gel formation with respect to the slower cooling ramp.

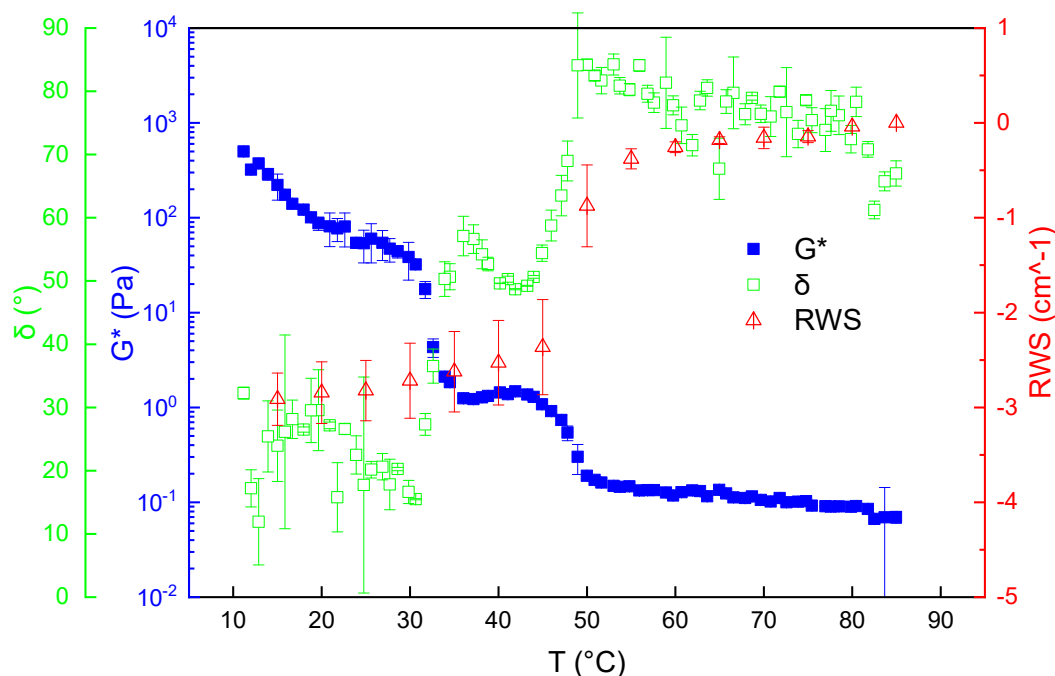


Fig 3.18: Time cure test and RWS for sample OC1, cooling rate $-5^{\circ}\text{C}/\text{min}$

On the other hand, RWS on SRTRT also shows a significant decrease, and this lead to an higher viscosity of the system (~ 1 order of magnitude). Therefore, for sample OC1, higher cooling ramp lowers the T_{co} for SAOTs, increases final viscosity in SRTRTs and decreases RWS for both the performed tests. It has to be bared in mind that carnauba wax is a very heterogeneous system due to the wide number of different compounds at different concentrations (Fig. 1.3), therefore different components may react in different ways and at a different extent leading to apparently contradictory results.

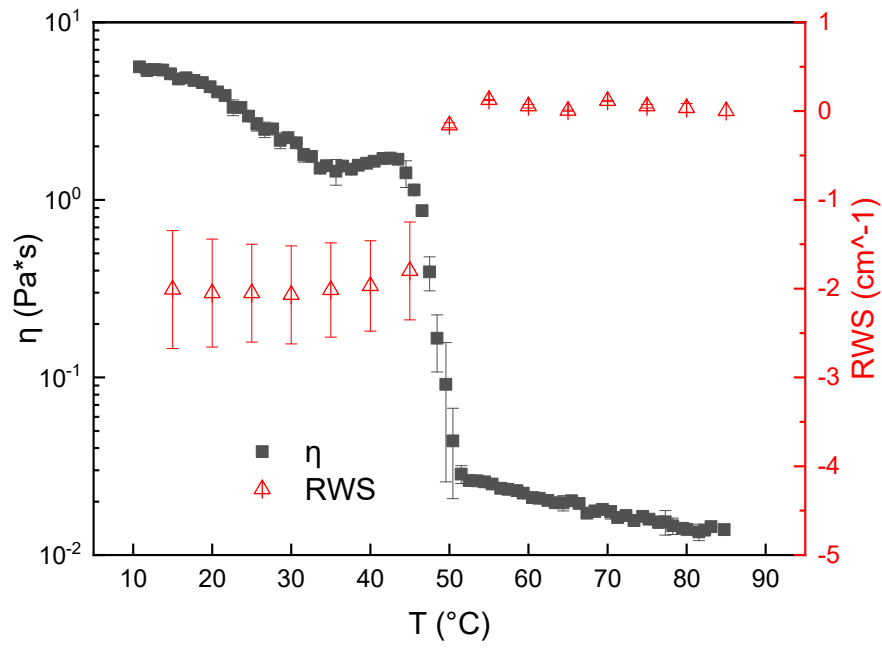


Fig 3.19: SRTRT and RWS for sample OC1, cooling rate $-5^\circ\text{C}/\text{min}$

3.2.3.2 DSC Analysis

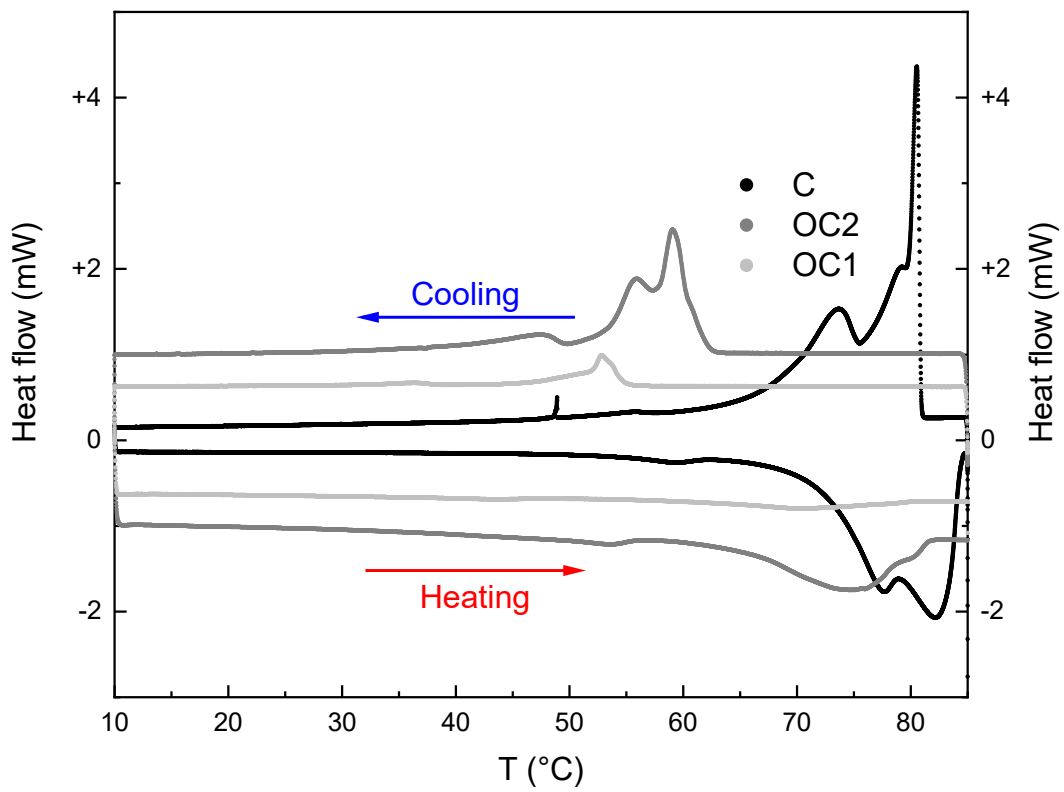


Fig 3.20: DSC thermogram of Carnauba-based samples, rate $1^\circ\text{C}/\text{min}$

DSC thermogram of Carnauba –based samples depicted in fig 3.20 shows that crystallisation of sample C starts suddenly, like policosanol, but it is not a single peak and is also very broad. This is because of the high degree of heterogeneity of components of the system and typical for waxes [6], as will be later seen. It is also worthy to note that the OC1 crystallisation peak is similar, although of course shifted toward lower temperatures and to a smaller and a broader extent, to the crystallisation peak of sample OC2 while for C is much smaller and characterised by a single peak. Furthermore, OC1 peak, which is around 55°C, is coherent with both the rheological tests performed at the same cooling rate; it can be concluded that the crystallisation onset of OC1 is hindered by a higher cooling rate. 3.2.3.3 SFC

Solid fat content of samples OC1 and OC2 is reported in fig. 3.21. The final values at low temperatures are very close to the respective % of mass fraction, which means that Carnauba wax maintain a certain degree of crystallinity in the gelled system. Both the samples seem to reach a SFC plateau below 40°C, and for OC1 this is consistent with the fact that the structuring degree of the system is already reached at that T, given by the fact that δ is very low and constant after that temperature value in the SAOTs (fig. 3.16).

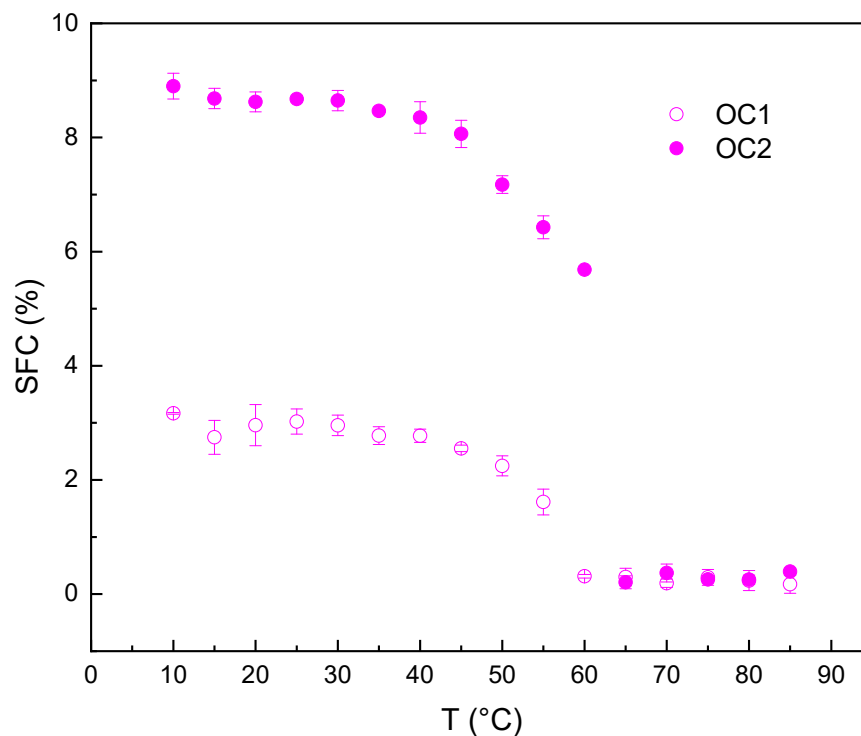


Fig 3.21: SFC of samples OC1 and OC2

3.2.4 Beeswax

3.2.4.1 Rheological and FTIR Analysis

Results on sample OB1 reporting the oscillatory time cure test are shown in figure 3.22.

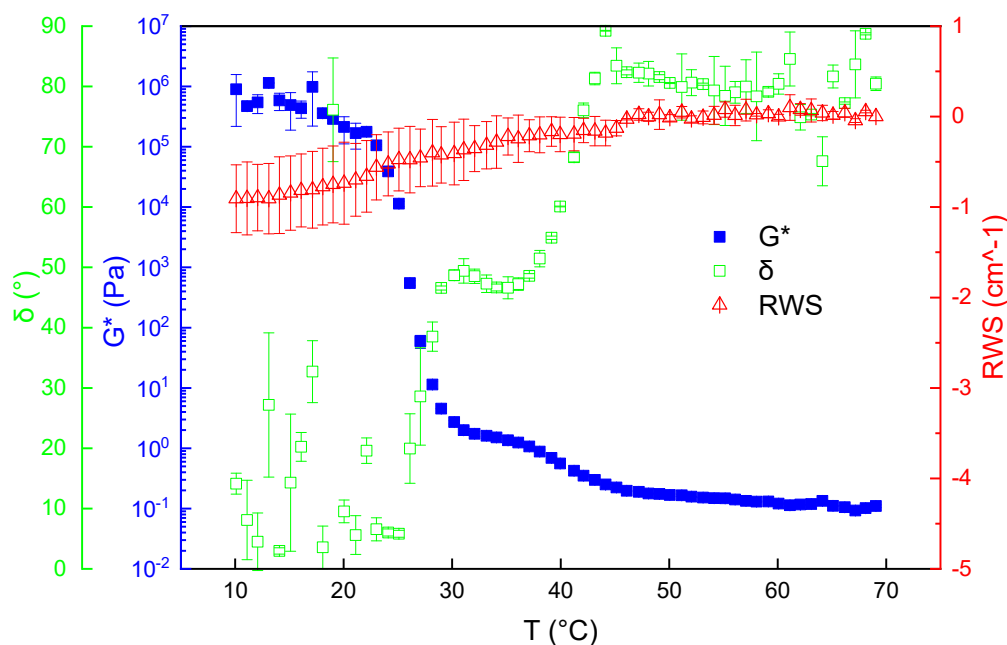


Fig 3.22: Time cure test and RWS for sample OB1, cooling rate $-1^{\circ}\text{C}/\text{min}$

OB1 sample in oscillatory regime has a lower crystal onset temperature with respect to the previous tested substances. That is clearly visible when looking at δ rather than G^* , even though a change in the slope of G^* is also noticeable. Once the system has reached 30°C , the complex modulus grows exponentially and the phase angle reaches zero within few degrees. Even if the scatter on phase angle is evident, the stress sweep tests performed at low temperature, which are necessary in order to find the linear viscoelasticity region, confirm that the system is very structured, and, so far, it is the strongest one at low temperatures. Despite that, the RWS decrease is quite modest (at worst, it reaches the value of -1, which is about the highest kinetic shift of pure oil within the whole temperature range, see fig 3.1). The behaviour of the same sample in steady shear conditions is reported in fig. 3.23. Viscosity initially grows after temperature goes below 50°C ; later an initial exponential growth seems to take place, then it stops and goes on again, until the viscosity reaches a maximum. It can be noted that, in both cases, a triple change in slope is visible, between 50°C and 25°C . RWS decrease is low for SRTTRT as well.

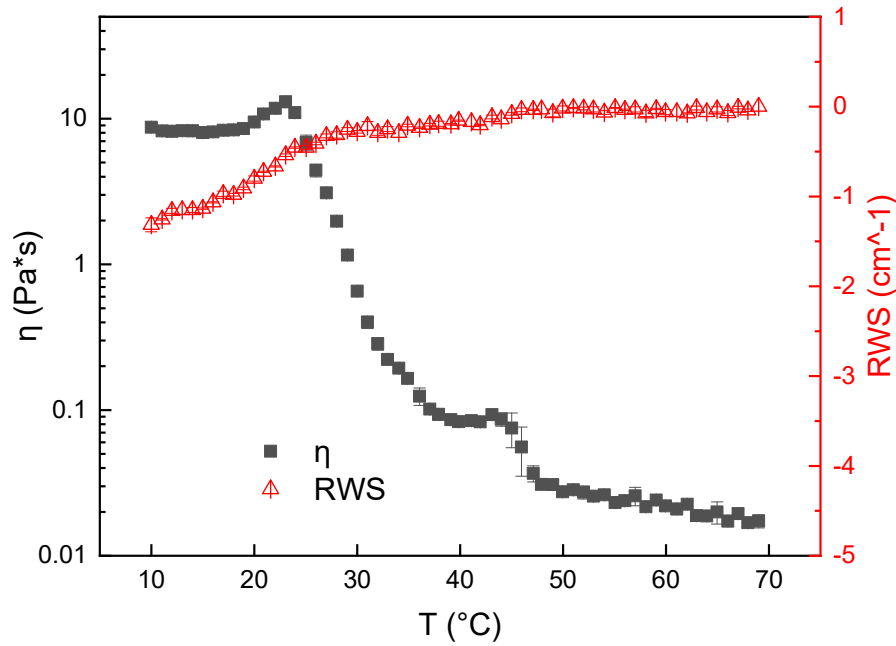


Fig 3.23: SRTRT and RWS for sample OB1, cooling rate -1°C/min

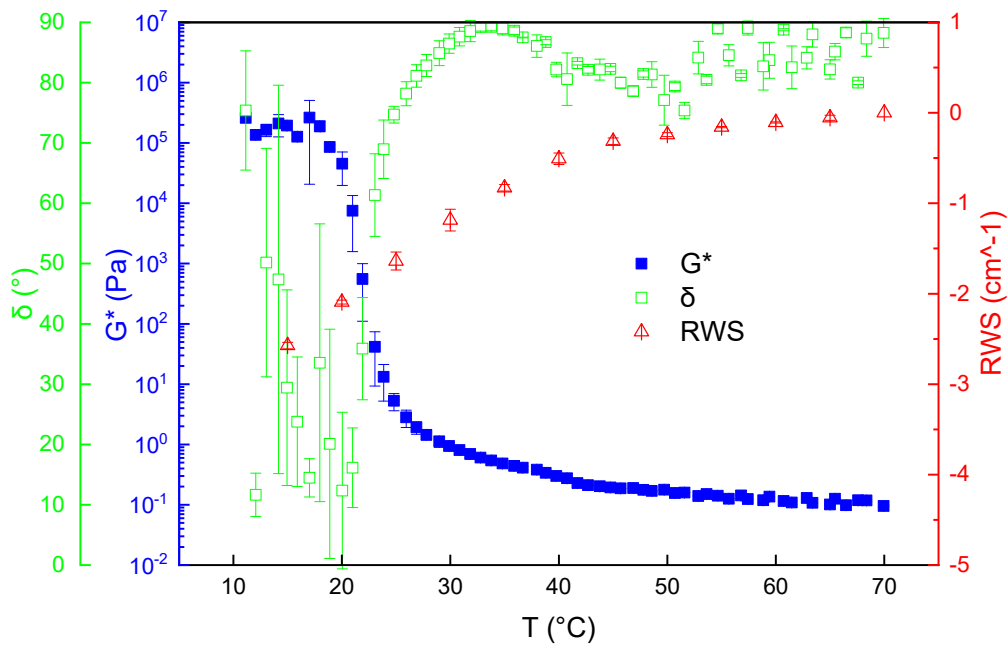


Fig 3.24: Time cure test and RWS for sample OB1, cooling rate -5°C/min

Results of the SAOT performed on sample OB1 at -5°C/min are showed in fig. 3.24. G^* seems to only grow because of kinetic effects, and simultaneously δ assumes values close to 90°, like sample O (fig. 3.1) up to about 30°C. When temperature reaches 30°C crystallisation occurs with a simultaneous decrease in δ and increase in G^* , with the latter reaching the value of the OB1 sample at a lower cooling rate. RWS parameter decreases from 0 to below -2 at low temperatures, indicating

the occurrence of a huge peak shift, which, as discussed did not happen in the previous oscillatory test examined. Results for SRTRT at the cooling rate -5°C min are depicted in fig. 3.25.

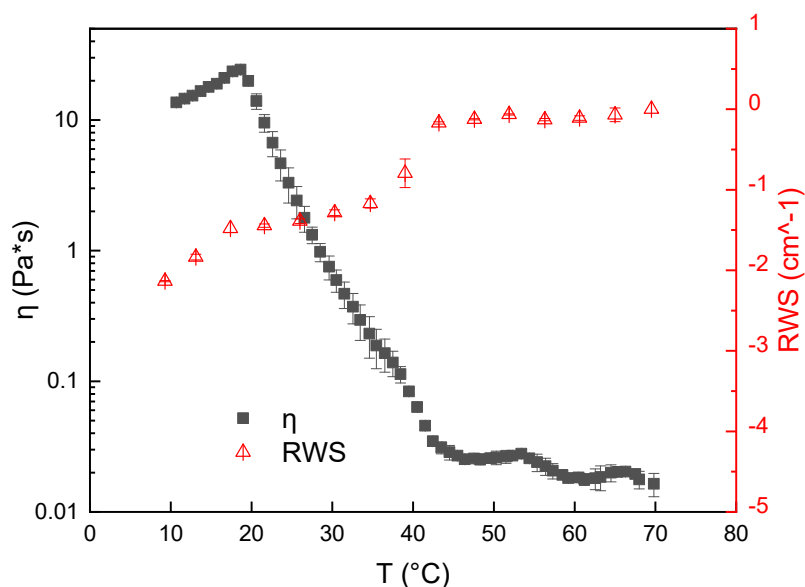


Fig 3.25: Time cure test and RWS for sample OB1, cooling rate -5°C/min

The temperature at which RWS decreases is similar to the temperature at which η increases abruptly; in the end, RWS seems to change its slope but the data are too spaced to speculate the existence of some polymorphic transformation as happened for sample OM1 (slope change of G^* and RWS at low temperature in fig. 3.3, confirmed by DSC test carried on that same sample). It can be highlighted that, at the respective cooling rates, T_{co} is higher in shear measurements than in oscillatory measurements. This could mean that, for this sample, shear flow promotes crystal aggregation while oscillation hinders it.

3.2.4.2 DSC Analysis

DSC thermogram for sample OB1 is reported in fig. 3.26. It reveals a very broad peak of crystallisation, which reflects the heterogeneity of beeswax and, more in general, of waxes. By looking at the cooling and melting profile of OB1 it is interesting to note that, despite beeswax-related gels exhibit important solid-like properties, which are desirable for a gel, this only happens at low temperatures and it is easy to form and also easy to melt: once formed, in fact, at room temperature it experiences transition toward molten state and this is not desirable especially for edible product.

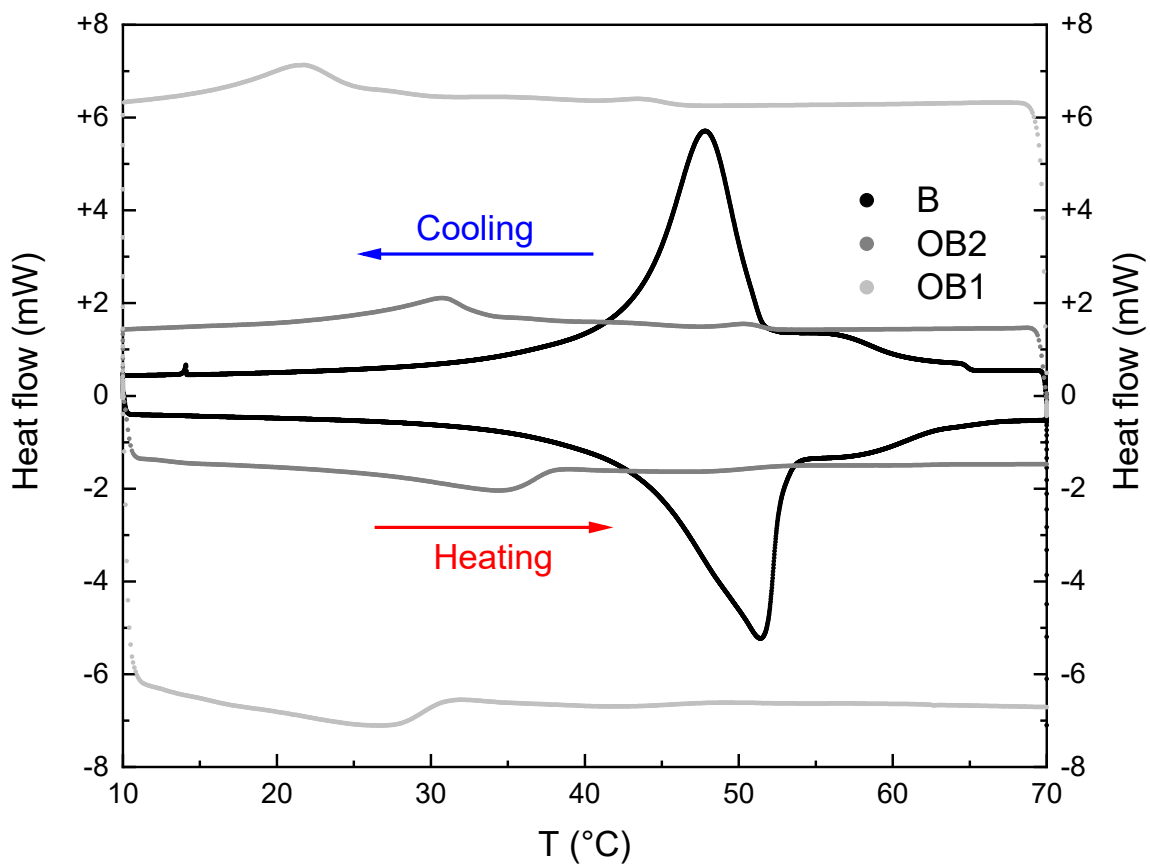


Fig 3.26: SRTRT and RWS for sample OB1, cooling rate $-1^{\circ}\text{C}/\text{min}$

3.2.4.3 SFC

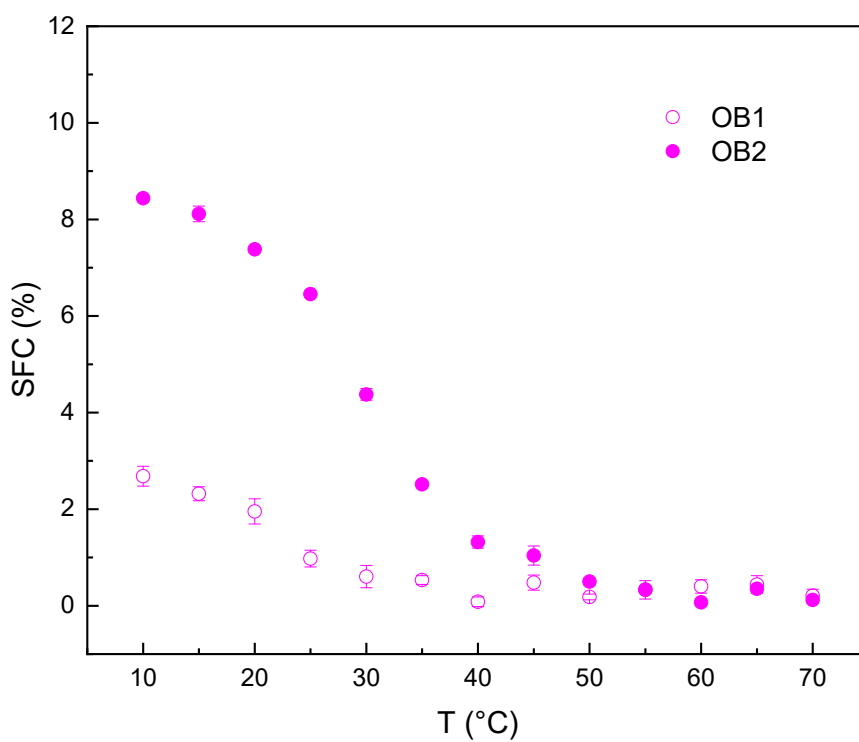


Fig 3.27: SFC of samples OB1 and OB2

Results of SFC for OB1 and OB2 are reported in fig. 3.27. Unlike other gelators at the same concentration, as the temperature is lowered the SFC for sample OB1 does not increase abruptly; although its final value increases almost until reaching its mass fraction, other gelators approach that value at the end of a plateau, which is consistent with the fact that above room temperature gel network in beeswax is not formed yet, as can be seen from rheological measurements.

3.2.5 Manuka Beeswax

3.2.5.1 Rheological and FTIR Analysis

Fig. 3.28 shows Time cure results on sample OU1 performed at the cooling rate $-1^{\circ}\text{C}/\text{min}$. The behaviour of rheological properties is typical of a oleogel system, with low G^* and high δ values until, at a critical T_{co} temperature, G^* begins to grow exponentially and δ assumes low values.

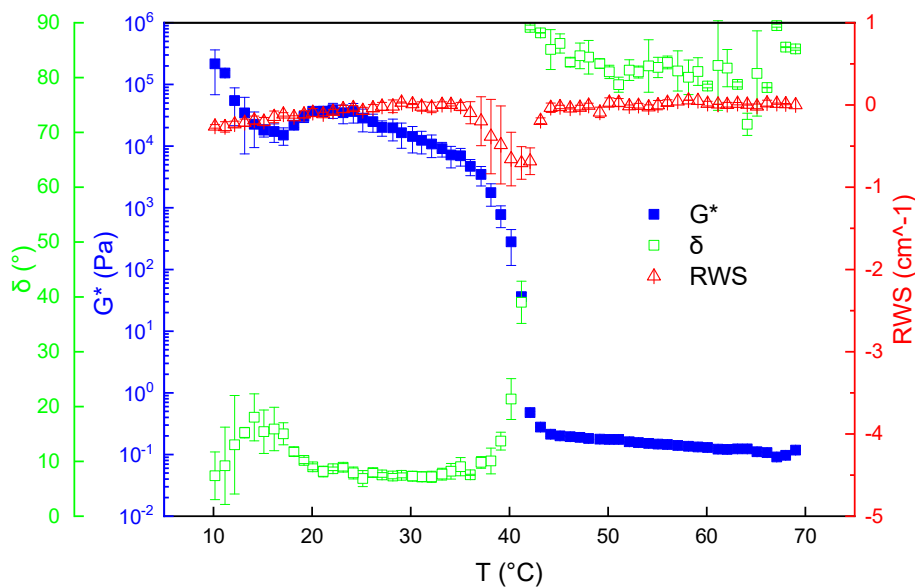


Fig 3.28: Time cure test and RWS for sample OU1, cooling rate $-1^{\circ}\text{C}/\text{min}$

RWS at first decreases in correspondence of the T_{co} , therefore a shift of the CH_2 absorption peak occurs, but then it returns to low values, meaning the peak re-shifts towards higher wavenumbers as the temperature decreases and the formation of the gel is ongoing, which is unexpected. Fig. 3.29 shows SRTRT measurement executed on sample OU1 at the cooling rate $-1^{\circ}\text{C}/\text{min}$. In the opposite way of what the time cure test on the same sample showed, beside a strong viscosity increase at the T_{co} , RWS decreasing in correspondence with the T_{co} is very clear despite the large error bars.

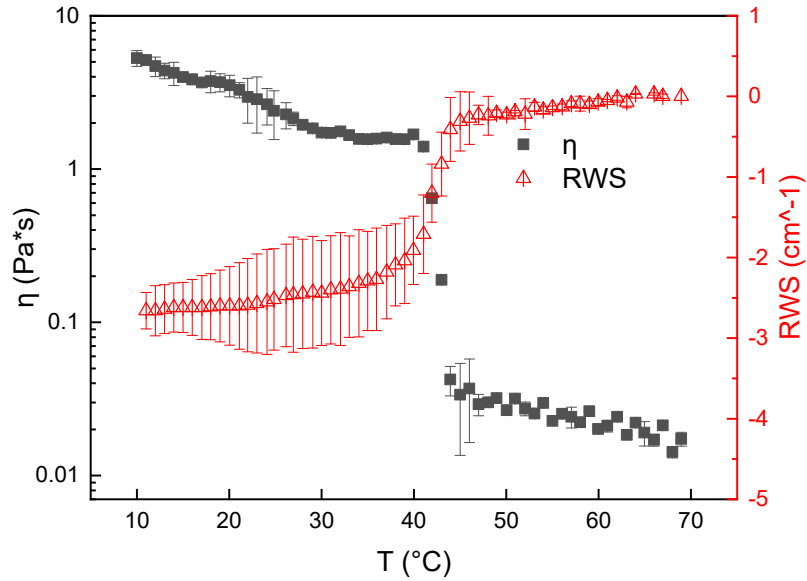


Fig 3.29: SRTRT and RWS for sample OU1, cooling rate -1°C/min

In fig 3.30 the Time cure for sample OU1 at cooling rate -5°C/min is reported. All of the examined properties suddenly change at T_{co} . A third slope change is visible for G^* , which corresponds to a faster decrease of δ . The RWS change in the SRTRT at the same cooling rate as shown in fig. 3.31 is clearly visible and similar to the one present in the previous measurement. Oscillatory time cure test at -1°C/min cooling rate was the only measurement which did not lead to a wavenumber shift, despite a very good structuring degree can be seen.

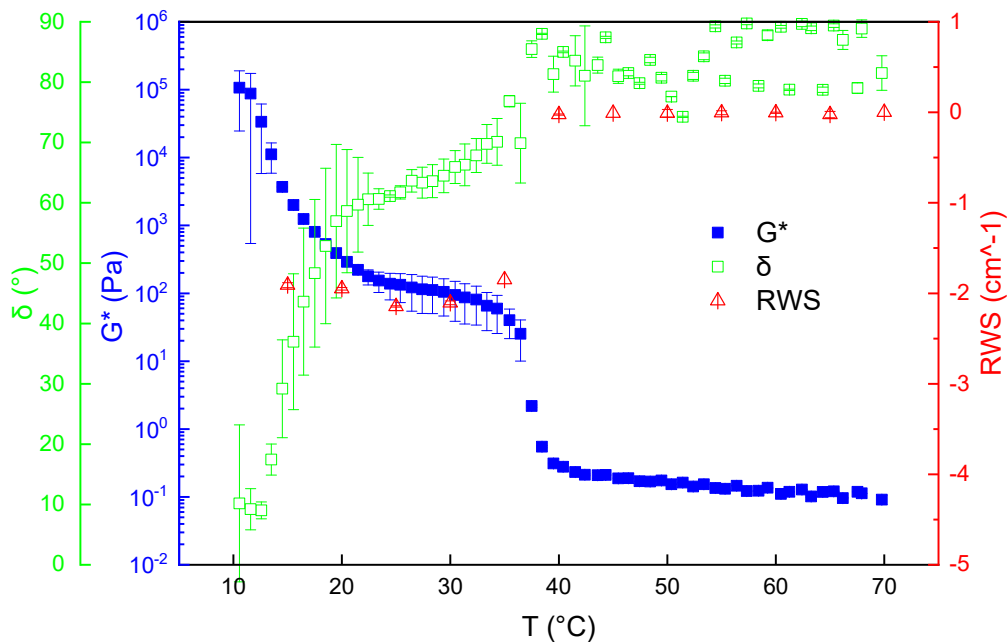


Fig 3.30: Time cure test and RWS for sample OU1, cooling rate -5°C/min

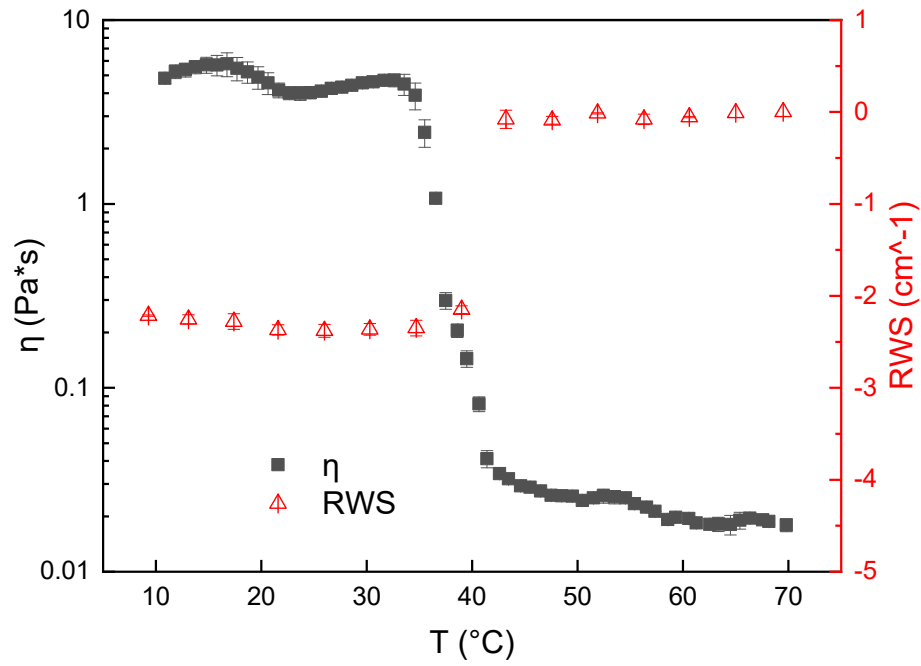


Fig 3.31: SRTRT and RWS for sample OU1, cooling rate -5°C/min

3.2.5.2 DSC Analysis

Fig. 3.32 shows DSC collected on U, OU1 and U2 samples. Despite being a kind of beeswax, The Manuka beeswax crystallisation and melting profile is more similar to the one exhibited by carnauba than the one of beeswax. The crystallisation peak of OU1 is located at about the same temperature at which Tco is found on rheological data.

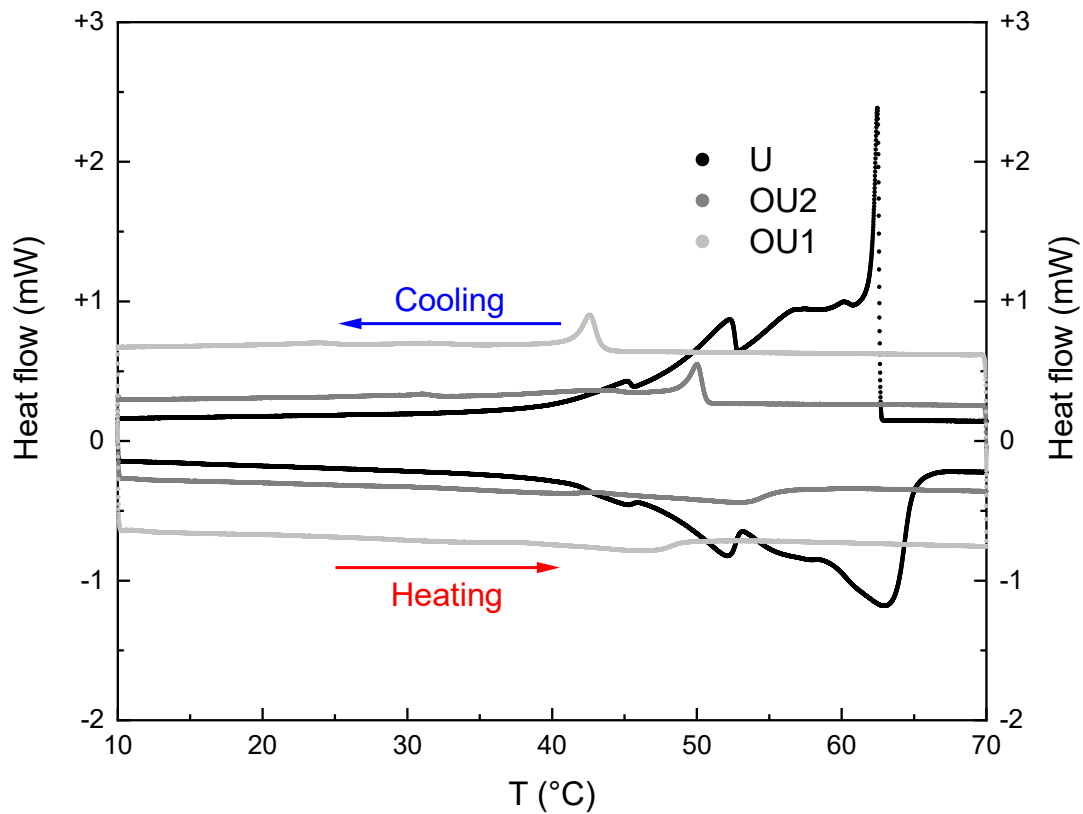


Fig 3.32: DSC thermogram, of Manuka beeswax-based samples, rate 1°C/min

3.2.5.3 SFC

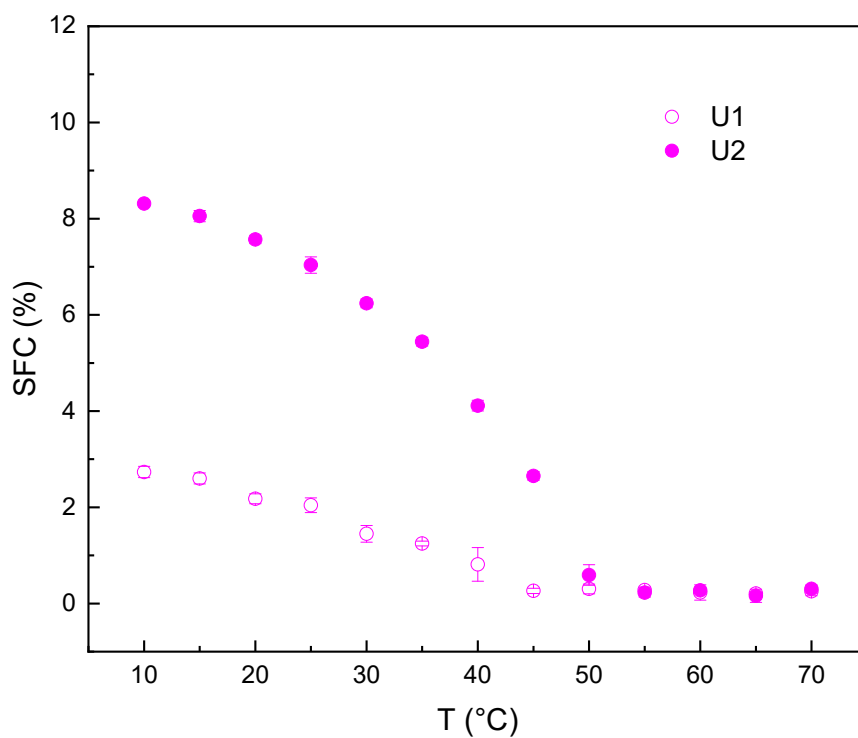


Fig 3.33: SFC of samples OU1 and OU2

SFC for samples OU1 and OU2 are reported in Fig. 3.33. Both values increase with decreasing temperature; furthermore, the onset of crystallisation is comparable to the one seen in DSC and rheological data.

3.3 Comparison between oleogelators

Given the previous results, a comparison between some relevant properties of the different gels will be made.

3.3.1 Crystal onset temperature

An overall comparison of crystal onset temperatures between selected oleogel properties is reported in fig. 3.34.

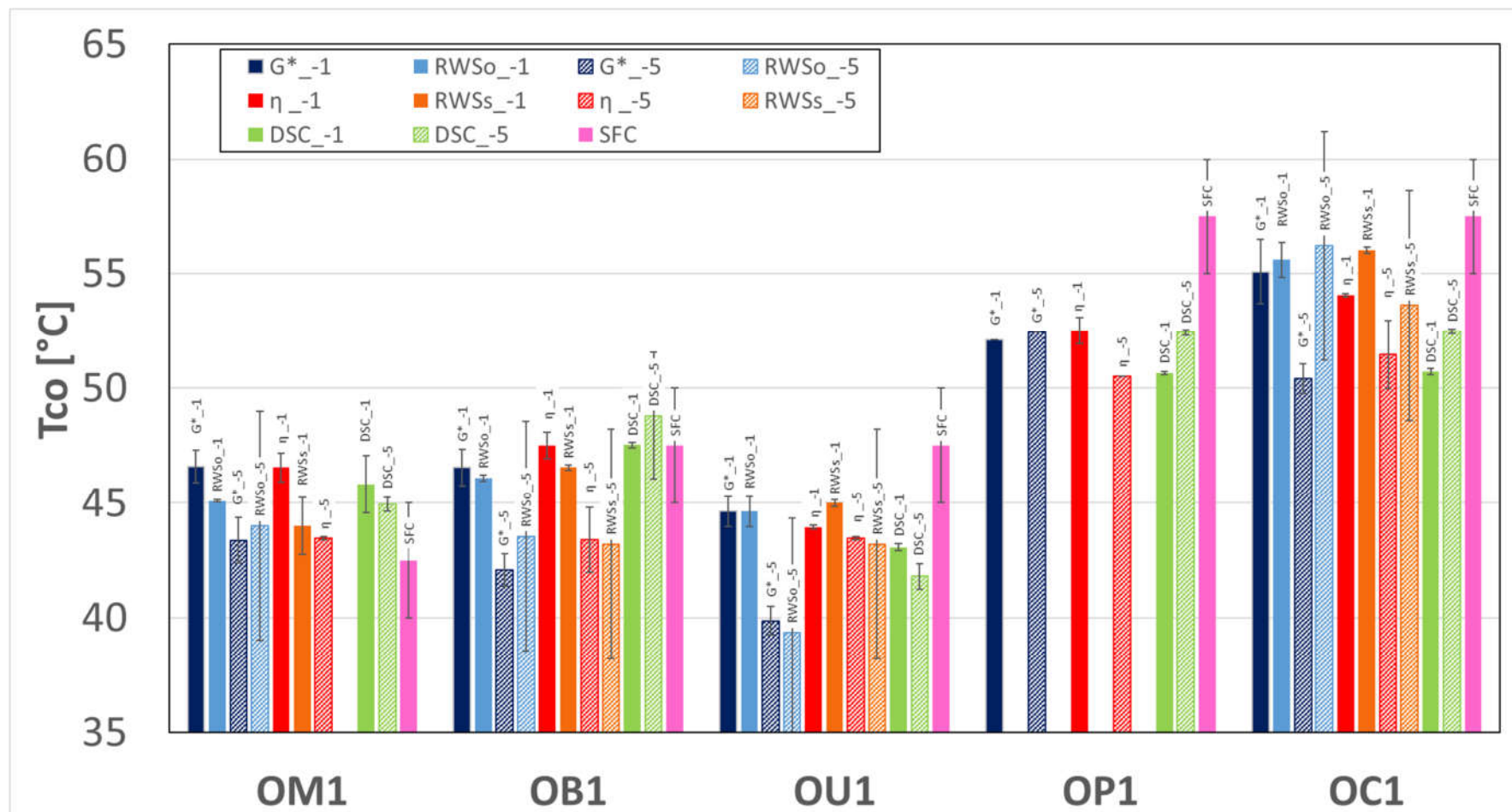


Fig. 3.34: Tco values calculated for different samples. Considered variables are highlighted both in legend and in each Tco value, and are referred to with the respective name along with the cooling rate at which they are measured: -1 for -1°C/min and -5 for -5°C/min. RWSO and RWSs are, respectively, the Relative Wavenumber Shift for oscillatory time cure and SRTRT. Full columns refer to -1°C/min except for SFC, which cooling ramp could not be properly controlled, and striped columns refer to -5°C/min.

Values of T_{co} calculated for the phase angle are not reported since they are very similar to the T_{co} values of their respective G^* for the same tests. Not all values are present. RWS for sample OP1 is never appreciable, as seen with time cure tests in section 3.2.2 in both tests and in both cooling rates. RWS for sample OM1 for SRTRT at $-5^\circ\text{C}/\text{min}$ is also not appreciable. OP1 and OC1 have overall higher crystal onset temperatures when comparing the same technique for different samples, and this is explained by the fact that P and C have higher melting points than M, B, and U; the preparation temperatures of the samples are, in fact, 85°C for OP1 and OC1 and 70°C for OM1, OB1 and OU1. So it is straightforward to say that the higher the melting temperature of the pure oleogelator, the higher the crystal onset temperature of the corresponding gel will be. Moreover, T_{co} seems to be affected by cooling rate. A lower cooling rate leads to higher T_{co} both in G^* and in η for all samples, except for OP1 which seems to have a slightly higher value of T_{co} for the faster cooling rate in G^* measurements. For DSC measurements no uniform behaviour is observed: cooling rate $-5^\circ\text{C}/\text{min}$ leads to higher T_{co} for OC1 and OP1; for OB1 the uncertainty of $T_{co_DSC_5}$ is too high, and for OM1 and OU1 cooling rate $-1^\circ\text{C}/\text{min}$ leads to higher T_{co} . Despite that, in all cases for DSC measurements the difference is lower than 2°C . RWS value, whereas present, is often close to the respective rheological property, and this is because such measurements are carried out simultaneously. Solid fat content T_{co} values have different behaviours but the wide error bars have to be considered as well.

3.3.2 Relative properties of gels during crystallisation

Another way to compare gels is by following the behaviour of relevant properties with respect to their crystal onset temperature, as described in chapter 2, section 2.2.1. Once T_{co} is calculated for each variable, this will be set as the first point. Then, 5°C are subtracted several times to obtain a new set of temperatures, and chosen properties are evaluated at each of those temperatures. So, for example, T_5 is the temperature 5°C lower than T_{co} for that particular sample and for that particular variable, T_{10} is the temperature 10°C lower than T_{co} and so on; in general, until T_{30} . The latter is the maximum value at which a comparison can be done in this study, since the minimum T_{co} value is $\sim 40^\circ\text{C}$ (fig. 3.34, OU1 sample) and the lowest temperature reached in measurements is 10°C . Considered properties were, for both cooling rates $-1^\circ\text{C}/\text{min}$ and $-5^\circ\text{C}/\text{min}$, G^* and δ for oscillatory tests and η for steady shear tests. Results are reported below. Fig 3.35 shows the behaviour of G^* for each sample with increasing distance from T_{co_OSC} , towards lower temperatures.

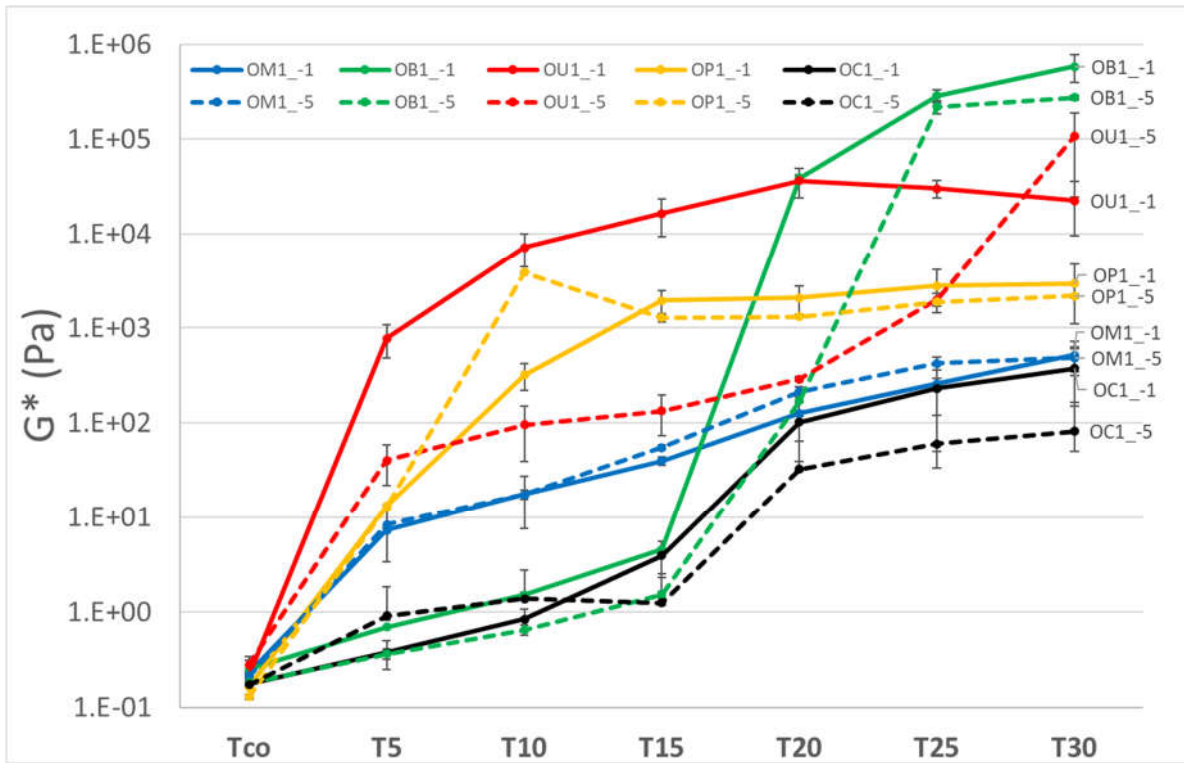


Fig. 3.35: G^* plotted against distance from T_{co_OSC} . Full line refers to cooling ramp $-1^\circ\text{C}/\text{min}$, dashed line refers to $-5^\circ\text{C}/\text{min}$.

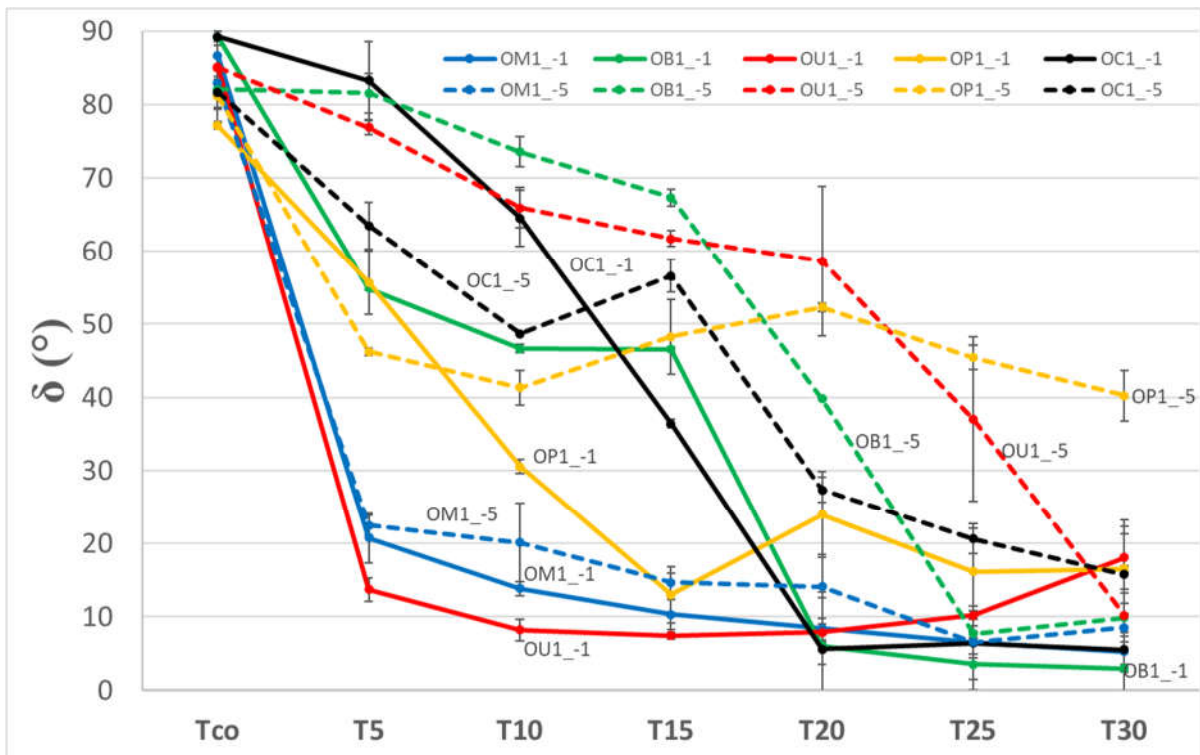


Fig. 3.36: δ plotted against distance from T_{co_OSC} . Full line refers to cooling ramp $-1^\circ\text{C}/\text{min}$, dashed line refers to $-5^\circ\text{C}/\text{min}$.

All samples at T_{co} have very low values of G^* , because crystallisation has not started yet. As temperature is lowered, G^* increases with different slopes for different samples. This means that every sample has a different crystallisation kinetics. Although all lines are distinguishable, the same

sample at different cooling rates seems to behave in the same way except for sample OU1_-1 at lower temperatures. G^* value reaches a plateau value at low temperatures. Overall, a slower cooling rate seems to promote higher G^* values for all samples during oleogelation. Sample OB1 has the same G^* behaviour as OC1 until T15, after which an impetuous increase in G^* is observed of about 5 orders of magnitude in 5°C. Fig 3.36 shows the same plot with δ as considered property. In correspondence of T_{co} all samples exhibit liquid-like behaviour, as δ is close to 90°. Sample OM1 and OU1 become solid-like within the first few degrees after crystallisation onset, except for OU1_-5°C/min which crystallisation is delayed, although its correspondent G^* is one of the highest. Therefore, G^* and δ have to be simultaneously examined to have a more complete idea of the mechanical behaviour of the system. As seen in fig 3.35, higher cooling rates hinders crystallisation, as lower δ values are reached by the samples cooled down with slower cooling rates first. Plotting of steady shear viscosity with increasing distance from T_{co_ROT} is reported in fig. 3.37.

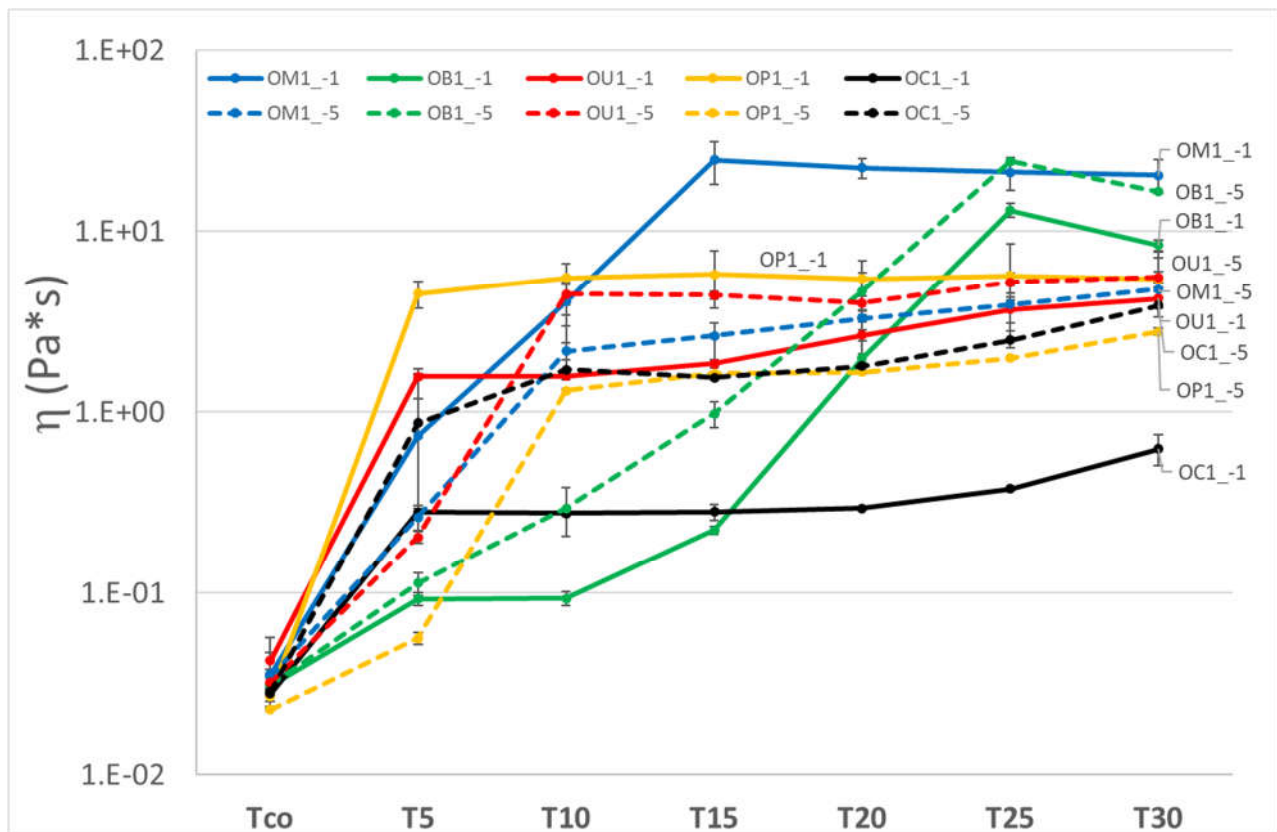


Fig. 3.37: η plotted against distance from T_{co_ROT} . Full line refers to cooling ramp -1°C/min, dashed line refers to -5°C/min.

As depicted in the figure it is clear that most of the samples' viscosities grow for the most part until T10, after which the viscosity does not significantly increase anymore; a small positive slope can be seen but this is probably due to kinetic effects within the crystal network. This is visible for the sample OC1_-1, which reaches the plateau at T5: this could mean that shear flow promotes gel formation,

although no information about the solid-like and liquid-like contributions can be gathered through a shear flow experiment. Moreover, a higher cooling rate has a positive effect on samples OB1, OU1 and OC1 and a negative effect on OM1 and OP1 samples. It is interesting to note that B, U and C are waxes which chemical composition is complex [7], while M and P are much simpler substances [8] [9], with less distributed and smaller molecules.

3.3.3 Structure Development Rate: Kinetics of gel structuring

Fig. 3.34 gives an insight of which system gels first with different techniques. Further analysis on gel structuring is carried out by considering the parameter SDR defined in eqs. 2.1 and 2.2, the former being the point derivative of G' with respect to time and the latter being an average of the SDR until a certain time (or temperature). SDR for the samples at -1°C cooling rate are reported in fig. 3.38 below.

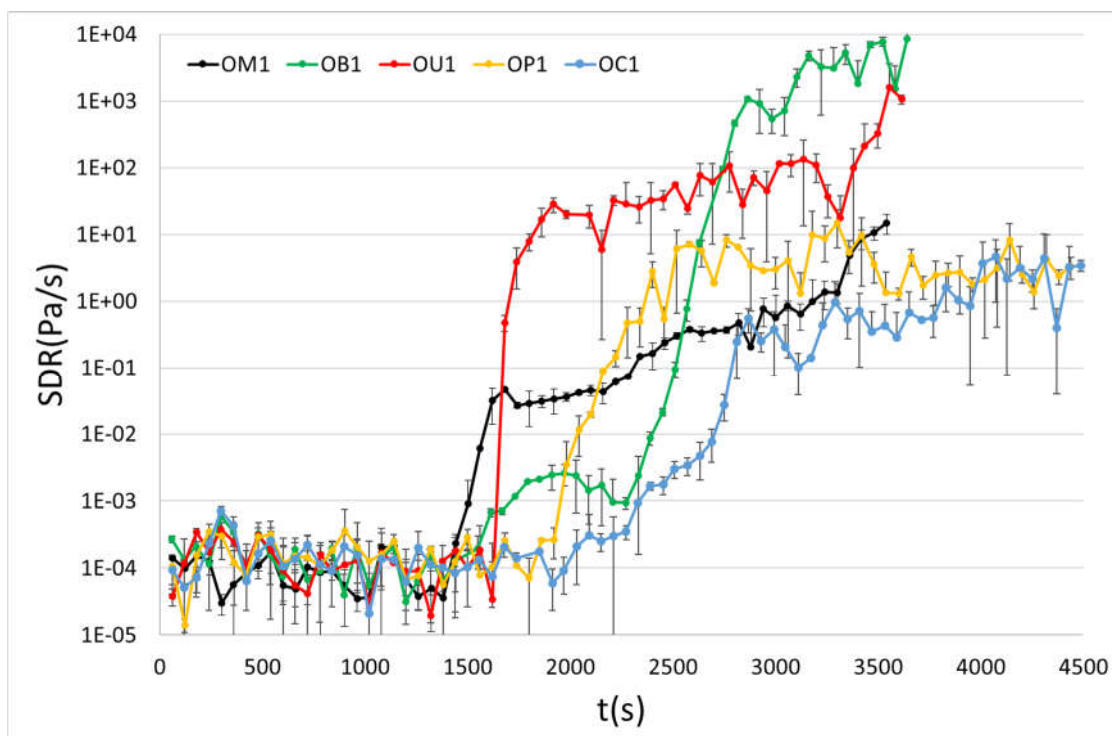


Fig. 3.38: SDR as a function of time for samples at cooling rate $-1^\circ\text{C}/\text{min}$

All of the samples exhibit similar gelling behaviour although at different numeric values. An initial plateau (although all of the derivatives scatter at the beginning due to the low stresses used, they do not increase significantly), at the beginning of the cooling process; an abrupt increase of G' , meaning the structuring process is taking place; a constant or slightly increasing of the derivative meaning the gelling process is substantially completed. OM1 sample is the first structuring system: this seems to be in contrast with results in fig. 3.34 where samples OP1 and OC1 have overall higher onset

temperatures, but it has to be kept in mind that OP1 and OC1 start from a temperature (85°C) which is significantly higher than the starting temperature of the other samples (70°C). The highest derivative belongs to sample OB1, meaning is the system to structure the most, while the fastest (in terms of derivative increasing a lot in a short timeframe) is the sample OU1. In order to compare the relative gelling ability of the oleogelators, the average SDR (SDr_{avg}) was considered. Plot in fig. 3.39 illustrates SDr_{avg} for the previous samples at different T_x , x being the distance from the crystal onset temperature.

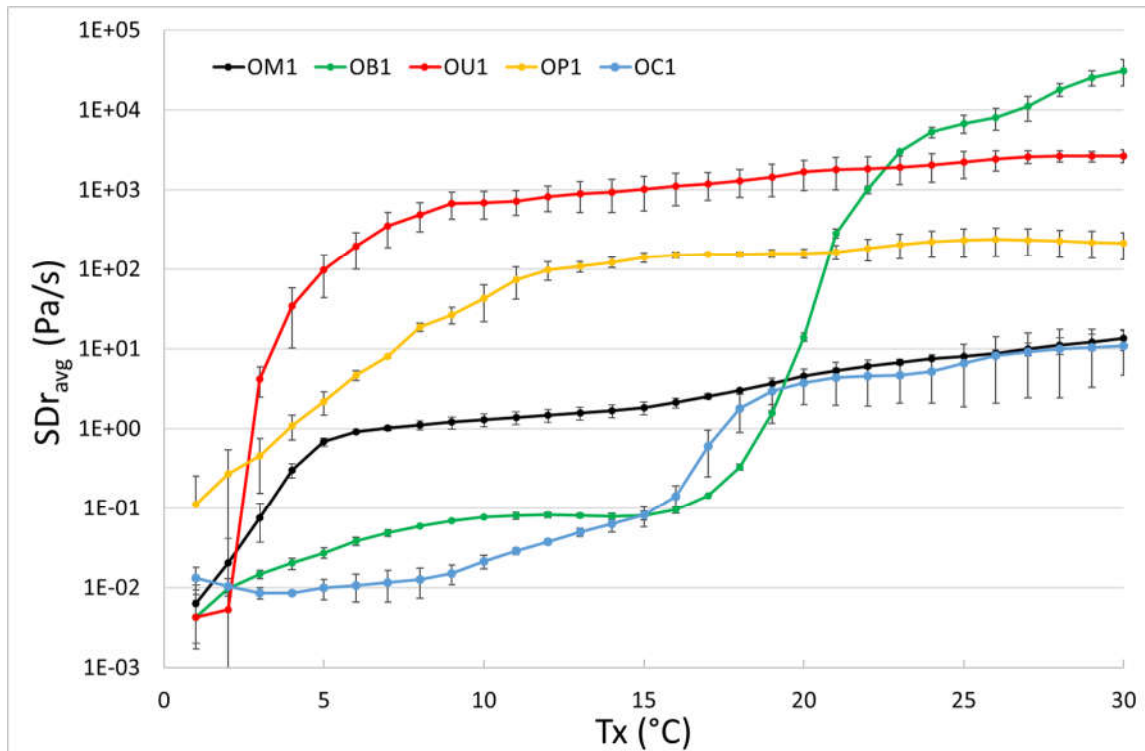


Fig. 3.39: SDr_{avg} as a function of distance from the respective onset temperature T_{co} for samples at cooling rate $-1^\circ\text{C}/\text{min}$

The parameter SDr_{avg} gives us information on the progression of the gelling process. It is interesting to acknowledge that, while samples OM1, OP1 and OU1 gain their structure for the most part within the first 10°C from the crystallisation onset, sample OC1 has a slow and limited overall SDR while OB1 has the highest SDR, although delayed similarly to OC1.

3.4 Edible oleogels as fat phase for emulsion preparation

Lupi et al [10] used myverol-based oleogel as the fat phase of a structured emulsion. The hosting company of this project, Reoli S.r.L., has interest in this research field since it produces spreadable emulsions as fat replacers. For this reason, the last part of this work focuses on a practical application of an oleogel as a structured fat phase for emulsion preparation.

3.4.1 R-based oleogels

The oleogelator used by the company to make spreadable emulsions, whose commercial name is not shown for the sake of confidentiality, is composed by monoacylglycerols like Myverol and has been used to prepare samples OR1 and SR1. Results of sample OR1 are shown in fig. 3.40 while results of sample SR1 are shown in fig. 3.41. Results show that the overall behaviour of OR1 and SR1 are consistent with the samples studied so far: they both are liquid-like at high temperatures, until temperature reaches a crystal onset value at which all the properties simultaneously change abruptly. Samples OR1 and SR1 also show almost identical behaviour. OH area was reported because it showed a very small deviation, unlike for OM1 sample; it seems to follow the increase of G^* very well. Change in RWS, on the other side, is not really appreciable, even though wide error bars suddenly appear whereas, at high temperatures, RWS was smoothly equal to zero until $T=T_{co}$. This suggests that a shift could be measurable.

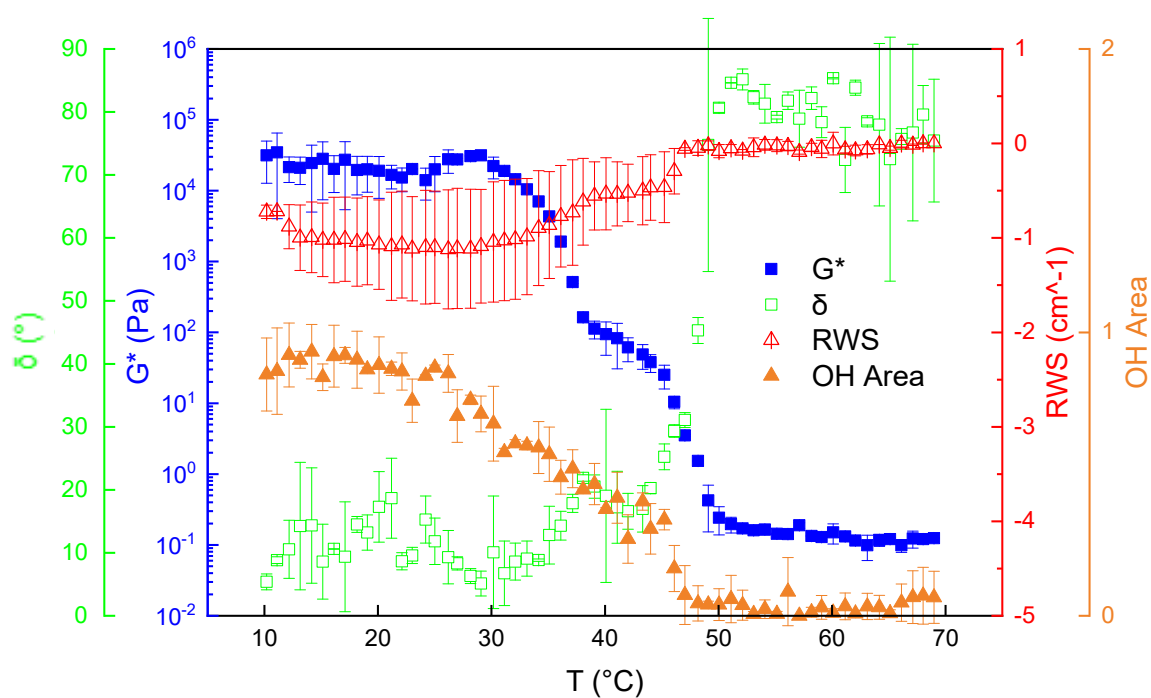


Fig 3.40: Time cure test and FTIR parameters for sample OR1, cooling rate $-1^{\circ}\text{C}/\text{min}$

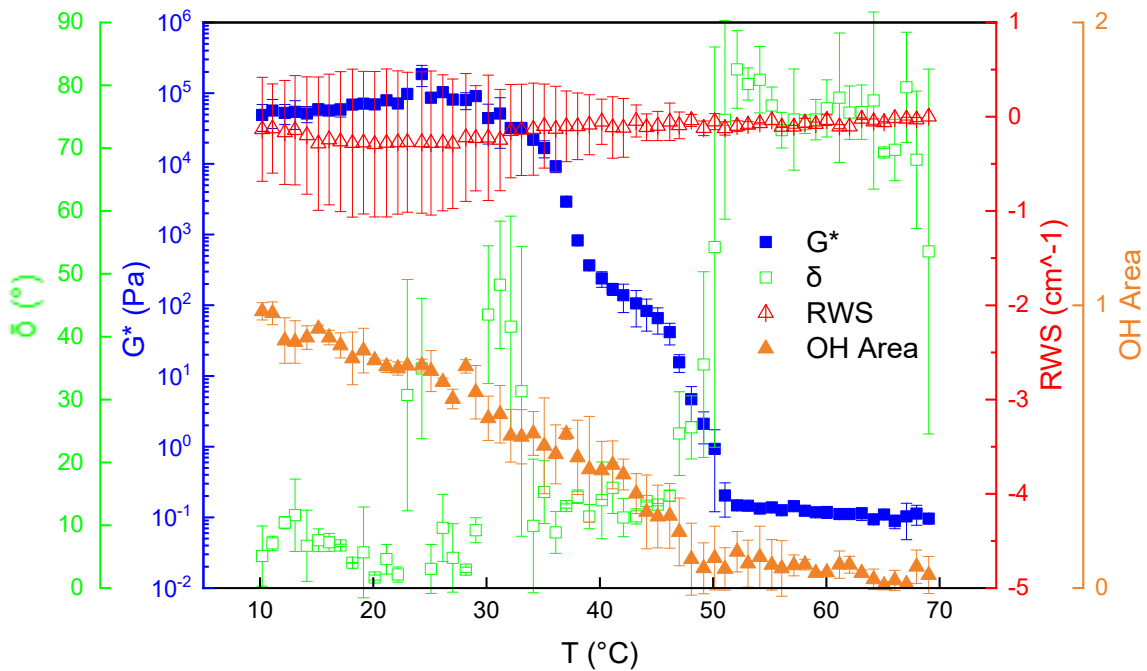


Fig 3.41: Time cure test and FTIR parameters for sample SR1, cooling rate -1°C/min

Since the only changing variable between the two samples is the oil used (O stands for olive oil, S stands for sunflower oil) no structural difference is observed when changing the oil for this test at this cooling rate, although more detailed tests should be carried out in order to exclude the influence of the oil type on this particular system. A study claimed that the change of oil type is not relevant to the rheological properties of fatty alcohols edible oleogels [11].

3.4.2 Rheological tests on a potentially marketable emulsion

Results of tests performed on a potentially marketable emulsion, as a part of the collaboration with the hosting company, are reported in fig. 3.42.

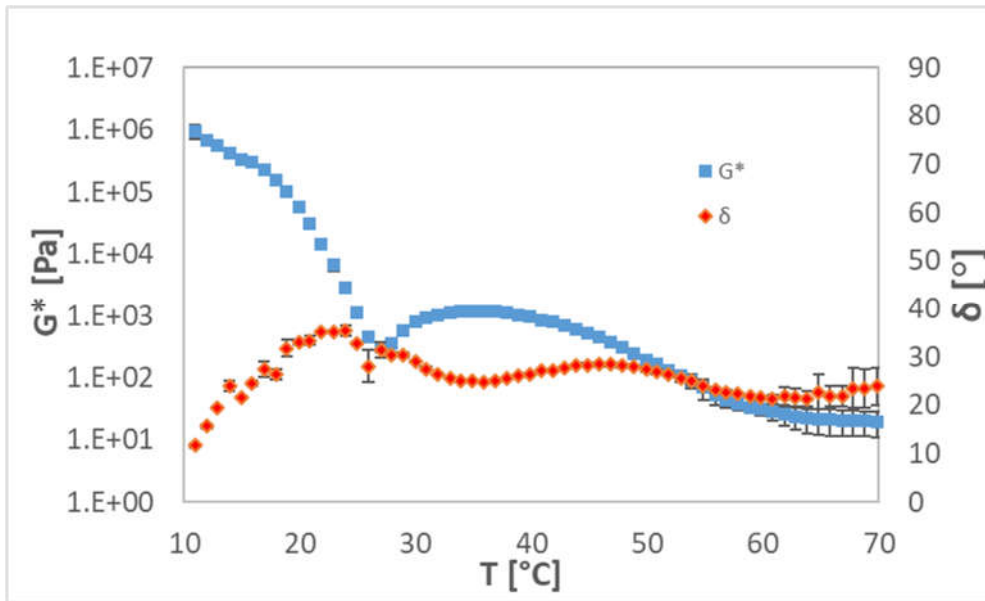


Fig 3.42: Time cure test of R-based emulsion with 21% w/w fruit juice applying a cooling rate of +1°C/min

The system is susceptible to temperature change but maintain good solid-like properties from starting temperature to room temperature, then an inflection in both G^* and δ is observed. After that, the system seems to keep its stability since the rheological properties do not change much, but actually a phase separation is happening. Results on frequency sweep tests are showed in fig. 3.43.

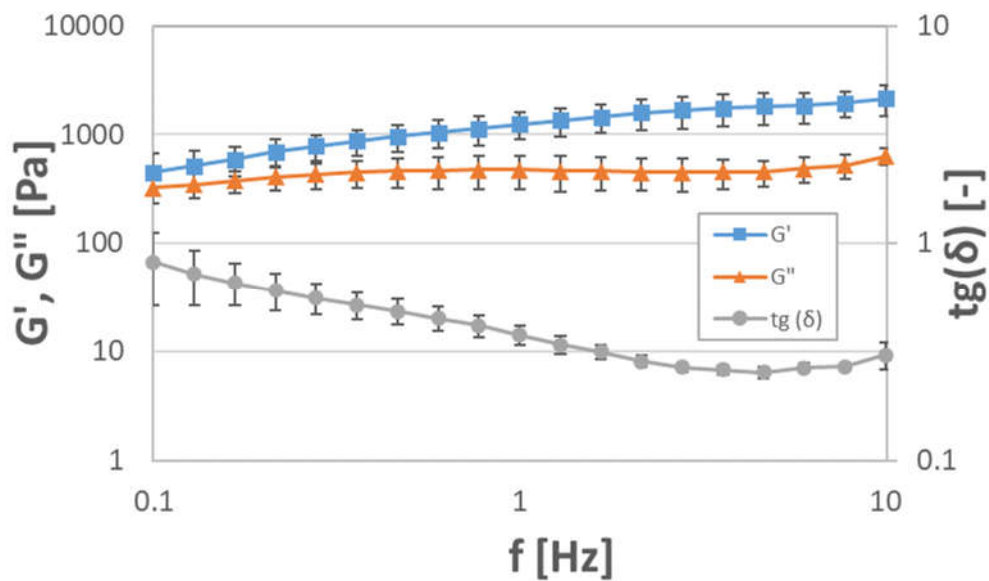


Fig 3.43: Frequency sweep test of R-based emulsion with 21% w/w fruit juice at 25°C without applying a heating ramp

Although storage modulus G' is always greater than loss modulus G'' no predominant solid-like behaviour is exhibited by the system, since $\tan(\delta)$, which equals to the ratio of loss modulus to storage modulus, is never significantly below 1.

References

- [1] N. Vlachos, Y. Skopelitis, M. Psaroudaki, V. Konstantinidou, A. Chatzilazarou, and E. Tegou, "Applications of Fourier transform-infrared spectroscopy to edible oils," *Anal. Chim. Acta*, vol. 573–574, pp. 459–465, 2006.
- [2] N. Yamada, T. Imai, and E. Koyama, "Lyotropic aggregate of tripeptide derivatives within organic solvents: relationship between interpeptide hydrogen bonding and packing arrangements of components," *Langmuir*, vol. 17, no. 4, pp. 961–963, 2001.
- [3] M. Suzuki, Y. Nakajima, M. Yumoto, M. Kimura, H. Shirai, and K. Hanabusa, "Effects of Hydrogen Bonding and van der Waals Interactions on Organogelation Using Designed Low-Molecular-Weight Gelators and Gel Formation at Room Temperature," *Langmuir*, vol. 19, no. 21, pp. 8622–8624, 2003.
- [4] F. R. Lupi, D. Gabriele, and B. de Cindio, "Effect of Shear Rate on Crystallisation Phenomena in Olive Oil-Based Organogels," *Food Bioprocess Technol.*, vol. 5, no. 7, pp. 2880–2888, 2012.
- [5] F. R. Lupi, V. Greco, N. Baldino, B. de Cindio, P. Fischer, and D. Gabriele, "The effects of intermolecular interactions on the physical properties of organogels in edible oils," *J. Colloid Interface Sci.*, vol. 483, pp. 154–164, 2016.
- [6] A. I. Blake, E. D. Co, and A. G. Marangoni, "Structure and physical properties of plant wax crystal networks and their relationship to oil binding capacity," *JAACS, J. Am. Oil Chem. Soc.*, vol. 91, no. 6, pp. 885–903, 2014.
- [7] A. I. Blake and A. G. Marangoni, "Plant wax crystals display platelet-like morphology,"

Food Struct., vol. 3, pp. 30–34, Jan. 2015.

- [8] F. R. Lupi, D. Gabriele, V. Greco, N. Baldino, L. Seta, and B. de Cindio, “A rheological characterisation of an olive oil/fatty alcohols organogel,” *Food Res. Int.*, vol. 51, no. 2, pp. 510–517, 2013.
- [9] F. R. Lupi, D. Gabriele, D. Facciolo, N. Baldino, L. Seta, and B. de Cindio, “Effect of organogelator and fat source on rheological properties of olive oil-based organogels,” *Food Res. Int.*, vol. 46, no. 1, pp. 177–184, 2012.
- [10] F. R. Lupi, D. Gabriele, B. De Cindio, M. C. Sánchez, and C. Gallegos, “A rheological analysis of structured water-in-olive oil emulsions,” *J. Food Eng.*, vol. 107, no. 3–4, pp. 296–303, 2011.
- [11] F. G. Gandolfo, A. Bot, and E. Flöter, “Structuring of Edible Oils by Long-Chain FA, Fatty Alcohols, and Their Mixtures,” *JAACS, J. Am. Oil Chem. Soc.*, vol. 81, no. 1, pp. 1–6, 2004.

Conclusions and perspectives

In this work, oil-based systems structured via organogelation, a non-invasive technique that allows edible oil to gain solid-like behaviour while keeping its properties were studied. The aim was to find suitable substances able to gel edible oils. The challenge is still open since the process of food innovation has to face strict rules regarding the use of food additives. Apart from policosanol and monoglycerides, two well-known oleogelators, waxes were also examined as possible oil structuring agents: Carnauba wax, beeswax and Manuka beeswax, all of them being suitable for producing organic fat phases. Results showed that beeswax-based-gels were very strong at low temperature but still too soft at room temperature, whereas carnauba wax and Manuka beeswax were the most promising choices in order to produce fat basis for the food industry. Tests on an oleogel-based emulsion were made, exhibiting a stiff behaviour especially at low temperatures. Another challenge faced was to understand the role of the interactions during gel formation. IR spectra are a useful tool for that purpose but some aspects still need to be clarified, as for example why during rheological measurements, spectra acquiring gives different results with respect to the same sample in steady conditions or in similar non-steady conditions. It would be interesting trying to understand whether is possible to link macroscopic properties to the information coming from infrared spectra.

La borsa di dottorato è stata cofinanziata con risorse del
Programma Operativo Nazionale Ricerca e Innovazione 2014-2020 (CCI 2014IT16M2OP005),
Fondo Sociale Europeo, Azione I.1 "Dottorati Innovativi con caratterizzazione Industriale"



UNIONE EUROPEA
Fondo Sociale Europeo



*Ministero dell'Istruzione,
dell'Università e della Ricerca*

